UNIVERSITA' DI NAPOLI FEDERICO II

DOTTORATO DI RICERCA
BIOCHIMICA E BIOLOGIA CELLULARE E MOLECOLARE
XXV CICLO

Properties of the thioredoxin system in microaerophiles from the *Streptococcus* genus

Salvatore Marco

Tutor
Prof. Emmanuele De Vendittis

Coordinator
Prof. Paolo Arcari

Academic Year 2011/2012

Ringraziamenti

Quando si va verso un obiettivo, è molto importante prestare attenzione al cammino. E' il cammino che ci insegna sempre la maniera migliore di arrivare, ci arricchisce mentre lo percorriamo, (Paulo Coelho).

A distanza di tre anni dal conseguimento della laurea specialistica, mi ritrovo a scrivere nuovamente i ringraziamenti. La sensazione che si prova è sempre piacevole, perché questo momento segna la fine di un percorso e forse l'inizio di qualcosa di nuovo e appassionante. In realtà, questa piacevole sensazione è accompagnata, mentre scrivo, da un pizzico di tristezza, dal timore di perdere qualcosa o qualcuno, ad esempio gli amici-colleghi, i professori, la mia seconda casa: il laboratorio 606.

Portare a termine un progetto di ricerca richiede molto impegno e soprattutto tanti sacrifici e solo l'amore per la scienza accompagnata dall'essere seguiti da persone molto qualificate hanno permesso la realizzazione di questo lavoro. Non sarà semplice questa volta scrivere dei ringraziamenti perché le persone che hanno collaborato al mio arricchimento professionale sono davvero tante e andrebbero tutte ringraziate ma ho poche righe a disposizione e loro lo sanno. Spero di aver dato delle conferme e di essere stato all'altezza di quanto mi è stato chiesto di fare, di certo l'impegno e la passione da parte mia non sono mai mancati. Il tempo è volato come sempre, in ogni caso ho cercato di dare il massimo di me stesso.

Ringrazio enormemente il mio docente guida, il Prof. Emmanuele De Vendittis, per i suoi pazienti e preziosi insegnamenti, per le risposte a tutti i miei dubbi e per la disponibilità mostrata nei miei confronti e nella stesura di questa tesi. Non avrei potuto avere una guida migliore, motivo in più che mi ha spinto a dare il massimo.

Ringrazio il prof. Luigi Servillo, per i suoi suggerimenti oltre che per essersi assunto l'onere di una lettura critica.

Ringrazio il Prof. Paolo Arcari, coordinatore del dottorato di ricerca in Biochimica e Biologia Cellulare e Molecolare per avermi dato l'opportunità di seguire corsi e seminari che hanno ampliato in particolar modo le mie conoscenze teoriche e per avermi dato la possibilità di partecipare a congressi nazionali e internazionali.

Ringrazio il Prof. Mariorosario Masullo per la disponibilità e la cortesia avute nei miei confronti da cui ho potuto trarre numerosi insegnamenti sia tecnici che teorici.

Ringrazio il Dott. Rosario Rullo la cui esperienza è stata per me un vero appiglio nei momenti d'indecisione fornendomi utili soluzioni nell'affrontare i vari quesiti sperimentali .

Antonella, ti ho tormentato lo so, Alessandra con te sono stato un po' più buono, grazie di cuore per avermi sopportato, siete state una vera compagnia oltre che delle validissime colleghe.

Ringrazio tutti i professori e i ricercatori del VI piano della torre biologica, il Prof. Antonio Dello Russo, il Prof. Gaetano Corso, le Dott.sse Rosaria Ruocco, Annalisa Lamberti, Lia Rippa, la Sig.ra

Alba simpaticissima e sempre disponibile, i giovani laureandi, dottorandi e contrattisti. Tutti insieme e ognuno a suo modo hanno contribuito a questa mia esperienza professionale oltre che umana e verso i quali esprimo una profonda gratitudine.

In ultimo, ma non di certo per importanza, desidero ringraziare i miei genitori, Grazie Mamma, grazie Papà per tutto quello che avete sempre fatto, il vostro sostegno è stato per me un aiuto imprescindibile che mi ha dato la forza per affrontare questo lungo percorso di studi.

Ah, dimenticavo!!!

Mio fratello Lino.

Uhmm?!!

In effetti, cosa ha fatto? Mi disturbava quando cercavo di studiare!!!!

Scherzo, e grazie anche a te per avermi sopportato, ti voglio bene fratello.

Riassunto

Gli streptococchi sono batteri gram-positivi di forma sferica (cocchi), che durante la crescita si dispongono in coppie o catenelle. Il loro fabbisogno energetico è assicurato dal metabolismo anaerobico in cui la glicolisi è seguita dalla formazione di acido lattico; tuttavia questi batteri fermentanti sono considerati anaerobi facoltativi, perché tollerano la presenza dell'ossigeno. Il genere *Streptococcus* raggruppa diverse specie, tra cui molte patogene per l'uomo, come *S. mutans*, che, colonizzando il cavo orale fin dalla comparsa dei primi denti decidui, è il principale responsabile dello sviluppo della carie dentaria. D'altra parte tra gli streptococchi si ritrovano anche specie non patogene come *S. thermophilus*, che assume grande rilevanza nell'industria alimentare, essendo adoperato per la produzione di molti derivati del latte.

Gli streptococchi sono dotati dei principali sistemi di difesa dalle specie reattive dell'ossigeno (ROS). In particolare, sia in *S. mutans* che in *S. thermophilus* è presente la superossido dismutasi (SOD), che eliminando l'anione superossido, il primo ROS generato dalla riduzione univalente dell'ossigeno, previene la formazione di altri ROS ancora più dannosi. Un altro elemento chiave per la difesa contro il danno indotto dai ROS è il sistema della tioredossina che provvede alla riduzione degli eventuali ponti disolfuro formati in proteine intracellulari durante condizioni di stress ossidativo. Tale sistema, costituito dal flavoenzima tioredossina riduttasi (TrxB) e dal

suo substrato proteico, la tioredossina (TrxA), utilizza il NADPH come donatore di equivalenti riducenti. Sia TrxA che TrxB possiedono un'attività tiolo-transferasica basata sull'ossido-riduzione reversibile del ponte disolfuro esistente tra due residui di cisteina della tipica sequenza di consenso (CXXC) di entrambe le proteine. Il ruolo di TrxB consiste nel catalizare il trasferimento di equivalenti riducenti dal coenzima NAPDH al FAD e poi al disolfuro del sito attivo. Gli elettroni sono successivamente trasferiti al disolfuro della TrxA, che a sua volta li trasferisce ad uno specifico substrato proteico ossidato, contribuendo in tal modo al mantenimento delle proteine citosoliche nel loro stato ridotto.

L'obiettivo di questa ricerca è stato quello di stabilire l'esistenza e il funzionamento del sistema della tioredossina in due membri rappresentativi del genere *Streptococcus*, *S. mutans* e *S. thermophilus*. Le precedenti notizie erano limitate all'annotazione dei putativi geni codificanti i componenti proteici di tale sistema. In particolare, il genoma di *S. mutans* contiene due geni per putative TrxB (*trxB* e *trxB1*) e tre geni per putative TrxA (*trxA*, *trxH1* e *trxL*). In *S. thermophilus* c'è una minore ridondanza, poichè sono stati annotati due geni per putative TrxB (*trxB1* e *trxB2*) e due geni per putative TrxA (*trxA1* e *trxA2*). L'ipotesi di una ridondanza di TrxB in *Streptococcus* è stata però subito scartata, perchè nella sequenza amminoacidica dedotta dai geni *trxB2* di entrambi i microrganismi mancava il motivo CXXC del sito attivo, un elemento indispensabile

per il ruolo delle TrxB. Non è stato invece possible scartare a priori l'ipotesi di una ridondanza di TrxA, anche se la lunghezza della sequenza amminoacidica dedotta dal gene *trxL* di *S. mutans* era circa doppia rispetto a quella solitamente ritrovata nelle TrxA batteriche. Pertanto, per identificare e caratterizzare i reali componenti proteici del sistema della tioredossina in *S. mutans* e *S. thermophilus*, è stata realizzata l'espressione eterologa dei suddetti geni con una strategia che consente di ottenere proteine fuse ad un peptide di sei istidine (His-tag). In particolare, sono state ottenute forme ricombinanti purificate di due putative tioredossine riduttasi (una per *S. mutans*, chiamata r*Sm*TrxB, e una per *S. thermophilus*, chiamata r*St*TrxB1) e di quattro putative tioredossine (due per *S. mutans*, chiamate r*Sm*TrxA e r*Sm*TrxH1, e due per *S. thermophilus*, chiamate r*St*TrxA1 e r*St*TrxA2). Invece non è stata ancora realizzata l'espressione eterologa del gene *trxL* di *S. mutans*. Dallo studio delle loro proprietà molecolari è emerso che le proteine espresse hanno la tipica massa delle TrxB (35 kDa) o delle TrxA (10.5 –12 kDa). Inoltre sia r*Sm*TrxB che r*St*TrxB1 hanno legato il FAD e possiedono la tipica organizzazione struttutale omodimerica.

La funzionalità delle proteine espresse è stata valutata mediante dosaggi specifici, con cui è stata misurata la tipica attività tiolo-disolfuro riduttasica dei componenti proteici del sistema tioredossina, sia da soli che in combinazione. In particolare, r*Sm*TrxB e *St*TrxB1 catalizzano la riduzione del ditionitrobenzoato (DTNB) in presenza di

NADPH come donatore di equivalenti. Sono stati anche misurati i parametri cinetici di tale reazione a 37°C, da cui è emerso che i due flavoenzimi hanno un'efficienza catalitica un po' inferiore rispetto a quella ritrovata nei corrispondenti enzimi di organismi aerobici. L'attività delle tioredossine è stata valutata con il dosaggio di riduzione dell'insulina umana in presenza di DTT come donatore di equivalenti riducenti. Delle quattro tioredossine, solo r*Sm*TrxA e r*St*TrxA1 sono risultate attive in questo dosaggio. L'assenza di attività delle altre due putative tioredossine, r*Sm*TrxH1 e r*St*TrxA2, è forse correlata alla presenza di residui amminoacidici insoliti all'interno della sequenza CXXC. Pertanto questi dati sembrano indicare che *S. thermophilus*, oltre ad un'unica tioredossina riduttasi, possieda una sola tioredossina. Per *S. mutans* non è invece ancoa possibile esculdere una ridondanza di tioredossine a causa della mancata espressione del gene *TrxL*.

La disponibilità dei rispettivi componenti proteici, una tioredossina ed una tioredossina riduttasi per ciascun microrganismo, ha consentito poi di ricostituire *in vitro* il sistema della tioredossina sia per *S. mutans* che per *S. thermophilus*. In particolare la funzionalità è stata studiata con il dosaggio di riduzione dell'insulina, adoperando in questo caso il NADPH come donatore di elettroni. In particolare, dai risultati ottenuti è emerso che il sistema della tioredossina è pienamente attivo sia con l'uso di componenti autologhi (r*Sm*TrxB + r*Sm*TrxA oppure r*St*TrxB1 + r*St*TrxA1) che di componenti misti

provenienti dai due microrganismi (r*Sm*TrxB + r*St*TrxA1 oppure r*St*TrxB1 + r*Sm*TrxA). Dagli studi cinetici sui sistemi ricostituiti autologhi e misti sembra che il flavoenzima di *S. mutans* r*Sm*TrxB abbia una lieve minore affinità sia per la tioredossina autologa che per quella di *S. thermophilus*, mentre entrambi i flavoenzimi abbiano una qualche maggiore affinità per la tioredossina di *S. thermophilus* r*St*TrxA1.

È stata anche studiata la reversibilità del passaggio di elettroni dal NADPH alla tioredossina mediato dalla tioredossina riduttasi, da cui è stato possibile misurare il potenziale redox della tioredossina nei sistemi autologhi e misti. Il potere riducente misurato con il sistema autologo di *S. thermophilus*, simile a quello di altri sistemi della tioredossina da batteri aerobici, è risultato maggiore rispetto a quello autologo di *S. mutans*. Questo comportamento suggerisce un diverso adattamento del meccanismo preposto al mantenimento delle proteine citosoliche nel loro stato ridotto, anche considerando il funzionamento della SOD dei due microrganismi. In *S. mutans* il più basso potere riducente della tioredossina potrebbe essere sufficiente, perchè la sua SOD cambialistica, finememnte regolata dal tipo di metallo legato nel sito attivo, esplica un efficientissimo controllo preventivo dei ROS. Invece in *S. thermophilus* occorre un maggior potere riducente della tioredossina perchè la sua SOD cambialistica è meno efficiente nel controllo preventivo dei ROS. I dati dei potenziali redox misurati nei sistemi misti sono risultati simili a quello ottenuto con il sistema

autologo di *S. thermophilus*. Sembra quindi che la magiore reattività di r*Sm*TrxA, insieme alla sua maggiore affinità per entrambi i flavoenzimi, possa compensare la minore reattività r*Sm*TrxB.

Sono stati infine condotti studi sulla termofilicità e termostabilità dei due flavoenzimi. In particolare, la temperatura fa aumentare solo lievemente l'attività di r*St*TrxB1, che quindi possiede un insolito basso valore di energia attivazione. Questo modesto effetto positivo della temperatura sull'attività addirittura scompare per r*Sm*TrxB. Gli studi di termostabilità hanno evidenziato una discreta resistenza al calore di entrambi i flavoenzimi e che tra i due enzimi quello più resistente è r*St*TrxB1. Infine è emerso che per entrambi i flavoenzimi il processo di inattivazione termica è concomitante a quello di denaturazione.

In conclusione, la ricerca svolta ha consentito di identificare e caratterizzare i componenti proteici del sistema della tioredossina in due anaerobi facoltativi del genere *Streptococcus*. Tale sistema è quindi attivo anche in questo tipo di microrganismi, contribuendo così alla riparazione dei danni causati da uno stress ossidativo in seguito ad un aumento dei livelli di ROS.

Summary

The *Streptococcus* genus includes the pathogenic species *S. mutans*, the main responsible of dental caries, and the safe microorganism *S. thermophilus*, used for the manufacture of dairy products. These facultative anaerobes control the levels of reactive oxygen species (ROS) and indeed, both *S. mutans* and *S. thermophilus* possess a cambialistic superoxide dismutase, the key enzyme for a preventive action against ROS. To evaluate the properties of a crucial mechanism for repairing ROS damages, the molecular and functional characterization of the thioredoxin system in these streptococci was investigated. The putative genes encoding its protein components in *S. mutans* and *S. thermophilus* were analysed and the corresponding recombinant proteins were purified. A single thioredoxin reductase was obtained from either *S. mutans* (*Sm*TrxB) or *S. thermophilus* (*St*TrxB1), whereas two thioredoxins were prepared from either *S. mutans* (*Sm*TrxA and *Sm*TrxH1) or *S. thermophilus* (*St*TrxA1 and *St*TrxA2). Both *Sm*TrxB and *St*TrxB1 reduced the synthetic substrate DTNB in the presence of NADPH, whereas only *Sm*TrxA and *St*TrxA1 accelerated the insulin reduction in the presence of DTT. To reconstitute an *in vitro* streptococcal thioredoxin system, the combined activity of the thioredoxin components was tested through the insulin precipitation in the absence of DTT. The assay functions with a combination of *Sm*TrxB or *St*TrxB1 with either *Sm*TrxA or *St*TrxA1. These results suggest that the streptococcal members of the

thioredoxin system display a direct functional interaction between them and that these protein components are interchangeable within the *Streptococcus* genus. In conclusion, our data prove the existence of a functioning thioredoxin system even in these microaerophiles.

Index

List of tables and figures

1. Introduction

1.1 *Oxygen tolerance in the* Streptococcus *genus*

Streptococci belong to the group of gram–positive facultative anaerobic bacteria,[1] whose energetic metabolism mainly depends on the glycolytic pathway, followed by the lactic fermentation.[2] Most of the *Streptococcus* species are known to be human pathogens, and some of them are highly virulent, such as *S. pneumoniae* or *S. agalactiae*, the causative agents of serious acute infections.[3,4] Other pathogens, such as *S. mutans* or *S. sobrinus*, are much less virulent, being part of the resident microflora of the human body. For instance, *S. mutans*, the main responsible in the aetiology of dental caries, colonizes the oral cavity from the early teeth eruption in infants.[5,6] Conversely, another species, the *S. salivarius* subsp. *thermophilus*, hereafter called *S. thermophilus*, is non pathogenic, being generally considered as a safe microorganism.[7,8] Indeed, *S. thermophilus* is massively used for the manufacture of dairy products and therefore has a great importance in food industry.[9-11]

Streptococci, such as *S. mutans* and *S. thermophilus*, are unable to respire by using oxygen as an electron acceptor. This anaerobic metabolism is consistent with the absence of genes encoding heme–containing proteins, such as catalase and cytochrome oxidase, in the streptococcal genomes.[12–14] However, streptococci, usually growing in almost anaerobic ecological niches, tolerate moderate oxygen concentrations, being able to promote the induction of some specific

scavengers of the reactive oxygen species (ROS) generated during the oxygen exposure.[15–19] For instance, streptococci eliminate the superoxide anion, the first ROS produced from the univalent reduction of oxygen, through the action of the enzymatic scavenger superoxide dismutase (SOD).[20,21] In particular, *S. mutans* and *S. thermophilus* possess a cambialistic SOD, which is adapted to the anaerobic or aerobic growth environment, thanks to the different properties exhibited by the Fe– and Mn–isoform of this metal enzyme.[22,23]

1.2 *Properties of the thioredoxin system*

Another key element for the cellular protection against ROS damages is the thioredoxin system, aimed at the removal of disulfide bridges eventually formed in intracellular proteins during an oxidative stress.[24-26] This system is composed by two protein components, thioredoxin (TrxA) and thioredoxin reductase (TrxB). TrxA is a small monomeric protein (10 – 15 kDa) containing the conserved CXXC sequence motif, in which the cysteine residues form a reversible disulfide bridge.[24] A similar sequence element is present also in TrxB, the NADPH–dependent flavoenzyme with a homodimeric organization and whose mass in bacteria is around 35 kDa/subunit.[27,28] The reparative mechanism of the thioredoxin system involves oscillation between oxidised and reduced form of both cysteine motifs of TrxA and TrxB; the role of NADPH as electron donor and the FAD/$FADH_2$ oscillation in the TrxB active site are also required for

the activity.[24,26] Briefly, TrxB catalyses the NADPH–dependent electron transfer to the active disulfide of the oxidised form of TrxA, via an intermediate step involving the bound FAD molecule; in turn, the dithiolic form of TrxA reduces the disulfide bridge of the target proteins, thus contributing to the maintenance of the reducing intracellular environment. A schematic representation of the thioredoxin system is shown in Table 1.

Table 1: General scheme of the molecular components and reactions involved in the thioredoxin system

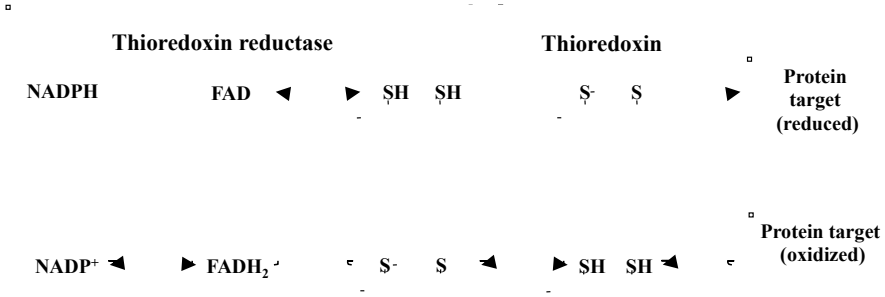

The thioredoxin system is often redundant in some eubacteria, because of the presence of more than one TrxA and/or TrxB.[29] This finding could be related to the necessity of specific TrxAs for different groups of target proteins; furthermore, the different TrxAs could interact with specific TrxBs or with the same TrxB. Redundancy of the thioredoxin system could also suggest the relevance of this reparative mechanism for the survival of the microorganism, a role becoming more crucial when the source is exposed to a prolonged oxidative stress.

1.3 *Scientific hypothesis and aim of the work*

This work reports a study on the thioredoxin system in *S. mutans* and *S. thermophilus*. Until now, the information on this antioxidant repairing system is limited to the annotation of the putative genes encoding TrxA and TrxB in these sources, with a certain gene redundancy either in *S. mutans* or *S. thermophilus*.[13,14] To assess the functionality and the role of the corresponding protein components, a biochemical investigation was carried on the purified recombinant forms of TrxA and TrxB obtained through the heterologous expression of the corresponding genes from these sources. The studies included measurements of the activity of all recombinant components either alone or in combination, evaluation of their thermophilicity and thermostability, as well as an assessment of the reversibility of the electron transfer within the thioredoxin components. All these investigations were carried out with the aim at the identification of the true TrxA and TrxB components from *S. mutans* and *S. thermophilus*, that positively interact in these sources for the reparation of the damages produced during an oxidative stress suffered from these streptococci.

2. Materials and methods

2.1 Chemicals, Enzymes, and Buffers

FAD, β–NADPH, β–$NADP^+$, 5,5'–dithiobis–2–nitrobenzoic acid (DTNB), dithiothreitol (DTT), β–mercaptoethanol, isopropyl–β–thiogalactopyranoside (IPTG) and a solution of human insulin (10 mg•mL^{-1}) were from Sigma–Aldrich. Restriction/modifying enzymes were from Promega or GE Healthcare. Plasmid pGEM–T Easy was Promega. Vectors pET–22b(+) and pET–28a(+) and the *E. coli* BL21(DE3) strain were from Novagen. The chromatographic medium Ni–NTA agarose was from Qiagen. Oligonucleotide synthesis and nucleotide sequencing was carried out at CEINGE, Italy. Synthesis of pET derivatives was carried out by GenScript, USA. HPLC–grade solvents were obtained from Carlo Erba. All other chemicals were of analytical grade.

The following buffers were used: buffer A, 20 mM Tris•Cl, pH 7.8; buffer B, 100 mM potassium phosphate, pH 7.8, 10 mM EDTA; buffer C, 20 mM Tris•Cl, pH 7.8, 150 mM KCl.

2.2 Engineering of vectors for thioredoxin and thioredoxin reductase genes in S. mutans *and* S. thermophilus

Transformation of bacterial strains, preparation of plasmids and other details of DNA recombinant technology were as previously described.[30] For the preparation of vectors producing

recombinant forms of the streptococcal thioredoxins and thioredoxin reductases, the corresponding genes annotated in the genome of *S. mutans* UA159 and *S. thermophilus* LMG 18311 were considered.[13,14] *S. mutans* UA159 contains two genes encoding putative thioredoxin reductases (*trxB* with ID: 1029596; *trxB2* with ID: 1029447) and three genes encoding putative thioredoxins (*trxA* with ID: 1029078; unnamed gene encoding a putative thioredoxin H1, hereafter called *trxH1*, with ID: 1029541; unnamed gene encoding a putative longer thioredoxin, hereafter called *trxL*, with I.D. 1028478).[13] A somehow lower redundancy exists in the genome of *S. thermophilus* LMG 18311, as it contains two genes for putative thioredoxin reductases (*trxB1* with ID: 3164148; *trxB2* with ID: 3165597) and two genes for putative thioredoxins (*trxA1* with ID: 3163813; *trxA2* with ID: 3164959).[14] The heterologous expression regarded all these genes, with the exclusion of the *trxB2* gene from either *S. mutans* or *S. thermophilus*, as explained in the Results section. The complete coding sequence of each gene was amplified by PCR, using the genomic DNA from *S. mutans* UA159 or *S. thermophilus* LMG 18311 as a template, and the couples of oligonucleotide primers reported in Table 2, annealing to the 5'– or 3'–untranslated region of the gene. Each PCR product was subcloned into the pGEM T–Easy plasmid and sequenced to confirm the identity with the corresponding gene. These recombinant plasmids were then digested with appropriate restriction endonucleases, to obtain appropriate DNA fragments for their cloning

into the prokaryotic expression vector pET–22b(+) or pET–28a(+). In particular, the pGEM T–Easy derivatives containing the amplified *trxA* and *trxH1* gene from *S. mutans*, or the amplified *trxB1*, *trxA1* and *trxA2* gene from *S. thermophilus* were digested with *Nde*I + *Xho*I; in the case of the plasmid containing the *trxB* gene from *S. mutans*, two separate digestions with *Nde*I + *Sac*II, and *Sac*II + *Xho*I allowed the obtainment of two consecutive DNA segments representing the entire *trxB* gene. After their purification on agarose gel, the *Nde*I→*Xho*I fragments were individually cloned into pET–22b(+), previously digested with *Nde*I and *Xho*I; for reconstructing the entire *trxB* gene from *S. mutans*, both *Nde*I→*Sac*II and *Sac*II→*Xho*I segments were cloned in the *Nde*I→*Xho*I fragment from pET–22b(+). For the remaining *trxL* gene from *S. mutans*, the corresponding pGEM T–Easy derivative was digested with *Nco*I + *Xho*I and the purified fragment cloned into pET–28a(+), previously digested with the same endonucleases. All the new constructs were controlled by nucleotide sequencing to exclude any undesired mutation occurring during the amplification/cloning procedure. These expression vectors were named v*Sm-trxB*, v*Sm-trxA*, v*Sm-trxH1*, v*Sm-trxL*, v*St-trxB1*, v*St-trxA1* and v*St-trxA2*, according to source of origin (*Sm* for *S. mutans* and *St* for *S. thermophilus*) and name assigned to each gene.

Table 2: Primers for the amplification of genes encoding the putative protein components of the thioredoxin system in *S. mutans* and *S. thermophilus*

Source	Gene	Primer [a]	
		Forward	Reverse
S. mutans	*trxB*	5'd–A_{-14}AGGAAAGTAACAT·*ATG*·TAC·GAT·ACA_{12}–3'	5'd–T_{925}TTCAAATCC·CTC·GAG·GTT·ATT·GAC·AAT·A_{897}–3'
	trxA	5'd–A_{-15}AGGAGAAATAACAT·*ATG*·ACA·AAA·GTA_{12}–3'	5'd–C_{325}CTGCTTATA·CTC·GAG·AAG·TTC·GGC·T_{300}–3'
	trxH1	5'd–A_{-15}TGAGGAGGATACAT·*ATG*·ATT·GTT·CCA·AAA_{15}–3'	5'd–T_{345}ATTATATGTAAAAA*CTC*GAG*TTT*CTC*CTC*TGT*TAA_{310}–3'
	trxL	5'd–T_{-17}TAAAAAGGAGATAGCC*ATG*GAA*AAG*GTT*ATT*T_{16}–3'	5'd–A_{579}GACGGGGAATTTAG·CTC·GAG·CAA·TTT·TTT·TAG_{547}–3'
S. thermophilus	*trxB1*	5'd–T_{-13}AAGGAGTTACAT·*ATG*·TAC·GAT·AC_{11}–3'	5'd–T_{931}CCATTTATG·CTC·GAG·ATC·ACC·AAG·TG_{905}–3'
	trxA1	5'd–A_{-14}GGAGGATAATCAT·*ATG*·ACA·AAA·GT_{11}–3'	5'd–C_{325}CATGATTAC·CTC·GAG·AAG·CTC·AGA_{301}–3'
	trxA2	5'd–G_{-14}AGGAGGAACACAT·*ATG*·ATT·ATT·CC_{11}–3'	5'd–T_{325}GGATTCTCC·CTC·GAG·TGT·TTC·CAA_{301}–3'

[a] Numbering begins from the starting codon shown in italics; underlined nucleotides indicate the mismatches introduced to create the cloning sites *Nde*I, *Nco*I or *Xho*I; dots in nucleotide sequence separate coding triplets.

2.3 Purification of recombinant forms of thioredoxin and thioredoxin reducatse from S. mutans *and* S. thermophilus

Transformants of the *E. coli* BL21(DE3) strain with the new engineered vectors were selected on LB–Agar plates containing ampicillin or kanamycin for pET–22b(+) or pET–28a(+) derivative, respectively. This expression system is under the control of the IPTG induction and allows the production of heterologous proteins fused to a His–tag; in particular, the C–terminal residue of each endogenous counterpart was replaced by the extrapeptide $LE(H)_6$; furthermore, in the heterologous product from v*Sm-trxL* a single amino acid substitution (Lys to Glu at amino acid position 2) was created by the engineering procedure. A previously described protocol for growth and induction of the transformants, and for purification of the heterologous products, was followed[31] with slight modifications. Indeed, each culture grew at 37°C up to 0.5 – 0.6 OD_{600} in 2 L of LB medium containing 0.1 mg mL^{-1} ampicillin or 0.06 mg mL^{-1} kanamycin. Upon the addition of 0.1 mg mL^{-1} IPTG, gene expression was induced at 37°C for 3 hours, with the exception of the v*Sm-trxB* or v*St-trxB1* transformant, where the induction time was limited to 2.5 hours. Bacterial cells were collected by centrifugation and resuspended in 20 mL buffer A and, immediately before cell lysis, 50 µM FAD was dissolved in cell suspensions from *vSm-trxB* or v*St-trxB1* transfortmant, in order to improve FAD incorporation into the flavoenzyme.[31] After cell lysis by French Press (Aminco), cellular

extracts were centrifuged at 30,000x*g* for 2 hour and supernatants (S–30) were used as starting materials for purification of the recombinant products. The His–tagged proteins were purified by Ni^{2+}–agarose affinity chromatography. To this aim, each S–30 (around 20 mL) was added in batch to 2 mL of Ni–NTA Agarose equilibrated in buffer A. After an overnight incubation, the slurry was poured in a column and the flow–through was discarded. Column was then extensively washed with 50 – 70 mL buffer A supplemented with 10 – 20 mM imidazole, in order to remove all unbound proteins. The heterologous products bound to the chromatographic medium were eluted with 20 mL buffer A supplemented with 200 mM imidazole and most of each recombinant enzyme eluted as a pure protein in few fractions, which were pooled together. After an eventual concentration step with Centricon (Aminco), each protein sample was dialysed against buffer A supplemented with 50% (v/v) glycerol and stored at –20°C. Under these conditions, the final yield for recombinant thioredoxin reductases or thioredoxins was nearly 3 – 10 mg or 5 – 15 mg from a 2–L culture, respectively.

2.4 Biochemical assays

Determination of the FAD amount bound to the purified samples of thioredoxin reductase was evaluated as previously reported.[31] In particular, measurements on the guanidinium chloride-denatured protein samples were realized on a Cary Eclipse

fluorescence spectrophotometer (Varian); the excitation and emission wavelengths were 375 nm and 528 nm, respectively. The FAD/flavoenzyme molar ratio was calculated after comparison with a FAD calibration curve.

Enzymatic assays for measuring the activity of the protein components of the thioredoxin system from *S. mutans* and *S. thermophilus* were carried out essentially as previously described in buffer B, using a Cary 1E spectrophotometer (Varian), equipped with an electronic temperature controller.[31,33] In particular, the activity of isolated thioredoxin reductase was followed by measuring its ability to reduce DTNB in the presence of NADPH as electron donor.[34] The absorbance increase at 412 nm due to TNB formation was followed kinetically, to determine the initial rate of the reaction. One unit (U) of activity was defined as the amount of enzyme that caused the conversion of 1 μmol DTNB in one min; the specific activity of thioredoxin reductase was expressed as U mg^{-1}. The activity of isolated thioredoxin was evaluated by its thiol–disulfide oxidoreductase activity in the presence of DTT as electron donor, and human insulin as substrate.[35] The reaction was followed kinetically by monitoring the increase in absorbance at 650 nm, due to precipitation of the reduced β–chain of insulin. The activity of thioredoxin was directly evaluated through the rate of insulin reduction, expressed as ΔA_{650} min^{-1}. To evaluate the combined activity of both protein components of the thioredoxin system, the assay mixture contained

thioredoxin and thioredoxin reductase, and used NADPH as electron donor and human insulin as substrate.[36,37] Also in this case the activity of the reconstituted thioredoxin system was evaluated through the rate of insulin reduction, expressed as ΔA_{650} min^{-1}.

In the complete thioredoxin system the reversibility of the thioredoxin reductase–mediated electron passage from the initial NADPH donor to the acceptor thioredoxin was evaluated in the absence of insulin and according to the following reaction scheme:

$$Trx–S_2 + NADPH + H^+ \leftrightarrows Trx–(SH)_2 + NADP^+$$

where $Trx–S_2$ and $Trx–(SH)_2$ are the oxidised and reduced form of thioredoxin, respectively[31]. The reaction was followed through the absorbance at 340 nm due to NADPH (ε_M = 6220 M^{-1} cm^{-1}). After an initial time–dependent decrease of the absorbance, indicating the NADPH consumption, the reaction reached the equilibrium and was then reverted upon the addition of a large excess of $NADP^+$. A new equilibrium was reached and the final concentrations of $Trx–(SH)_2$ or $Trx–S_2$ were derived from measurements of NADPH consumed or regenerated. These concentrations together with those of NADPH and $NADP^+$ allowed the calculation of the redox potential of the reaction according to the Nernst equation:

$$E^{0'}_{(Trx)} = E^{0'}_{(NADP+)} + RT/nF \ \ln [NADP^+] [Trx–(SH)_2]/[NADPH] [Trx–S_2]$$

using a value of – 0.324 V for $E^{0'}_{(NADP+)}$.[38]

The kinetic parameters K_M and V were calculated from Lineweaver–Burk plots drawn from measurements of the initial rate of the reaction in the presence of different substrate concentrations. The energy of activation was calculated from Arrhenius plots of the activity data.

2.5 Other methods

Thermal denaturation of the protein samples was followed by means of fluorescence measurements realised on Cary Eclipse fluorescence spectrophotometer (Varian), equipped with an electronic temperature controller, essentially as previously described.[31]

The mass spectrometry analysis was realised on protein samples desalted by RP–HPLC, as previously reported.[39,40] Protein concentration was determined by the method of Bradford,[41] using bovine serum albumin as standard. Protein purity was evaluated by SDS/PAGE according to standard protocols.[42] The quaternary structure of thioredoxin reductase was evaluated by gel filtration on a Superdex 75 10/300 GL column eluted with buffer C.

3. Results

3.1 Amino acid sequence analysis of the redundant components of the thioredoxin system in S. mutans *and* S. thermophilus

Redundancy of the genes encoding putative thioredoxin reductases or thioredoxins in the genome of *S. mutans* UA159[13] and *S. thermophilus* LMG 18311[14] was investigated. To this aim, the predicted amino acid sequence from the annotated genes was analysed in order to ascertain the presence of typical signatures for bacterial thioredoxin reductases or thioredoxins. Concerning the flavoenzyme, Table 3 reports the length of the deduced proteins, the presence of consensus motifs, and the homology with typical bacterial thioredoxin reductases.[27,43–45] The two gene products from either *S. mutans* or *S. thermophilus* have similar lengths (304 – 337 residues, corresponding to 33 – 37 kDa), in good agreement with that of the bacterial flavoenzyme. Moreover, all the predicted proteins have almost conserved sequence binding domains for NAD(P) and FAD.[44] On the other hand, the typical CXXC motif is present only in the gene products from *trxB* of *S. mutans* and *trxB1* of *S. thermophilus*, an indispensable requisite for the putative assignment as thioredoxin reductase.[27] To better discriminate in the membership to this family, a multiple alignment was realised in which each of the four gene products was aligned with five typical bacterial thioredoxin reductases, having a known 3D structure;[46–48] the number of identical

and similar residues obtained from these alignments is reported in Table 3. The most relevant finding is that the product of *trxB* from *S. mutans* or *trxB1* from *S. thermophilus* had a higher number of amino acid identities (56 or 54 residues, respectively), compared to that found with the *trxB2* gene products. Moreover, when the homology is evaluated from pairwise alignments within the *Streptococcus* genus, a high percentage of amino acid identities was obtained only when the product of *trxB* from *S. mutans* was aligned with that of *trxB1* from *S. thermophilus* (77.1 %) or in the alignment between the *trxB2* products from *S. mutans* and *S. thermophilus* (71.9 %); significantly lower values, ranging between 26.0 % and 27.1 %, were obtained in the other pairwise alignments within the *Streptococcus* genus. All these findings confirm that only the product of *trxB* from *S. mutans* or *trxB1* from *S. thermophilus* should belong to the family of thioredoxin reductases. Conversely, the gene products of *trxB2* from *S. mutans* and *S. thermophilus* could be better reassigned as putative ferredoxin NADP reductases, as also inferred from the homology with this class of enzymes. Therefore, the present study was focused on the products obtained from the expression vectors v*Sm-trxB* and v*St-trxB1* described in the Materials and Methods section; the corresponding purified heterologous proteins were called r*Sm*TrxB and r*St*TrxB1, respectively.

Table 3: Signatures for bacterial thioredoxin reductases in the putatively encoding genes from *S. mutans* and *S. thermophilus*

Source	Gene	Protein length (residues)	Consensus sequence [a]				Homology [c]	
			1st FAD-binding motif GXGXXGXXXAXXXXXXG	Cys motif CXXC	NAD(P)+–binding motif GXGXXAXXXAXXXXXXG	2nd FAD-binding motif [b] TXXXX*hyhh*GD	Identical residues	Similar residues [d]
S. mutans	*trxB*	304	8GSGPAGMTAALYAARSN	130CAVC	147GGGDSAVEEALFLTRFA	263TKVAGVFAIGD	56 (18.4%)	86 (28.3%)
S. mutans	*trxB2*	337	19GGGPVGLFTAFYAGLRG	none	167GGGDSAVDWANALDKIA	282TSQTGVFAIGD	33 (9.8%)	84 (24.9%)
S. thermophilus	*trxB1*	306	8GAGPAGMTAALYAARAN	130CAVC	147GGGDSAVEEGIYLTRFA	263TSVPGIFAIGD	54 (17.6%)	87 (28.4%)
S. thermophilus	*trxB2*	332	13GGGPVGLWAAFYAGLRG	none	161GGGDSAVDWANHLDGVA	276TSQEGVYAIGG	32 (9.6%)	84 (25.3%)

[a] Shadowed residues indicate accordance with the consensus.
[b] In this consensus sequence *h* or *y* represent hydrophobic or aromatic residues, respectively.
[c] Homology was evaluated through a multiple sequence alignment with the following thioredoxin reductases, with known 3D structure: *Campylobacter jejuni*, PDB 3R9U; *Deinococcus radiodurans*, PDB 2Q7V; *Escherichia coli*, PDB 1TDE; *Helicobacter pylori*, PDB 3ISH; *Mycobacterium tuberculosis*, PDB 2A87; the number of identical and similar residues among these five sequences was 62 and 97, respectively. Percentages indicated in brackets are referred to total residues of each protein.
[d] Conservative and semi-conservative substitutions.

Table 4 reports typical signatures for bacterial thioredoxins in terms of length, consensus motif and homology.[24,25,49,50] Concerning the length of the proteins deduced from the corresponding putative genes (three from *S. mutans* and two from *S. thermophilus*), four out of five proteins span 104 – 109 residues, corresponding to 11.5 – 12.8 kDa, the typical size of a bacterial thioredoxin. On the other hand, the longer *trxL* gene product of *S. mutans* spans 187 residues, corresponding to 20.9 kDa, a value outside of that usually found for a thioredoxin. The sequence of the thioredoxin family active site, including the absolutely required CXXC motif, is well conserved in the *trxA* and *trxL* product from *S. mutans*, as well as in the *trxA1* product from *S. thermophilus*; a lower conservation is found in the other gene products (*trxH1* from *S. mutans* and *trxA2* from *S. thermophilus*), mainly for the P→D replacement in the position immediately before the second cysteine of the motif.[25,49,50] For a better evaluation of the membership to the thioredoxin family, a multiple alignment was realised using the amino acid sequence of five typical bacterial thioredoxins with known 3D structure.[51–54] Interestingly, the products of *trxA* from *S. mutans* and *trxA1* form *S. thermophilus* has a significantly higher number of amino acid identities (28 residues) compared to that found in the other three gene products, including the longer one. However, taken together, all these findings do not allow any certain exclusion among the five gene products, even considering the thioredoxin redundancy already reported for other bacteria.[29] For

Table 4: Signatures for bacterial thioredoxins in the putatively encoding genes from *S. mutans* and *S. thermophilus*

Source	Gene	Protein length (residues)	Thioredoxin family active site [a]	Homology [b]	
				Identical residues	Similar residues [c]
S. mutans	*trxA*	104	20LVDFWATWCGPCLMQAPIL	28 (26.9%)	24 (23.1%)
S. mutans	*trxH1*	109	21VLFFTADWCSDCQFIYPAM	14 (12.8%)	32 (29.4%)
S. mutans	*trxL*	187	67YINVWATWCGPCMREIPDL	14 (7.5%)	30 (16.0%)
S. thermophilus	*trxA1*	104	20LIDFWATWCGPCLMQAPIL	28 (26.9%)	24 (23.1%)
S. thermophilus	*trxA2*	104	21VFFFTADWCPDCQFIYPVM	14 (12.8%)	29 (26.6%)

[a] As reported in the SwissProt Prosite Database (http://prosite.expasy.org/) under the accession number PDOC00172, the consensus sequence of the thioredoxin family active site is [LIVMF]-[LIVMSTA]-X-[LIVMFYC]-[FYWSTHE]-X(2)-[FYWGTN]-C-[GATPLVE]-[PHYWSTA]-C-{I}-X-{A}-X(3)-[LIVMFYWT]. Shadowed residues indicate accordance with the consensus. The Cys motif is underlined.

[b] Homology was evaluated through a multiple sequence alignment with the following Trxs, with known 3D structure: *Bacillus subtilis*, PDB 2GZZ; *Escherichia coli*, PDB 2TRX; *Mycobacterium tuberculosis*, PDB 2I1U; *Staphilococcus aureus*, PDB 2O7K; *Thermus thermophilus*, PDB 2YZU; the number of identical and similar residues among these five sequences was 30 and 30, respectively. Percentages indicated in brackets are referred to total residues of each protein.

[c] Conservative and semi-conservative substitutions.

these reasons, all the gene products were considered in the present study and the corresponding heterologous proteins were hereafter called r*Sm*TrxA, r*Sm*TrxH1, r*Sm*TrxL, r*St*TrxA1 and r*St*TrxA2, according to each gene name. At moment, all these recombinant proteins were obtained in a purified form, with the exception of r*Sm*TrxL.

3.2 Molecular properties of the streptococcal components of the thioredoxin system

The purified recombinant proteins putatively involved in the streptococcal thioredoxin system were analysed by SDS/PAGE (Fig. 1); in particular, the electrophoretic mobility of the macromolecules from *S. mutans* or *S. thermophilus* is shown in Figs. 1A or 1B, respectively. All the protein samples were homogenous and their mobilities were in agreement with the size deduced from the amino acid sequence. In particular, the apparent mass of both r*Sm*TrxB (Fig. 1A) or r*St*TrxB1 (Fig. 1B) was 35 kDa, corresponding to that of a monomer of the flavoenzyme. On the other hand, the mass value measured for both r*Sm*TrxA and r*Sm*TrxH1 (Fig. 1A), as well as for r*St*TrxA1 (Fig. 1B) was 12 kDa, whereas a smaller mass value of 10.5 kDa was measured for r*St*TrxA2 (Fig. 1B). However, these values were in a sufficient agreement with those expected from the size of these recombinant thioredoxins.

The mass of the recombinant proteins was also analysed by ESI/Q–TOF mass spectrometry. In all protein samples this investigation confirmed a good coincidence of the experimental M_r with the theoretical value deduced form the amino acid sequence, including His-tag and disulfide bridge within the Cys motif. Furthermore, the analysis revealed if the initial methionine was conserved in each recombinant protein and if the macromolecules were targets of any covalent adduct, as sometimes observed in proteins involved in the control of the redox homeostasis.[33,40,55] The results obtained indicated that only r*Sm*TrxA and r*St*TrxA1 did not contain the initial methionine, and that a sodium adduct was present in the r*Sm*TrxB sample.

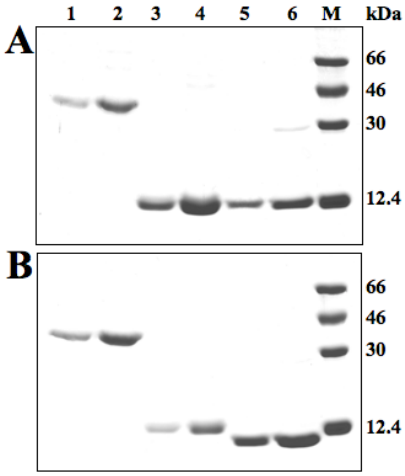

Fig. 1 SDS-PAGE of purified recombinant forms of putative thioredoxins and thioredoxin reductases from the *Streptococcus* genus. Increasing amounts of the purified proteins samples were analysed on a 14% polyacrylamide gel. Migration of molecular mass protein standards (*lane* M) is reported on the right. **A** Proteins from

S. mutans. 2 and 5 µg of r*Sm*TrxB (*lanes* 1 and 2), r*Sm*TrxA (*lanes* 3 and 4) and r*Sm*TrxH1 (*lanes* 5 and 6). **B** Proteins from *S. thermophilus*. 2 and 5 µg of r*St*TrxB1 (*lanes* 1 and 2), r*St*TrxA1 (*lanes* 3 and 4) and r*St*TrxA2 (*lanes* 5 and 6).

The M_r of r*Sm*TrxB and r*St*TrxB1 was also determined by gel–filtration chromatography under native conditions. Both proteins eluted as a single peak with an apparent molecular mass of 62 kDa or 67 kDa for r*Sm*TrxB or r*St*TrxB1, respectively; these data suggest that both thioredoxin reductases should have the expected homodimeric organisation (theoretical mass, 68 kDa).

The FAD content of both r*Sm*TrxB and r*St*TrxB1 was measured and the calculated content of the coenzyme in various r*Sm*TrxB samples ranged between 0.80 and 0.92 mol FAD/mol enzyme subunit, whereas the corresponding values for r*St*TrxB1 were in the range 0.95 – 0.99. It is worth mentioning that the addition of exogenous FAD during production of the recombinant flavoenzymes was crucial for reaching an almost stoichiometric FAD/flavoenzyme ratio and hence for the functionality of the thioredoxin reductase.[31] In the following biochemical assays the activity of each streptococcal thioredoxin reductase was referred to its specific FAD content.

3.3 Activity of the streptococcal thioredoxin components

In order to assess the functionality of the thioredoxin system in *S. mutans* and *S. thermophilus*, specific biochemical assays were carried out for the corresponding recombinant components either alone or in combination, as well as by studying the reversibility of the

electron passage between them. The activity of r*Sm*TrxB and r*St*TrxB1 alone was evaluated through the DTNB reduction assay in the presence of NADPH as electron donor. Both enzymes were able to reduce the synthetic substrate DTNB and their activity depended on the flavoenzyme concentration. Lineweaver-Burk plots of this activity at 37°C allowed the determination of the kinetic parameters K_M and V for both flavoenzymes (Fig. 2). In particular, the K_M for the synthetic substrate DTNB was 0.89 mM for r*Sm*TrxB and 1.25 mM for r*St*TrxB1, whereas the corresponding V values were 0.60 U mg^{-1} and 0.91 U mg^{-1}, respectively. These data indicate that the recombinant forms of the streptococcal flavoenzymes were obtained in their active form. Upon conversion of V into a k_{cat} value (0.68 s^{-1} for r*Sm*TrxB and 1.03 s^{-1} for r*St*TrxB1), the catalytic efficiency at 37°C of the streptococcal flavoenzymes, evaluated through the k_{cat}/K_M ratio, was 0.76 s^{-1} mM^{-1} and 0.82 s^{-1} mM^{-1} for r*Sm*TrxB and r*St*TrxB1, respectively. These values were somehow lower when compared with the corresponding data from aerobic sources, mainly because of the lower k_{cat} values possessed by the streptococcal flavoenzymes. For instance, the higher k_{cat}/K_M ratios reported for the catalytic efficiency of thioredoxin reductase from the aerobic psychrophile *Pseudoalteromonas haloplanktis* in the 10 – 30°C interval (from 2.72 to 5.04 s^{-1} mM^{-1}) were essentially due to significantly higher k_{cat} values (from 3.78 to 8.10 s^{-1}), whereas the K_M remained almost

constant in the whole temperature interval (1.01 – 2.33 mM) and almost similar to that measured for the streptococcal flavoenzymes.[31]

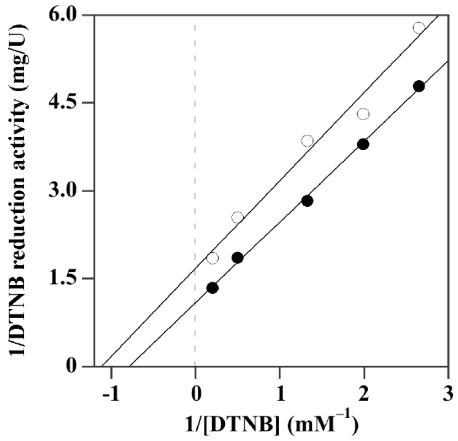

Fig. 2 Lineweaver–Burk plots of the DTNB reduction activity sustained by the streptococcal thioredoxin reductases. The reaction mixture contained 200 µM NADPH, 0.45 µM r*Sm*TrxB (○) or *St*TrxB1 (●) and the indicated concentrations of DTNB in 1 mL final volume of buffer B. The reaction started at 37°C with the addition of NADPH and was followed kinetically through the absorbance at 412 nm. The specific activity was expressed as U mg^{-1} and was calculated through the ΔA_{412} s^{-1} values, corresponding to the initial rates of the reaction.

The activity of the recombinant thioredoxins from *S. mutans* or *S. thermophilus* was evaluated through the insulin precipitation assay in the presence of DTT as electron donor. The behaviour of the putative thioredoxins from *S. mutans* and *S. thermophilus* in this assay is shown in Figs. 3A and 3B, respectively. The data show that r*Sm*TrxA accelerates the rate of insulin reduction at 37°C in a dose-dependent manner and that the lag phase from insulin precipitation progressively decreases with the r*Sm*TrxA concentration; on the other

hand, r*Sm*TrxH1 is absolutely unable to promote the insulin precipitation, even when present at high concentration (Fig. 3A). Similarly, among r*St*TrxA1 and r*St*TrxA2, only the first one is active in the insulin precipitation assay (Fig. 3B). From the comparison of the lag phases observed for the onset of the reaction, it appears that insulin precipitation starts earlier with r*Sm*TrxA (Fig. 3A) than with r*St*TrxA1 (Fig. 3B).

For a better evaluation of the functionality of the active streptococcal thioredoxins, the r*Sm*TrxA or r*St*TrxA1 concentration leading to half maximum activity was calculated from a double reciprocal plot where the rate of insulin precipitation measured in the linear increase of the absorbance at 650 nm was analysed as a function of thioredoxin concentration (Fig. 4). Similar values were obtained for the thioredoxin concentration leading to half maximum activity, namely 3.0 µM for r*Sm*TrxA and 2.3 µM for r*St*TrxA1. These data, even similar to those already reported for the thioredoxin from the aerobic psychrophile *P. haloplanktis*,[33] indicate that r*Sm*TrxA and r*St*TrxA1 are active in the electron passage from the donor DTT to the final synthetic acceptor human insulin.

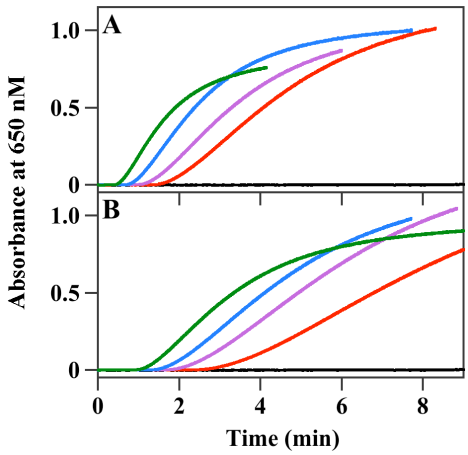

Fig. 3 Insulin precipitation promoted by streptococcal thioredoxins. The reaction mixture contained 200 µM DTT, 0.79 mg mL^{-1} human insulin and various dilutions of the thioredoxin samples in 700 µL final volume of buffer B. The reaction started at 37°C with the addition of DTT and was followed kinetically through the absorbance at 650 nm, due to insulin precipitation. **A** Analysis of thioredoxins from *S. mutans*. Insulin reduction curves obtained without thioredoxin (black line) or with a r*Sm*TrxA concentration equal to 2.06 µM (red line), 2.94 µM (purple line), 5.14 µM (blue line), or 10.3 µM (green line). The curve obtained with 9.9 µM r*Sm*TrxH1 was superimposable with that without thioredoxin. **B** Analysis of thioredoxins from *S. thermophilus*. Same conditions as in A with the exception that the r*St*TrxA1 concentration was 1.95 µM (red line), 3.00 µM (purple line), 4.88 µM (blue line), or 9.75 µM (green line). The curve obtained with 10.2 µM r*St*TrxA2 was superimposable with that without thioredoxin.

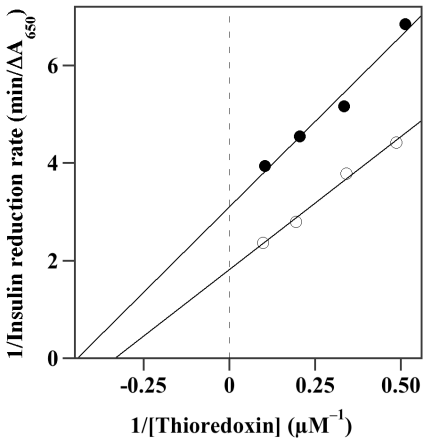

Fig. 4 Affinity of the streptococcal thioredoxins for the thiol-disulfide oxidoreductase activity. The rate of insulin precipitation, evaluated through the ΔA_{650} min^{-1} value measured in the linear increase of the absorbance of each curve reported in Fig. 3, was plotted versus the r*Sm*TrxA (○) or r*St*TrxA1 (●) concentration in a double reciprocal plot.

3.4 Reconstitution of the streptococcal thioredoxin system

The availability of the corresponding components allowed an *in vitro* reconstitution of the streptococcal thioredoxin system. To this aim, the combined activity of the involved proteins was measured at 37°C with the insulin reduction assay, which in this case contained one thioredoxin reductase, one thioredoxin, NADPH and human insulin. The data reported in Fig. 5 describe the features of thioredoxin systems realised through the combination of mixed components within the *Streptococcus* genus. In particular, in the presence of r*Sm*TrxB, the rate of insulin precipitation increases with the concentration of either the autologous r*Sm*TrxA (Fig. 5A) or the

heterologous r*St*TrxA1 (Fig. 5B), whereas r*Sm*TrxH1 (Fig. 5A) or r*St*TrxA2 (Fig. 5B) are unable to promote the insulin reduction.

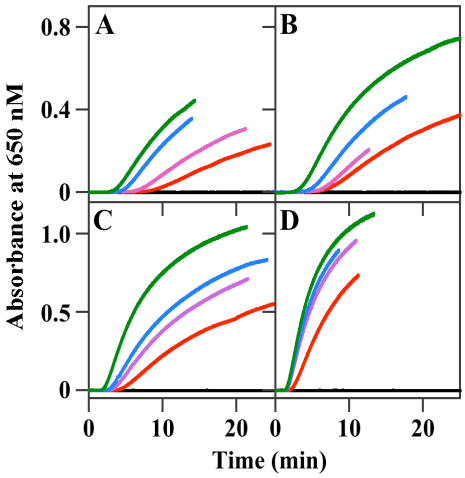

Fig. 5 Reconstitution of the streptococcal thioredoxin system. The reaction mixture contained 202 µM NADPH, 0.79 mg mL^{-1} human insulin and various combinations of thioredoxin and thioredoxin reductase in 700 µL final volume of buffer B. The reaction started at 37°C with the addition of NADPH and was followed kinetically through the increase of the absorbance at 650 nm, due to insulin precipitation. **A** Combination of r*Sm*TrxB with thioredoxins from *S. mutans*. Insulin reduction curves obtained in the presence of 1.03 µM r*Sm*TrxB without thioredoxin (black line) or with a r*Sm*TrxA concentration equal to 1.03 µM (red line), 2.06 µM (purple line), 5.14 µM (blue line), or 10.3 µM (green line). The curve obtained with 9.9 µM r*Sm*TrxH1 was superimposable with that without thioredoxin. **B** Combination of r*Sm*TrxB with thioredoxins from *S. thermophilus*. Same conditions as in A with the exception that the r*St*TrxA1 concentration was 4.95 µM (red line), 7.50 µM (purple line), 12.0 µM (blue line), or 49.9 µM (green line). The curve obtained with 10.2 µM r*St*TrxA2 was superimposable with that without thioredoxin. **C** Combination of r*St*TrxB1 with thioredoxins from *S. thermophilus*. Insulin reduction curves obtained in the presence of 1.03 µM r*St*TrxB1 without thioredoxin (black line) or with a r*St*TrxA1 concentration equal to 0.98 µM (red line), 1.95 µM (purple line), 4.13 µM (blue line), or 9.75 µM (green line). The curve obtained with 10.2 µM r*St*TrxA2 was superimposable with that without thioredoxin. **D** Combination of r*St*TrxB1 with thioredoxins from *S. mutans*. Same conditions as in C with the exception that the r*Sm*TrxA concentration was 1.10 µM (red line), 5.00

μM (purple line), 7.50 μM (blue line), or 12.5 μM (green line). The curve obtained with 9.9 μM r*Sm*TrxH1 was superimposable with that without thioredoxin.

Similarly, in the presence of r*St*TrxB1, either the autologous r*St*TrxA1 (Fig. 5C) or the heterologous r*Sm*TrxA (Fig. 5D) promote the insulin reduction, whereas no activity is observed with r*St*TrxA2 (Fig. 5C) or r*Sm*TrxH1 (Fig. 5D). Also in this case, from the comparison of the lag phases observed for the onset of the reaction, insulin precipitation starts earlier in the presence of r*Sm*TrxA, especially when in combination with r*St*TrxB1 (Fig. 5D). All these findings indicate that a streptococcal thioredoxin system was efficiently reconstituted *in vitro*, because the combination of specific protein components allowed the electron transfer from the initial donor NADPH to the final acceptor insulin. In particular, the positive interaction between r*Sm*TrxB and either r*Sm*TrxA or r*St*TrxA1, and similarly between r*St*TrxB1 and either r*St*TrxA1 or r*Sm*TrxA indicates that the streptococcal thioredoxin system functions with mixed components within the *Streptococcus* genus. The missing activity of r*Sm*TrxH1 and r*St*TrxA2 also in a reconstituted thioredoxin assay suggests that these molecules cannot be considered as redundant forms of thioredoxin in *S. mutans* and *S. thermophilus*, respectively.

In order to evaluate the affinity of thioredoxin reductases for the active thioredoxins in the reconstituted thioredoxin system, the r*Sm*TrxA and r*St*TrxA1 concentration leading to half maximum activity was calculated from double reciprocal plots (Fig. 6). Indeed, the values obtained in the presence of r*Sm*TrxB were 3.0 μM for

r*Sm*TrxA and 12.0 µM for r*St*TrxA1 (Fig. 6A); those calculated in the presence of r*St*TrxB1 were 1.2 µM for r*Sm*TrxA and 2.6 µM for r*St*TrxA1 (Fig. 6B). All these values, roughly similar to those obtained when assaying the activity of thioredoxin alone, were of the same order of magnitude of those reported for thioredoxin systems from aerobic sources.[33,56,57] Moreover, the data confirm the interchangeability between thioredoxin components from *S. mutans* or *S. thermophilus*, and probably suggest that the *S. mutans* tioredoxin has a higher affinity towards both thioredoxin reductases.

The reversibility of the electron passage is another useful parameter for validating the direct interaction between the molecular components of the thioredoxin system. This biochemical property was investigated at 25°C through a reconstituted assay, where the combined activity of autologous or mixed components of the thioredoxin system was evaluated in the absence of human insulin (Fig. 7).

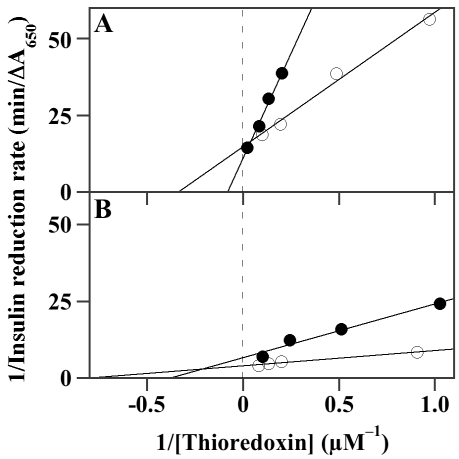

Fig. 6 Affinity of the streptococcal thioredoxins in the reconstituted thioredoxin system. The rate of insulin precipitation, evaluated through the ΔA_{650} min^{-1} value measured in the linear increase of the absorbance of each curve reported in Fig. 5, was plotted versus the thioredoxin concentration in a double reciprocal plot. **A** Combined presence of r*Sm*TrxB with r*Sm*TrxA (○) or r*St*TrxA1 (●). **B** Combined presence of r*St*TrxB1 with r*Sm*TrxA (○) or r*St*TrxA1 (●).

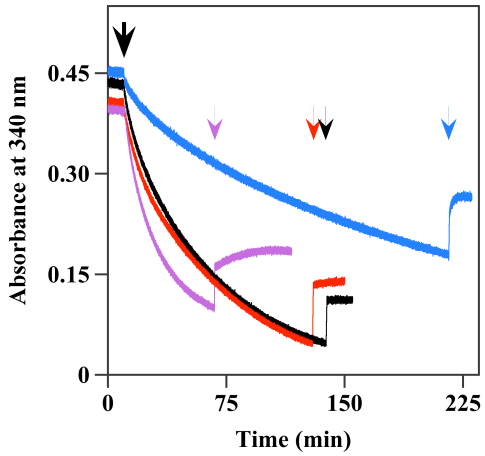

Fig. 7 Reversibility of the electron passage from NADPH to thioredoxin in reconstituted streptococcal thioredoxin systems. The reaction mixture contained 55 μM NADPH and 15.4 μM r*Sm*TrxA (black and purple lines) or 15.7 μM r*St*TrxA1 (red and blue lines) in 1 mL final volume of buffer B. A first addition of

50.4 nM r*Sm*TrxB (black and blue lines) or 50.7 nM r*St*TrxB1 (red and purple lines) provoked the NADPH consumption, and a second addition of 1050 μM $NADP^+$ (all lines) allowed its reformation (1^{st} or 2^{nd} addition indicated by a bold or a coloured arrow, respectively). The reaction, carried out at 25°C, was continuously monitored by the absorbance at 340 nM due to NADPH. When the reaction reached the final equilibrium, the concentration of reduced thioredoxin, oxidised thioredoxin and NADPH was calculated through the amount of NADPH reformed after its consumption, whereas the $NADP^+$ concentration was assumed to remain 1050 μM. For calculation, the reported A_{340} values were corrected for dilution or the overlapping absorption by the $NADP^+$ spectrum.

The initial NADPH consumption, observed in the first step of the reaction after the addition of thioredoxin reductase, is followed by the reformation of this coenzyme, when an excess of the oxidised form $NADP^+$ is added in the reaction mixture. Therefore, the new equilibria reached between oxidised and reduced components in the autologous and mixed streptococcal thioredoxin systems indicate that the thioredoxin reductase–mediated electron passage from NADPH to thioredoxin is fully reversible. The equilibrium concentrations of reagents and products measured from the data of Fig. 7 allow the calculation of the corresponding redox potentials. In particular, the reaction in the autologous systems of *S. mutans* or *S. thermophilus* proceeds at a very similar rate and the calculated $E^{0'}_{(Trx)}$ value is – 0.221 V or – 0.258 V for the autologous system from *S. mutans* or *S. thermophilus*, respectively. These findings indicate that the autologous system from *S. thermophilus* is endowed with a reducing power higher than that of *S. mutans*. Furthermore, the redox potential of the *S. thermophilus* system approaches that reported for some aerobic sources, such as the psychrophile *P. haloplanktis* (– 0.276 V),[31] the

mesophile *E. coli* (– 0.270 V),[58] or the hyperthermophile *Aeropyrum pernix* (– 0.262 V).[57] A reversible electron passage takes place also in mixed thioredoxin systems, containing r*Sm*TrxB plus r*St*TrxA1 or r*St*TrxB1 plus r*Sm*TrxA; however, in the former case the overall reaction proceeds at a significantly slower rate compared to the autologous systems, whereas in the other case the reaction is even slightly faster (Fig. 7). In the system containing r*Sm*TrxB plus r*St*TrxA1, the calcutated $E^{0'}_{(Trx)}$ is – 0.263 V, whereas in that containing r*St*TrxB1 plus r*Sm*TrxA the $E^{0'}_{(Trx)}$ is – 0.258 V, both values approaching that determined for the autologous system from *S. thermophilus*. These results confirm that the presence of one component from *S. thermophilus* is sufficient in producing a reducing power of the streptococcal thioredoxin system higher than that obtained in the presence of the autologous components from *S. mutans*.

3.5 Effect of temperature on the streptococcal thioredoxin reductases

The study of the effect of temperature on components of the thioredoxin system in *Streptococcus* was focused on thioredoxin reductase. To study the temperature dependence of the activity sustained by r*Sm*TrxB or r*St*TrxB1, the DTNB reduction assay was carried out at various temperatures ranging between 15°C and 45°C. The values of specific activity measured for each flavoenzyme were

reported as a function of temperature and shown in Fig. 8. Only the activity of r*St*TrxB1 moderately increases with temperature, whereas that of r*Sm*TrxB remains approximately constant up to 37°C and then slightly decreases above this temperature. Therefore, only the data of r*St*TrxB1 can be treated according to the Arrhenius equation to determine the energy of activation (E_a) of the oxidoreductase reaction (inset in Fig. 8).

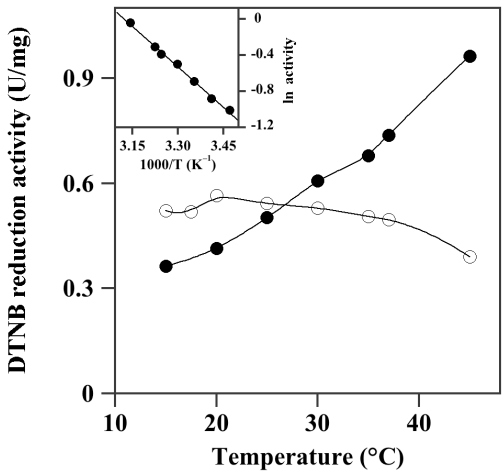

Fig. 8 Effect of temperature on the DTNB reduction activity catalysed by streptococcal thioredoxin reductases. The reaction mixture, containing 209 μM NADPH and 5 mM DTNB in 1 mL final volume of buffer B, was carried out at the indicated temperature in the absence or in the presence of two different concentrations (0.016 or 0.022 mg mL^{-1}) of r*Sm*TrxB or r*St*TrxB1. The reaction started with the addition of NADPH and was followed kinetically through the absorbance at 412 nm. The reported values of specific activity were averaged from the initial rates of the reaction obtained at the different concentrations of r*Sm*TrxB or r*St*TrxB1. Blanks in the absence of any thioredoxin reductase were subtracted. The inset reports the analysis of the specific activity values measured for r*St*TrxB1 according to the Arrhenius equation.

The low E_a value of 25.1 kJ mol^{-1} points to a poor thermophilicity for r*St*TrxB1; curiously, the psychrophilic thioredoxin reductase from *P. haloplanktis* possessed a higher E_a value, ranging between 30.3 and 30.9 kJ mol^{-1}.[31,33] Concerning the unusual lack of thermodependence for r*Sm*TrxB, no clear-cut explanation exists for such a behaviour. Indeed, the finding that the activity remains approximately constant over a large temperature interval should exclude a heat inactivation of the *S. mutans* enzyme up to 37°C. To better address this point and to evaluate the heat resistance of r*Sm*TrxB and r*St*TrxB1, samples of each flavoenzyme were incubated for 10 min at different temperatures and the residual activity of the treated samples was then measured by the DTNB reduction assay and reported as a function of the treatment temperature (Fig. 9). The half–inactivation temperature of the flavoenzymes calculated from their heat inactivation profiles is 53°C for r*Sm*TrxB and 60°C for r*St*TrxB1. These data indicate that the *S. thermophilus* flavoenzyme is more heat resistant than the *S. mutans* counterpart and exclude that the lack of thermodependence found in the activity of r*Sm*TrxB analysed in the 15–37°C interval is due to a measurable heat inactivation of the flavoenzyme.

The heat stability of the flavoenzymes was also analysed by thermal denaturation profiles obtained through fluorescence measurements (Fig. 10). The melting temperature calculated for the

flavoenzymes is 52°C for r*Sm*TrxB and 64°C for r*St*TrxB1. These values are similar to those obtained from the heat inactivation profiles.

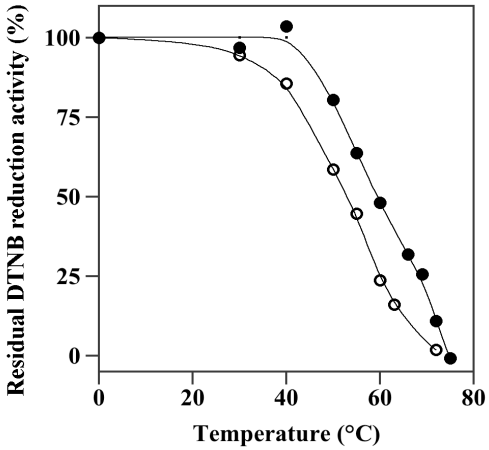

Fig. 9 Heat inactivation profiles of the streptococcal thioredoxin reductases. Aliquots (110 µL) from a 0.3 mg mL^{-1} solution of r*Sm*TrxB (○) or r*St*TrxB1 (●) in buffer B were incubated for 10 min at the indicated temperatures. After the treatment, the samples were immediately chilled on ice for at least 30 min. The residual activity of 50–µL aliquots form the various r*Sm*TrxB or r*St*TrxB1 samples was measured in duplicates through the DTNB reduction assay, carried out at 37°C, essentially as indicated in Fig. 8. The activity of an untreated aliquot kept at 0°C was considered as 100% activity.

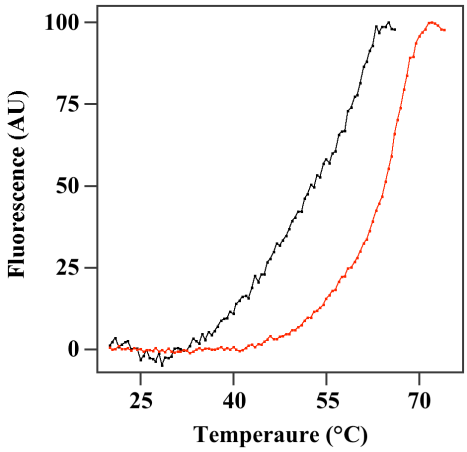

Fig. 10 Fluorescence melting curves of the streptococcal thioredoxin reductases. A solution containing 0.13 mg mL^{-1} r*Sm*TrxB (black line) or r*St*TrxB1 (red line) in buffer B was placed in a 500–µL stoppered fluorescence cuvette. Measurements were realised on a Cary Eclipse fluorescence spectrophotometer (Varian), equipped with an electronic temperature controller. Excitation and emission wavelengths were 280 and 335 nm, respectively; excitation and emission slits of 10 nm were used. The increase in temperature was set at 0.2°C min^{-1} and emission was recorded at every 0.5°C increase. Fluorescence values were corrected for the temperature–dependent quenching and expressed as arbitrary units (AU).

4. Discussion

The characterization of the thioredoxin system in *S. mutans* and *S. thermophilus* was realised with the aim at investigating how functions the enzymatic mechanism for the preservation of the reduced state of intracellular proteins in two representative members of the *Streptococcus* genus. Indeed, the facultative anaeorobic metabolism of streptococci implies an oxygen tolerance of these species in their specific habitats; as a consequence, the functionality of the enzyme systems involved in prevention/repair of the oxidative damages occurring during ROS exposure assumes great relevance for the survival of these microaerophiles. Previous works showed that the early ROS defence in *Streptococcus* is provided by the cambialistic character of SOD, implying a regulation of its activity, indispensable for the adaptive response of the microbial sources to oxidant insults.[22,23] The greater regulation of the activity found in SOD from *S. mutans* compared to the *S. thermophilus* enzyme was explained with the observation that *S. mutans*, living in the ecological niche of the oral cavity, is probably more adapted than *S. thermophilus* to prolonged oxidative stress conditions.

The characterization of the thioredoxin system in *S. mutans* and *S. thermophilus* sheds light on a key repair mechanism of ROS damages on cellular proteins. The study was first approached with the identification and assessment of the functionality of its protein components. The analysis of the typical signatures for thioredoxin

reductase allowed the exclusion of a putative *trxB2* gene from both streptococci, because the required Cys motif was absent in the deduced amino acid sequence. The other putative thioredoxin reductase genes (*trxB* in *S. mutans* and *trxB1* in *S. thermophilus*) were expressed and their recombinant products were found to be fully active in a typical thioredoxin reductase assay. The flavoenzymes had the typical affinity for the synthetic substrate DTNB, although their catalytic efficiencies were lower compared with the values found in the analogous enzyme from aerobic bacteria. This finding could be related to the lower exposure to oxidant insults that these facultative anaerobic species tolerate compared to aerobic bacteria. Concerning thioredoxins, the gene products of *trxA* from *S. mutans* and *trxA1* from *S. thermophilus* were endowed with the typical thioredoxin activity, as proved by the insulin reduction assay; moreover, the affinity of these enzymes for the reaction was similar to that typically found in aerobic microbial sources. On the other hand, the lack of activity in the *trxH1* and *trxA2* gene products from *S. mutans* and *S. thermophilus*, respectively, indicated that these proteins cannot be considered as functional thioredoxins. This finding is probably related to a different CXXC motif in r*Sm*TrxH1 and r*St*TrxA2, because the second X of the motif, a proline in r*Sm*TrxA and r*St*TrxA1 as usually found in typical thioredoxins, is instead occupied by aspartate. The proline substitution in r*Sm*TrxH1 and r*St*TrxA2 could impair the reversible formation of the disulfide bridge within the Cys loop required for the thioredoxin

activity, as also hypothesized by mutagenic studies on the *E. coli* thioredoxin.[58] Another question related to a possible thioredoxin redundancy is the presence of a putative longer thioredoxin gene, called *trxL*, in the *S. mutans* genome. The size of its corresponding protein would be outside of that usually found in bacterial thioredoxin; on the other hand, the sequence of its Cys motif is identical to that present in the functional thioredoxins r*Sm*TrxA and r*St*TrxA1. Unfortunately, the corresponding gene product was not obtained yet, and its possible functioning as thioredoxin cannot be excluded. In conclusion, the functional thioredoxin components obtained from *S. mutans* and *S. thermophilus* are limited to one thioredoxin reductase (r*Sm*TrxB and r*St*TrxB1, respectively) and one thioredoxin (r*Sm*TrxA and r*St*TrxA1, respectively); at moment, a redundancy in the thioredoxin components can be excluded only for *S. thermophilus*.

The characterization of the streptococcal thioredoxin system also included its *in vitro* reconstitution with the usage of the purified active recombinant components. The results obtained indicate that a functional thioredoxin system was reconstituted with the usage of either autologous or mixed components within the *Streptococcus* genus. Indeed, the thioredoxin reductase from *S. mutans* positively interacted either with the autologous thioredoxin or with the corresponding enzyme from *S. thermophilus*; a similar positive interaction existed between thioredoxin reductase from *S.*

thermophilus and the autologous/heterologous thioredoxin. The functionality and interchangeability between streptococcal components was also confirmed by the affinity values determined for the autologous and mixed systems, similar to those reported for thioredoxin systems from aerobic sources.[33,56,57] However, the data suggest a moderate higher affinity of both thioredoxin reductases for r*Sm*TrxA and a faster onset of its reactivity, compared to r*St*TrxA1, a behaviour confirmed also with the studies on the reversibility of the electron passage from NADPH to thioredoxin. Indeed, this latter investigation was another proof of the efficient reconstitution of the streptococcal thioredoxin system; moreover, it allowed the calculation of the redox potential of autologous and mixed systems. The reducing power measured for the autologous *S. thermophilus* system approached that reported for aerobic sources belonging to bacterial or archaeal kingdom and adapted from low to hot temperatures;[31,57,58] on the other hand, the autologous system of *S. mutans* possessed a significantly lower value. These finding could suggest a somehow different adaptation of these facultative anaerobes in the mechanism involved in keeping the reduced state of cytosolic proteins: in *S. thermophilus* a reducing power similar to that observed in aerobic sources is required, whereas in *S. mutans* a lower value is probably sufficient. When analysing the redox potential of mixed systems containing an *S. thermophilus* component, either thioredoxin or thioredoxin reductase, and the other component from *S. mutans*, the

measured value approached that obtained in the autologous *S. thermophilus* system. We could speculate that the faster reactivity of r*Sm*TrxA, together with its moderately higher affinity for both thioredoxin reductases, could compensate for a low reactivity of r*Sm*TrxB, thus leading to the high reducing power of the mixed thioredoxin systems.

Finally, the characterization of the thioredoxin system in *Streptococcus* included the study of the effect on temperature on the activity and stability of thioredoxin reductases. The study of the temperature–dependence of the activity showed for the *S. thermophilus* enzyme a moderate increase of the activity with temperature, as better evaluated by its low value of the energy of activation. The low thermophilicity of r*St*TrxB1 is a curious property for an enzyme isolated from *S. thermophilus*, adapted to tolerate moderate thermal treatments. The modest effect of temperature on the activity even disappeared for the *S. mutans* enzyme, whose activity remained almost constant over a large temperature interval. The lack of thermodependence of the activity of r*Sm*TrxB was not caused by an inactivation process, which for the *S. mutans* enzyme occurred at more elevated temperatures. Among the possible explanations, a differential effect of temperature on the large conformational changes of the flavoenzyme during its activity, and on the affinity for the substrate, cannot be excluded. The heat stability of the streptococcal flavoenzymes was evaluated by heat inactivation and denaturation

profiles. In both experiments r*St*TrxB1 resulted significantly more heat resistant than r*Sm*TrxB, which however possessed a discrete heat resistance. The similarity between half–inactivation and half–denaturation temperatures indicates that heat inactivation and heat denaturation are concomitant processes for both flavoenzymes.

Conclusions

In conclusion, our data prove the existence of a functioning thioredoxin system in two representative members of the *Streptococcus* genus, thus indicating that this key mechanism for the preservation of the reduced state of cytosolic proteins is present also in these facultative anaerobes. The results also showed that the direct interaction between the streptococcal protein components of the thioredoxin system could involve mixed factors from *S. mutans* and *S. thermophilus*, a behaviour confirming the close taxonomic relationship between these microaerophiles, in spite of their different role towards the human health.

References

1. R. Facklam, What happened to the Streptococci: overview of taxonomic and nomenclature changes, *Clin. Microbiol. Rev.*, 2002, **15**, 613–630.
2. B. Poolman, Energy transduction in lactic acid bacteria, *FEMS Microbiol. Rev.*, 1993, **12**, 125–147.
3. T. J. Mitchell, The pathogenesis of streptococcal infections: from tooth decay to meningitis, *Nat. Rev. Microbiol.* 2003, **1**, 219–230.
4. H. Tettelin, Streptococcal genomes provide food for thought, *Nat. Biotechnol.*, 2004, **22**, 1523–1524.
5. S. Hamada, H. D. Slade, Biology, immunology, and cariogenicity of *Streptococcus mutans*, *Microbiol. Rev.*, 1980, **44**, 331–384.
6. W. J. Loesche, Role of *Streptococcus mutans* in human dental decay, *Microbiol. Rev.*, 1986, **50**, 353–380.
7. P. Hols, F. Hancy, L. Fontaine, B. Grossiord, D. Prozzi, N. Leblond-Bourget, B. Decaris, A. Bolotin, C. Delorme, S. Dusko Ehrlich, E. Guedon, V. Monnet, P. Renault, M. Kleerebezem, New insights in the molecular biology and physiology of *Streptococcus thermophilus* revealed by comparative genomics. *FEMS Microbiol. Rev.*, 2005, **29**, 435–463.
8. C. Delorme, Safety assessment of dairy microorganisms: *Streptococcus thermophilus*, *Int. J. Food Microbiol.*, 2008, **126**, 274–277.
9. R. K. Thunell, W. E. Sandine, In: *Bacterial starter culture for foods*, S. E. Gilliland, ed., CRC Press Inc., Boca Raton, Fla, 1985, pp. 127–144.
10. P. F. Fox, *Cheese: chemistry, physics and microbiology*, Chapman & Hall, London, 1993.
11. A. Y. Tamime, H. C. Deeth, Yogurt: technology and biochemistry, *J. Food Protect.*, 1980, **43**, 939–977.
12. M. I. Dolin, Cytochrome-independent electron transport enzymes of bacteria, In: *The Bacteria*, I. C. Gunsalus and R. Y. Stainer, eds., Academic Press, New York, 1961, vol. **2**, pp. 425–460.
13. D. Ajdic, W. M. McShan, R. E, McLaughlin, G. Savic, J. Chang, M. B. Carson, C. Primeaux, R. Tian, S. Kenton, H. Jia, S. Lin,

Y. Qian, S. Li, H. Zhu, F. Najar, H. Lai, J. White, B. A. Roe, J. J. Ferretti, Genome sequence of *Streptococcus mutans* UA159, a cariogenic dental pathogen. *Proc. Natl. Acad. Sci. USA*, 2002, **99**, 14434–14439.

14. A. Bolotin, B. Quinquis, P. Renault, A. Sorokin, S. Dusko Ehrlich, S. Kulakauskas, A. Lapidus, E. Goltsman, M. Mazur, G. D. Pusch, M. Fonstein, R. Overbeek, N. Kyprides, B. Purnelle, D. Prozzi, K. Ngui, D. Masuy, F. Hancy, S. Burteau, M. Boutry, J. Delcour, A. Goffeau, P. Hols, Complete sequence and comparative genome analysis of the dairy bacterium *Streptococcus thermophilus*. *Nat. Biotechnol.*, 2004, **22**, 1554–1558.
15. M. Higuchi, The effect of oxygen on the growth and mannitol fermentation of *Streptococcus mutans*, *J. Gen. Microbiol.*, 1984, **130**, 1819–1826.
16. M. Higuchi, Reduced nicotinamide adenine dinucleotide oxidase involvement in defense against oxygen toxicity of *Streptococcus mutans*, *Oral Microbiol. Immunol.*, 1992, **7**, 309–314.
17. M. Higuchi, M. Shimada, Y. Yamamoto, T. Koga, Y. Kamio, Identification of two distinct NADH oxidases corresponding to H_2O_2–forming oxidase and H_2O–forming oxidase induced in *Streptococcus mutans*, J. Gen. Microbiol., 1993, **139**, 2343–2351.
18. M. Higuchi,Y. Yamamoto, Y. Kamio, Molecular biology of oxygen tolerance in lactic acid bacteria: functions of NADH oxidases and Drp in oxidative stress, *J. Biosci. Bioeng.*, 2000, **90**, 484–493.
19. A. Thibessard, A. Fernandez, B. Gintz, N. Leblond-Bourget, B. Decaris, Hydrogen peroxide effects on *Streptococcus thermophilus* CNRZ368 cell viability, *Res. Microbiol*., 2001, **152**, 593–596.
20. P.G. Vance, B. B. Jr Keele, K. V. Rajagopalan, Superoxide dismutase from *Streptococcus mutans*. Isolation and characterization of two forms of the enzyme, *J. Biol. Chem.*, 1972, **247**, 4782–4786.

21. S. K. Chang, H. M. Hassan, Characterization of superoxide dismutase in *Streptococcus thermophilus*, *Appl. Environ. Microbiol.*, 1997, **63**, 3732–3735.
22. A. De Vendittis, M. Amato, A. Michniewicz, G. Parlato, A. De Angelis, I. Castellano, R. Rullo, F. Riccitiello, S. Rengo, M. Masullo, E. De Vendittis, Regulation of the properties of superoxide dismutase from the dental pathogenic microorganism *Streptococcus mutans* by iron– and manganese–bound co–factor, *Mol. BioSyst.*, 2010, **6**, 1973–1982.
23. A. De Vendittis, S. Marco, A. Di Maro, A. Chambery, A. Albino, M. Masullo, A. Michniewicz, G. Parlato, A. De Angelis, E. De Vendittis, R. Rullo, Properties of a putative cambialistic superoxide dismutase from the aerotolerant bacterium *Streptococcus thermophilus* strain LMG 18311, *Protein Pept. Lett.*, 2012, **19**, 333–344.
24. A. Holmgren, Thioredoxin, *Annu. Rev. Biochem.*, 1985, **54**, 237–271.
25. A. Holmgren, Thioredoxin and glutaredoxin systems, *J. Biol. Chem.*, 1989, **264**, 13963–13966.
26. E. S. J. Arner, A. Holmgren, Physiological functions of thioredoxin and thioredoxin reductase, *Eur. J. Biochem.*, 2000, **267**, 6102–6109.
27. R. P. Hirt, S. Müller, T. M. Embley, G. H. Coombs, The diversity and evolution of thioredoxin reductase: new perspectives, *Trends Parasitol.*, 2002, **18**, 302–308.
28. C. H. Williams Jr, Mechanism and structure of thioredoxin reductase from *Escherichia coli*, *FASEB J.*, 1995, **9**, 1267–1276.
29. F. Åslund, J. Beckwith, The thioredoxin superfamily: redundancy, specificity, and gray–area genomics, *J. Bacteriol.*, 1999, **181**, 1375–1379.
30. J. Sambrook, E. F. Fritsch, T. Maniatis, *Molecular cloning: a laboratory manual*, 2nd ed., Cold Spring Harbor, Laboratory Press, New York, 1989.
31. R. Cotugno, M.R. Ruocco, S. Marco, P. Falasca, G. Evangelista, G. Raimo, A. Chambery, A. Di Maro, M. Masullo, E. De Vendittis, Differential cold–adaptation among protein

components of the thioredoxin system in the psychrophilic eubacterium *Pseudoalteromonas haloplanktis* TAC 125, *Mol. BioSyst.*, 2009, **5**, 519–528.
32 T. E. Creighton, in: *Protein Structure a Practical Approach*, T. E. Creighton, ed., Oxford University Press, Oxford, UK, 1989, pp. 155–167.
33. P. Falasca, G. Evangelista, R. Cotugno, S. Marco, M. Masullo, E. De Vendittis, G. Raimo, Properties of the endogenous components of the thioredoxin system in the psychrophilic eubacterium *Pseudoalteromonas haloplanktis* TAC 125, *Extremophiles*, 2012, **16**, 539–552.
34. A. Holmgren, M. Björnstedt, Thioredoxin and thioredoxin reductase, *Methods Enzymol.*, 1995, **252**,199–208.
35. A. Holmgren, Thioredoxin catalyzes the reduction of insulin disulfides by dithiothreitol and dihydrolipoamide, *J. Biol. Chem.*, 1979, **254**, 9627–9632.
36. A. Holmgren, Reduction of disulfides by thioredoxin. Exceptional reactivity of insulin and suggested functions of thioredoxin in mechanism of hormone action, *J. Biol. Chem.*, 1979, **254**, 9113–9119.
37. G. Spyrou, E. Enmark, A. Miranda-Vizuete, J. Gustaffson, Cloning and expression of a novel mammalian thioredoxin, *J. Biol. Chem.*, 1997, **272**, 2936–2941.
38. P. A. Loach, in: *Handbook of Biochemistry and Molecular Biology*, G. D. Fasman, ed., CRC Press, Boca Raton FL, 3rd edn, 1976, vol. **1**, pp. 122–130.
39. R. Dosi, A. Di Maro, A. Chambery, G. Colonna, S. Costantini, G. Geraci, A. Parente, Characterization and kinetics studies of water buffalo (*Bubalus bubalis*) myoglobin, *Comp. Biochem. Physiol. B: Biochem. Mol. Biol.*, 2006, **145**, 230–238.
40. I. Castellano, A. Di Maro, M. R. Ruocco, A. Chambery, M. T. Di Martino, G. Parlato, M. Masullo, E. De Vendittis, Psychrophilic superoxide dismutase from *Pseudoalteromonas haloplanktis*: biochemical characterization and identification of a highly reactive cysteine residue, *Biochimie*, 2006, **88**, 1377–1389.

41 M. Bradford, A rapid and sensitive method for the quantitation of microgram quantities of protein utilizing the principle of protein-dye binding, *Anal. Biochem.*, 1976, **72**, 248–254.
42. U. K. Laemmli, Cleavage of structural proteins during the assembly of the head of bacteriophage T4, *Nature*, 1970, **227**, 680–685.
43. R. K. Wierenga, P. Terpstra, W. G. Hol, Prediction of the occurrence of the ADP–binding beta alpha beta–fold in proteins, using an amino acid sequence fingerprint, *J. Mol. Biol.*, 1986, **187**, 101–107.
44. I. Hanukoglu, T. Gutfinger, cDNA sequence of adrenodoxin reductase. Identification of NADP–binding sites in oxidoreductases, *Eur. J. Biochem.*, 1989, **180**, 479–484.
45. G. Eggink, H. Engel, G. Vriend, P. Terpstra, B. Witholt, Rubredoxin reductase of *Pseudomonas oleovorans*. Structural relationship to other flavoprotein oxidoreductases based on one NAD and two FAD fingerprints, *J. Mol. Biol.*, 1990, **212**, 135–142.
46. J. Obiero, V. Pittet, S. A. Bonderoff, D. A. Sanders, Thioredoxin system from *Deinococcus radiodurans*, *J. Bacteriol.*, 2010, **192**, 494–501.
47. G. Waskman, T. S. Krishna, C. H. Williams Jr, J. Kuriyan, Crystal structure of *Escherichia coli* thioredoxin reductase refined at 2 Å resolution. Implications for a large conformational change during catalysis, *J. Mol. Biol.*, 1994, **236**, 800–816.
48. M. Akif, K. Suhre, C. Verma, S. C. Mande, Conformational flexibility of *Mycobacterium tuberculosis* thioredoxin reductase: crystal structure and normal-mode analysis, *Acta Cryst.*, 2005, **D61**, 1603–1611.
49. F. K. Gleason, A. Holmgren, Thioredoxin and related proteins in procaryotes, *FEMS Microbiol. Rev.*, 1988, **4**, 271–297.
50. H. Eklund, F. K. Gleason, A. Holmgren, Structural and functional relations among thioredoxins of different species, *Proteins*, 1991, **11**, 13–28.
51. Y. Li, Y. Hu, X. Zhang, H. Xu, E. Lescop, B. Xia, C. Jin, Conformational fluctuations coupled to the thiol-disulfide transfer

between thioredoxin and arsenate reductase in *Bacillus subtilis*, *J. Biol. Chem.*, 2007, **282**, 11078–11083.
52. S. K. Katti, D.M. LeMaster, H. Eklund, Crystal structure of thioredoxin from *Escherichia coli* at 1.68 Å resolution, *J. Mol. Biol.*, 1990, **212**, 167–184.
53. G. Hall, M. Shah, P. A. McEwan, C. Laughton, M. Stevens, A. Westwell, J. Emsley, Structure of *Mycobacterium tuberculosis* thioredoxin C, *Acta Cryst.*, 2006, **D62**, 1453–1457.
54. G. Roos, A. Garcia-Pino, K. Van belle, E. Brosens, K. Wahni, G. Vandenbussche, L. Wyns, R. Loris, J. Messens, The conserved active site proline determines the reducing power of *Staphylococcus aureus* thioredoxin, *J. Mol. Biol.*, 2007, **368**, 800–811.
55. I. Castellano, M.R. Ruocco, F. Cecere, A. Di Maro, A. Chambery, A. Michniewicz, G. Parlato, M. Masulo, E. De Vendittis, Glutathionylation of the iron superoxide dismutase from the psychrophilic eubacterium *Pseudoalteromonas haloplanktis*, *Biochim. Biophys. Acta*, 2008, **1784**, 816–826.
56. A. Miranda-Vizuete, A.E. Damdimopoulos, J.Å. Gustafsson, G. Spyrou, Cloning, expression, and characterization of a novel *Escherichia coli* thioredoxin, *J. Biol. Chem.*, 1997, **272**, 30841–30847.
57. S.J. Jeon, K. Ishikawa, Identification and characterization of thioredoxin and thioredoxin reductase from *Aeropyrum pernix* K1, *Eur. J. Biochem.* 2002, **269**, 5423–5430.
58. G. Krause, J. Lundstrom, J.L. Barea, C. Pueyo de la Cuesta, A. Holmgren, Mimicking the active site of protein disulfide–isomerase by substitution of proline 34 in *Escherichia coli* thioredoxin, *J. Biol. Chem.*, 1991, **266**, 9494–9500

List of pubblications of Dr. Salvatore Marco

Full pubblications

1. Albino A, **Marco S**, Di Maro A, Chambery A, Masullo M, De Vendittis E.
   Characterization of a cold-adapted glutathione synthetase from the psychrophile *Pseudoalteromonas haloplanktis.*
   Molecular BioSystems. 2012 Sep;8(9):2405-14.

2. Falasca P, Evangelista G, Cotugno R, **Marco S**, Masullo M, De Vendittis E, Raimo G.
   Properties of the endogenous components of the thioredoxin system in the psychrophilic eubacterium *Pseudoalteromonas haloplanktis* TAC 125.
   Extremophiles. 2012 May;16(3):539-52.

3. De Vendittis A, **Marco S**, Di Maro A, Chambery A, Albino A, Masullo M, Michniewicz A, Parlato G, De Angelis A, De Vendittis E, Rullo R.
   Properties of a putative cambialistic superoxide dismutase from the aerotolerant bacterium *Streptococcus thermophilus* strain LMG 18311.
   Protein & Peptide Lettetters. 2012 Mar;19(3):333-44.

4. Merlino A, Russo Krauss I, Rossi B, Vergara A, De Vendittis A, **Marco S**, De Vendittis E, Sica F. Identification of an active dimeric intermediate populated during the unfolding process of the cambialistic superoxide dismutase from *Streptococcus mutans*.
   Biochimie. 2012 Mar;94(3):768-75.

5. Cotugno R, Rosaria Ruocco M, **Marco S**, Falasca P, Evangelista G, Raimo G, Chambery A, Di Maro A, Masullo M, De Vendittis E.

Differential cold-adaptation among protein components of the thioredoxin system in the psychrophilic eubacterium *Pseudoalteromonas haloplanktis* TAC 125.
Molecular BioSystems. 2009 May;5(5):519-28.

Abstracts with ISSN

6. Albino A, **Marco S**, De Vendittis E, Masullo M.
The glutathione biosynthesis in the psychrophile *Pseudoalteromonas haloplanktis*.
36th FEBS Congress, Torino, June 25-30, 2011.
FEBS Journal 278, suppl. 1, 389 (Abs. P26.1).

7. **Marco S**, Albino A, De Vendittis A, Rullo R, De Vendittis E.
Biochemical properties of the superoxide dismutase from the pathogenic bacterium *Helicobacter pylori.*
36th FEBS Congress, Torino, June 25-30, 2011.
FEBS Journal 278, suppl. 1, 399 (Abs. P26.32).

Abstracts of International Meetings

8. **Marco S**, Albino A, De Vendittis A, Masullo MR, Rullo R, Amato M, Riccitiello F, De Vendittis E.
Properties of the thioredoxin system in microaerophiles from the Streptococcus Genus.
37th FEBS Congress, Sevilla, September 4-9, 2012, (Abs. P26.32)

Abstracts of National Meetings

9. **Marco S**, Albino A, Martucci N.M, Rullo R, De Vendittis E.
Caratterizzazione biochimica della superossido dismutasi dal batterio patogeno *Helicobacter pylori*.
Giornate Scientifiche di Ateneo, Università Federico II, Facoltà di Medicina e Chirurgia, Facoltà di Scienze Biotecnologiche, Napoli, Novembre 24-26, 2010 (Abs. 056).

10. De Vendittis A, Caiazza S, Cocchiaro P, **Marco S**, De Vendittis E, Rullo R.
    Proprietà biochimiche della superossido dismutasi dal batterio d'interesse agro-alimentare *Streptococcus thermophilus*.
    Giornate Scientifiche di Ateneo, Università Federico II, Facoltà di Medicina e Chirurgia, Facoltà di Scienze Biotecnologiche, Napoli, Novembre 24-26, 2010 (Abs. 090).

11. Cotugno R., Ruocco M.R., **Marco S**., Masullo M., De Vendittis E.
    Proprietà molecolari e funzionali del sistema della tioredossina nell'eubatterio psicrofilo *Pseudoalteromonas haloplanktis*.
    Giornate Scientifiche di Ateneo, Università Federico II, Facoltà di Agraria, Portici, Dicembre 10-12, 2008 (Abs. 072).

Pubblications of Dr. Salvatore Marco during Doctoral training

Molecular BioSystems

Dynamic Article Links

Cite this: *Mol. BioSyst.*, 2012, **8**, 2405–2414

www.rsc.org/molecularbiosystems

PAPER

Characterization of a cold-adapted glutathione synthetase from the psychrophile *Pseudoalteromonas haloplanktis*

Antonella Albino,[a] Salvatore Marco,[a] Antimo Di Maro,[b] Angela Chambery,[b] Mariorosario Masullo[ac] and Emmanuele De Vendittis*[a]

Received 27th March 2012, Accepted 6th June 2012
DOI: 10.1039/c2mb25116g

Glutathione (GSH) biosynthesis occurs through two ATP-dependent reactions, usually involving distinct enzymes; in the second step of this process, catalysed by glutathione synthetase (GshB), GSH is formed from γ-glutamylcysteine and glycine. A recombinant form of GshB from the cold-adapted source *Pseudoalteromonas haloplanktis* (r*Ph*GshB) was purified and characterised. The enzyme formed a disulfide adduct with β-mercaptoethanol, when purified in the presence of this reducing agent. The homotetrameric form of r*Ph*GshB observed at high protein concentration disassembled into two homodimers at low concentration. A new method for directly determining the r*Ph*GshB activity was developed, based on [γ-^{32}P]ATP hydrolysis coupled to the GSH synthesis. The ATPase activity required the presence of both γ-glutamylcysteine and glycine and its optimum was reached in the 7.4–8.6 pH range; a divalent cation was absolutely required for the activity, whereas monovalent cations were dispensable. r*Ph*GshB was active at low temperatures and had a similar affinity for ATP (K_m 0.26 mM) and γ-glutamylcysteine (K_m 0.25 mM); a lower affinity was measured for glycine (K_m 0.75 mM). The oxidised form of glutathione (GSSG) acted as an irreversible inhibitor of r*Ph*GshB (K_i 10.7 mM) and formed disulfide adducts with the enzyme. r*Ph*GshB displayed a great temperature-dependent increase in its activity with an unusually high value of energy of activation (75 kJ mol^{-1}) for a psychrophilic enzyme. The enzyme was moderately thermostable, its half inactivation temperature being 50.5 °C after 10 min exposure. The energy of activation of the heat inactivation process was 208 kJ mol^{-1}. To our knowledge, this is the first contribution to the characterization of a GshB from cold-adapted sources.

Introduction

Glutathione (GSH) is an abundant low molecular weight thiol, which displays its antioxidant cellular functions in virtually all eukaryotes[1–5] and also in many prokaryotes.[6–10] Several investigations demonstrated that GSH is the main regulator of the physiological redox environment through an intracellular balance with its oxidised form (GSSG).[5,10] Defence against oxidative damages, detoxification of foreign compounds, and protection of protein sulfhydryls from irreversible oxidation are among the most common antioxidant functions exerted by the GSH/GSSG redox couple. On the other hand, GSH, GSSG and/or *S*-nitrosoglutathione (GSNO) are responsible for the S-thiolation reaction, a covalent modification forming a glutathionyl adduct on reactive cysteine residues and possibly regulating the function of the target protein.[11–13]

In both eukaryotes and prokaryotes the biosynthesis of this tripeptide takes place through an enzyme system including two sequential reactions.[1] In the first reaction, the enzyme glutamylcysteine ligase (GshA) catalyses the formation of L-γ-glutamylcysteine (γ-Glu-Cys) from L-glutamate and L-cysteine; in the second one, another enzyme, glutathione synthetase (GshB) leads to the formation of GSH from γ-Glu-Cys and glycine, as reported in the following scheme.

$$\text{L-Glutamate} + \text{L-cysteine} + \text{ATP} \xrightarrow{\text{GshA}} \gamma\text{-Glu-Cys} + \text{ADP} + \text{P}_i \quad (1)$$

$$\gamma\text{-Glu-Cys} + \text{glycine} + \text{ATP} \xrightarrow{\text{GshB}} \text{GSH} + \text{ADP} + \text{P}_i \quad (2)$$

In both catalysed reactions, one molecule of ATP is hydrolysed to ADP and inorganic phosphate in the presence of Mg^{2+} ions. Some organisms contain a single bifunctional enzyme displaying both GshA and GshB activities.[14–16] The rate limiting step of the whole process is reaction (1),[17] which is also feedback inhibited by GSH.[18,19] Furthermore, Mn^{2+} can replace Mg^{2+} ions,

[a] *Dipartimento di Biochimica e Biotecnologie Mediche, Università di Napoli Federico II, Via S. Pansini 5, 80131 Napoli, Italy. E-mail: devendittis@dbbm.unina.it; Fax: +39 081 7463653*
[b] *Dipartimento di Scienze dela Vita, II Università di Napoli, Via Vivaldi 43, 81100 Caserta, Italy*
[c] *Dipartimento di Studi delle Istituzioni e dei Sistemi Territoriali, Università di Napoli "Parthenope", Via Medina 40, 80133 Napoli, Italy*

at least in this reaction; however, the substitution reduces the GshA activity and modifies the affinity towards different substrates.[20–22]

Biosynthesis of GSH and its functional role have been the object of several investigations in eukaryotes. In prokaryotes GSH is biosynthesized in almost all Gram-negative bacteria,[6] although its antioxidant role is somehow controversial. Indeed, GSH acts as a sacrificial nucleophile for the detoxification of chlorine compounds;[23] conversely, it is dispensable for H_2O_2 resistance or gamma radiation.[24] A diversified picture emerges for Gram-positive bacteria, because GSH is absent in some anaerobic or microaerophilic sources,[6] is replaced by other thiols in actinomycetes,[9] or is produced through a bifunctional enzyme in *Streptococcus agalactiae*,[14] *Listeria monocytogenes*,[15] or *Pasteurella multocida*;[16] moreover, in *Streptococcus mutans*, GSH is taken up from the external medium, although this microorganism possesses the gene encoding a bifunctional enzyme.[25]

To our knowledge, glutathione biosynthesis was never reported in a cold-adapted source, where the antioxidant role of GSH could be more relevant for the survival of the psychrophilic source at cold temperatures. *Pseudoalteromonas haloplanktis* TAC125 is a psychrophilic eubacterium isolated from the Antarctic sea, growing in the 4–20 °C temperature interval.[26] The presence of GSH in this Gram-negative gamma-proteobacterium was inferred by previous works, in which glutathionyl adducts were formed on enzymes involved in the redox balance of *P. haloplanktis*, such as superoxide dismutase[27] and thioredoxin reductase.[28] Glutathionylated proteins were detected even in a growing culture of this psychrophile and the extent of modification increased under oxidative growth conditions.[27] Furthermore, in the case of superoxide dismutase, the modified enzyme became more resistant to its physiological inactivator peroxynitrite.[27]

The object of the present work is the enzyme system aimed at GSH biosynthesis in *P. haloplanktis*. In particular, the research was focused on the characterization of a recombinant form of glutathione synthetase (*Ph*GshB), which was recently crystallised using a without-oil microbatch method.[29] A direct assay, based on the hydrolysis of radiolabelled ATP coupled to GSH formation, was set up for measuring the *Ph*GshB activity. Using this assay, the kinetic parameters for each substrate were measured and the effect of temperature on enzyme activity and stability was evaluated. The results obtained represent the first investigation of the biosynthetic route of GSH in a psychrophilic source and prove that the functionality of a key reaction aimed at GSH biosynthesis is relevant even in cold-adapted microorganisms.

Experimental

Materials

Restriction and modifying enzymes were from GE Healthcare or Promega. *Taq* DNA polymerase from Takara was used in PCR experiments. Plasmid pGEM-T Easy was from Promega, whereas vector pET-28a(+) and the *Escherichia coli* BL21(DE3) strain were from Novagen. Purification of plasmids and DNA fragments was realised with Qiagen kits from M-Medical. Oligonucleotide synthesis, nucleotide sequencing and synthesis of vectors were carried out at Primm (Italy). Ampicillin, kanamycin, isopropyl-β-thiogalactopyranoside (IPTG), dithiothreitol (DTT), β-mercaptoethanol, γ-Glu-Cys and 5,5′-dithiobis-2-nitrobenzoic acid (DTNB) were from Sigma-Aldrich. [γ-^{32}P]ATP (2 mCi mL^{-1}; 10 Ci mmol^{-1}) was purchased from Perkin Elmer. The chromatographic medium Ni-NTA agarose was from Qiagen. HPLC-grade solvents for mass spectrometry were obtained from Carlo Erba. All other chemicals were of analytical grade.

The following buffers were used: buffer A, 20 mM Tris–HCl, pH 7.8, 5 mM $MgCl_2$, 150 mM KCl, 20 mM imidazole–HCl; buffer B, 20 mM Tris–HCl, pH 7.8, 50% (v/v) glycerol; buffer C, 100 mM Tris–HCl, pH 7.8, 5 mM $MgCl_2$, 150 mM KCl; buffer D, 20 mM Tris–HCl, pH 7.8, 150 mM KCl.

Heterologous expression of the *gshB* gene from *Pseudoalteromonas haloplanktis*

The genomic DNA from *P. haloplanktis*, strain TAC125, was prepared as previously described.[30] Transformation of bacterial strains, preparation of plasmids and other details of DNA recombinant technology were carried out according to standard procedures.[31] Engineering of the vector for heterologous expression of the *PhgshB* gene (ID 3708001) was already reported.[29] Briefly, the vector, named v*Ph*gshB, was a derivative of pET-28a(+) and its expression occurred in the host strain BL21(DE3) from *E. coli* upon the IPTG induction. Moreover, in the recombinant *Ph*GshB (r*Ph*GshB), the C-terminal lysine of the endogenous enzyme was replaced by the extrapeptide LE(H)$_6$, useful for the one-step purification of the expression product by affinity chromatography. However, the following procedure modified and integrated the previously described protocol for purification of r*Ph*GshB.[29] A colony obtained from the BL21(DE3)/v*Ph*gshB transformation was grown at 37 °C in 1 L of LB medium containing 0.06 mg mL^{-1} kanamycin up to 0.6 OD_{600} and, upon the addition of 0.1 mg mL^{-1} IPTG, heterologous expression of the cloned gene was induced for 2 hours. The culture was divided into two 500 mL aliquots and cells were collected by centrifugation at 5000 rpm for 20 min. One bacterial pellet was resuspended in 20 mL buffer A (non-reducing buffer), whereas the other one was resuspended in 20 mL buffer A supplemented with 7 mM β-mercaptoethanol (reducing buffer). After cellular lysis by French Press (Aminco, USA) and centrifugation at 30 000×*g*, two supernatants were obtained and each of them was added in batch to 3 mL of Ni-NTA Agarose resin, equilibrated with the non-reducing or reducing buffer, respectively. After incubation overnight at 4 °C, each slurry was poured in a column, which was extensively washed with the corresponding buffer. The bound r*Ph*GshB was then eluted by raising the imidazole–HCl concentration up to 200 mM to either non-reducing or reducing buffer. Pure protein fractions, as analysed by SDS-polyacrylamide gel elecrophoresis, were pooled together, eventually concentrated by ultrafiltration, and stored at −20 °C in buffer B (non-reducing storage buffer) or buffer B supplemented with 7 mM β-mercaptoethanol (reducing storage buffer). Approximately 20–25 mg of r*Ph*GshB purified under non-reducing or reducing conditions were obtained from the 500 mL culture of the transformant.

Assay for the activity of r*Ph*GshB

A new assay was set up for measuring the r*Ph*GshB activity, based on the ATP hydrolysis coupled to the GSH synthesis (reaction (2)). The ATPase was evaluated as radioactive inorganic phosphate ($^{32}P_i$) released from [γ-^{32}P]ATP through the phosphomolybdate method.[32] The reaction was followed kinetically on 50 μL aliquots withdrawn from the reaction mixture at selected times. Unless otherwise indicated, the reaction was carried out in buffer C, supplemented with the substrates glycine and γ-Glu-Cys. The reaction was stopped at 0 °C by the addition of an equal volume of 1 M $HClO_4$ supplemented with 5 mM KH_2PO_4 as a $^{32}P_i$ carrier. Following the addition of 300 μL of 20 mM sodium molybdate, phosphate was converted into a phosphododecamolybdate complex, which was then extracted by a vigorous stirring for 30 s with 400 μL isopropylacetate. After a fast spinning to achieve phase separation, 200 μL of the organic phase were counted in 3 mL Emulsifier-Safe (Packard), using the liquid scintillation counter TriCarb 1500 (Packard). The rate constant of the reaction was calculated from the slope of linear kinetics and expressed as mole of $^{32}P_i$ released by one mole of r*Ph*GshB in one second. Blanks for spontaneous [γ-^{32}P]ATP hydrolysis determined in the absence of r*Ph*GshB were subtracted.

The kinetic parameters of the ATPase catalysed by r*Ph*GshB, including the K_m values for the three substrates γ-Glu-Cys, glycine and ATP and the V_{max} of the reaction, were derived from Lineweaver–Burk plots of the activity data. To this aim, the concentration of the substrate was almost equally distributed in the reciprocal x-axis around the K_m of the reaction, whereas the concentration of the other substrates was essentially saturating. Linearity in double reciprocal plots was evaluated through the squared correlation coefficient r^2, which in almost all cases was higher than 0.98. The inhibition constant (K_i) of GSSG was calculated from Lineweaver–Burk plots in which the affinity of r*Ph*GshB for ATP was evaluated in the absence or in the presence of two fixed GSSG concentrations. In particular, the K_i value was averaged from the decrease of V_{max} in the presence of the inhibitor, according to the equation $V^I_{max} = V_{max}/\{1 + ([I]/K_i)\}$, where V^I_{max} represents the V_{max} of the ATPase in the presence of the concentration [I] of the inhibitor.

The energy of activation E_a and the Arrhenius constant A of the reaction, as well as the related thermodynamic parameters of activation, namely enthalpy (ΔH^*), entropy (ΔS^*) and free energy (ΔG^*), were calculated as reported elsewhere.[33]

Other methods

Protein concentration was determined by the method of Bradford, using bovine serum albumin as a standard.[34] Purity of protein samples was assessed by 12% SDS-PAGE according to standard protocols.[35] The quaternary structure of r*Ph*GshB was evaluated by gel-filtration on a Superdex™ 200 10/300 GL column connected to a FPLC apparatus (GE Healthcare). The mass spectrometry analysis was realised on protein samples desalted by RP-HPLC, as previously reported.[36,37] The number of cysteine residues in r*Ph*GshB was determined by the Ellman assay.[38,39]

Results

Molecular properties of r*Ph*GshB

The putative genes encoding GshA and GshB in *P. haloplanktis* have been annotated in the genome of this psychrophilic eubacterium made of two chromosomes.[26] Concerning GshA, two genes were found and named *PhgshA*I (ID 3708000) and *PhgshA*II (ID 3711501) from their localisation in choromosome I and II, respectively; conversely, a single gene for GshB was identified in chromosome I (*PhgshB*; ID 3708001). In order to characterize the glutathione synthetase activity from a psychrophilic source, a recombinant form of *Ph*GshB (r*Ph*GshB) with the C-terminal lysine replaced by the extrapeptide $LE(H)_6$ was obtained, using the heterologous expression system constituted by the vector v*Ph*gshB, a pET-28a(+) derivative, and the *E. coli* strain BL21(DE3).[29] The molecular properties of two r*Ph*GshB samples purified in the absence or in the presence of β-mercaptoethanol were assessed by SDS/PAGE analysis (Fig. 1); both were homogenous and their electrophoretic mobility corresponded to a molecular mass of 36 kDa, the expected size for the r*Ph*GshB monomer. These protein samples were also analysed by ESI/Q-TOF mass spectrometry (Fig. 2). In the absence of β-mercaptoethanol, a single peak was obtained, whose calculated M_r 35 888.33 was in good agreement with the theoretical value of 35 887.03 assigned to the recombinant enzyme, considering the His-tail and the lack of initial methionine. On the other hand, in the presence of β-mercaptoethanol, another heavier peak with M_r 35 964.63 was found besides the most abundant peak with M_r 35 888.34. A tentative explanation for this additional peak, based on a similar behaviour observed for the superoxide dismutase from *P. haloplanktis*,[37] led to the suggestion that the 76.29 Da extra mass could be due to a disulfide adduct between β-mercaptoethanol and a cysteine residue of r*Ph*GshB.

The molecular mass of r*Ph*GshB purified in the absence of β-mercaptoethanol was also determined by gel filtration chromatography under non-denaturing conditions. Fig. 3 shows the elution profile of this sample at different concentrations on a Superdex™ 200 10/300 GL column. Position and broadness of peaks were significantly affected by protein concentration; for instance, the elution of 10 mg mL^{-1} r*Ph*GshB was significantly faster, although broader, than that of 0.5 mg mL^{-1}.

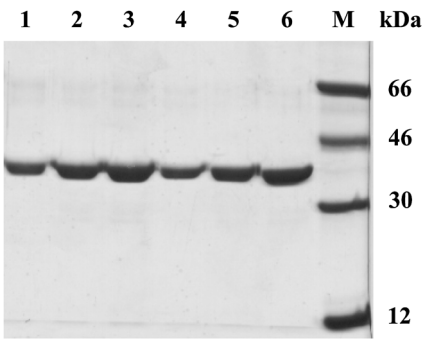

Fig. 1 SDS-PAGE of purified r*Ph*GshB samples. Increasing amounts (2, 4 and 6 μg) of r*Ph*GshB purified in the presence of β-mercaptoethanol (*lanes* 1–3) or in its absence (*lanes* 4–6) were analysed on a 12% polyacrylamide gel. Migration of molecular mass protein standards (*lane* M) is reported on the right.

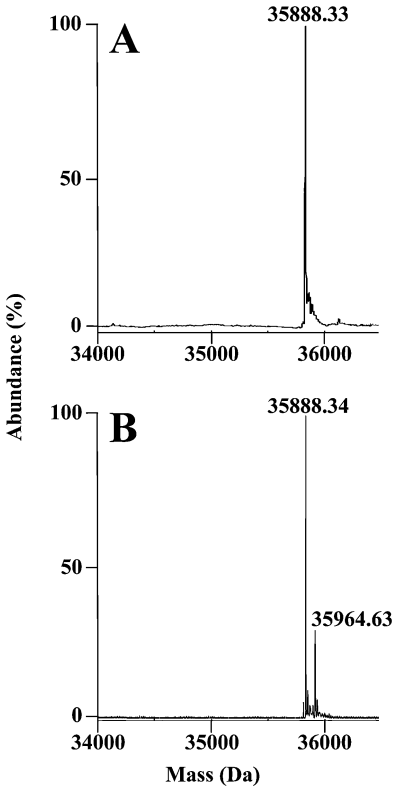

Fig. 2 Molecular mass of r*Ph*GshB. Electrospray mass spectrum of r*Ph*GshB purified in the absence (*panel* A) or in the presence of β-mercaptoethanol (*panel* B). The M_r values of the major peaks are indicated.

The elution times of peaks obtained at the various r*Ph*GshB concentrations were then compared with those of protein standards; the extrapolated molecular mass for r*Ph*GshB ranged between 74 and 136 kDa, which roughly corresponded to a homodimeric or homotetrameric organization, respectively. Similar profiles were obtained with r*Ph*GshB purified in the presence of β-mercaptoethanol. This behaviour could be explained with the assemblage of four r*Ph*GshB subunits at high protein concentration, and the disassemblage of the homotetramer in two homodimers at lower concentrations. We cannot exclude that the homotetramer/homodimer conversion takes place during gel filtration.

Three cysteine residues are present in the amino acid sequence of *Ph*GshB, namely at positions 185, 223 and 290 (numbering includes initial methionine). The Ellman assay was used to determine the number of free cysteines in the r*Ph*GshB samples purified in the absence or in the presence of β-mercaptoethanol and the values found were 2.75 and 2.17, respectively. These data suggest that when r*Ph*GshB was purified in the absence of reducing agents, its three cysteines were present as free sulfhydryl groups. The reduced number of free cysteines measured in the protein sample purified in the presence of β-mercaptoethanol reinforces the hypothesis of the formation of an adduct between cysteine(s) and β-mercaptoethanol. However, only part of the protein population harboured this adduct, as also confirmed by the presence of both unmodified and modified peaks in the mass spectrometry data; therefore, the postulated covalent modification of the cysteine residue(s) was understoichiometric.

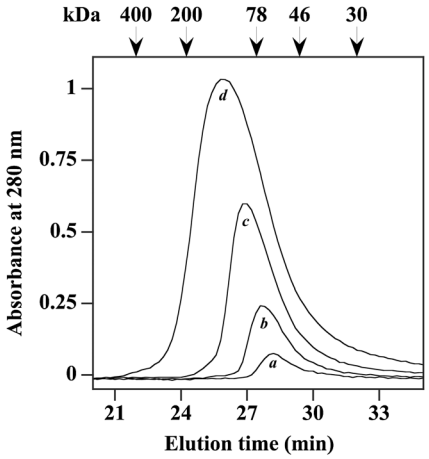

Fig. 3 Gel filtration behaviour of r*Ph*GshB under non-denaturing conditions. The elution profile of r*Ph*GshB purified in the absence of β-mercaptoethanol was analysed on a Superdex™ 200 10/300 GL column. 100 μL of r*Ph*GshB solutions at 0.5 mg mL^{-1} (line *a*), 1.5 mg mL^{-1} (line *b*), 4.0 mg mL^{-1} (line *c*) or 10.0 mg mL^{-1} (line *d*) final concentration in buffer D were loaded on the column. Elution was realised with buffer D at a flow rate of 0.5 mL min^{-1}. The column was calibrated with apoferritin (M_r 400 000), β-amylase (M_r 200 000), human transferrin (M_r 78 000), ovalbumin (M_r 46 000) and carbonic anhydrase (M_r 30 000); the corresponding elution positions are indicated by arrows on the top. Absorbance was continuously monitored at 280 nm.

Biochemical properties of r*Ph*GshB

Assays for GshB activity (reaction 2) are usually based on the determination of ADP formed during the GSH synthesis through an indirect enzyme-coupled method, which used pyruvate kinase and lactate dehydrogenase to measure ADP formation through NADH oxidation.[40] However, the employment of other enzymes impaired a direct evaluation of the effect of some parameters, such as temperature, pH, ions, on the biochemical properties of GshB. To this aim, another assay was developed, which directly evaluated the activity of GshB through the measurement of the radioactive $^{32}P_i$ released from the radiolabelled [γ-^{32}P]ATP. The rate of $^{32}P_i$ release promoted by r*Ph*GshB in the presence of glycine, γ-Glu-Cys or both compounds is shown in Fig. 4. No significant activity was measured in the presence of a single substrate in the reaction mixture; conversely, a well-measurable activity was detected in the presence of both glycine and γ-Glu-Cys. These results indicate that the ATPase catalysed by r*Ph*GshB required the presence of both substrates and was likely coupled to the GSH synthesis. The validity of the new method for measuring the glutathione synthetase activity was demonstrated by the linear dependence of the initial rate of $^{32}P_i$ release with the concentration of r*Ph*GshB, as expected for an enzyme activity (not shown). The usage of a direct assay for measuring the activity was judged more convenient for the biochemical characterization of r*Ph*GshB without the addition of other enzymes. Indeed, the results obtained with this assay were more confident, because the probable mixing effects on the investigated parameters by a cold-adapted enzyme (*Ph*GshB) and two mesophilic ones (lactate dehydrogenase and pyruvate kinase) were avoided.

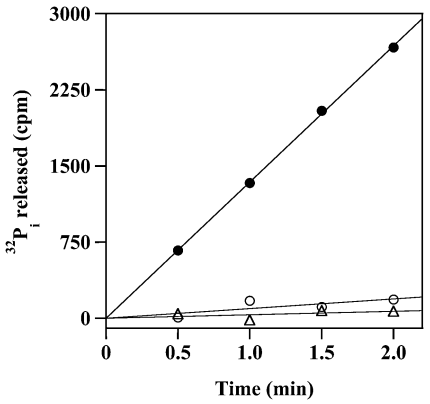

Fig. 4 Time course of ATP hydrolysis by r*Ph*GshB. The reaction mixture contained 0.15 μM r*Ph*GshB, supplemented with 10 mM glycine (○), or 2.5 mM γ-Glu-Cys (△), or both substrates (●), in 250 μL final volume of 100 mM Tris–HCl, pH 7.8 buffer, containing 20 mM $MgCl_2$ and 150 mM KCl. The reaction was carried out at 30 °C and started with the addition of 2 mM [γ-^{32}P]ATP (specific radioactivity 8.45 cpm pmol^{-1}). At the times indicated, aliquots were withdrawn and analysed for the $^{32}P_i$ released, as described in the Materials and Methods section.

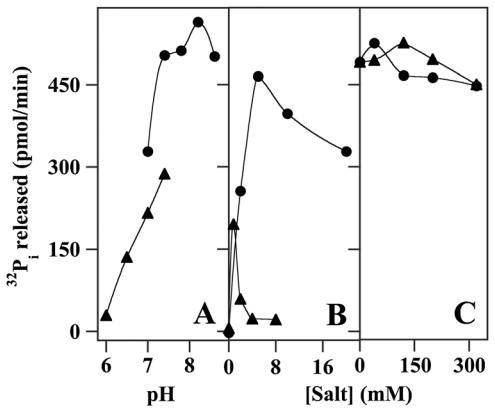

Fig. 5 pH and ionic dependence of the ATPase activity catalysed by r*Ph*GshB. (A) Effect of pH. The reaction mixture contained 0.17 μM r*Ph*GshB, 10 mM glycine and 2.5 mM γ-Glu-Cys in 250 μL final volume of 100 mM Tris–HCl (●) or 100 mM imidazole–HCl buffer (▲), at the pH indicated, supplemented with 5 mM $MgCl_2$ and 150 mM KCl. (B) Effect of divalent cations. The reaction mixture contained the same concentration of r*Ph*GshB, glycine and γ-Glu-Cys as in (A), in 250 μL final volume of 100 mM Tris–HCl, pH 7.8 buffer, supplemented with 150 mM KCl and the indicated concentration of $MgCl_2$ (●) or $MnCl_2$ (▲). (C) Effect of monovalent cations. The reaction mixture contained the same concentration of r*Ph*GshB, glycine and γ-Glu-Cys as in (A), in 250 μL final volume of 100 mM Tris–HCl, pH 7.8 buffer supplemented with 5 mM $MgCl_2$ and the indicated concentration of KCl (●) or NaCl (▲). All reactions were carried out at 15 °C, started with the addition of 2 mM [γ-^{32}P]ATP (specific radioactivity 1.27–2.19 cpm pmol^{-1}) and were followed kinetically. To this aim, aliquots were withdrawn at selected times and analysed for $^{32}P_i$ released. The data were expressed as rate of $^{32}P_i$ release, evaluated from the slope of linear kinetics.

The assessment of the biochemical properties possessed by the psychrophilic r*Ph*GshB was carried out with the enzyme sample purified in the absence of β-mercaptoethanol, to avoid any interference by an understoichiometric thiolic adduct on the enzyme. All the assays were carried out at 15 °C, the optimum growth temperature of *P. haloplanktis*. To establish the best experimental conditions for measuring the ATPase activity triggered by r*Ph*GshB, its pH and ionic dependence were investigated (Fig. 5). To study the effect of pH in the 6.0–8.6 interval, the chosen buffers were Tris–HCl or imidazole–HCl supplemented with 5 mM $MgCl_2$ and 150 mM KCl. As shown in Fig. 5A, the activity was affected by the pH; maximum levels of activity were reached with the Tris–HCl buffer in the 7.4–8.6 pH range. For this reason, the following experiments were all carried out in 20 mM Tris–HCl buffer, pH 7.8.

The ionic dependence of the r*Ph*GshB activity was focused on the assessment of possible specific requirements for monovalent and/or divalent cations. The buffer employed for investigating the effect of divalent cations contained 150 mM KCl and an increasing concentration of chlorides of Mg^{2+} or Mn^{2+} (Fig. 5B). The presence of a divalent cation was absolutely required for the activity and Mg^{2+} was significantly more effective than Mn^{2+}. Concerning the effect of magnesium, maximum activity was reached in the presence of 5 mM $MgCl_2$ and a further addition of this salt caused a little decrease in activity; a narrower bell-shaped curve was observed when the effect of manganese was analysed, and the best condition for the Mn-dependent activity was found in the presence of 0.8 mM $MnCl_2$. In the study related to monovalent cations, the buffer employed contained 5 mM $MgCl_2$ and an increasing concentration of chlorides of the most common monovalent cations, namely Na^+ or K^+ (Fig. 5C). An almost maximum level of activity was reached in the absence of these salts, thus indicating that r*Ph*GshB did not require the presence of monovalent cations for its activity. Moreover, no significant variation of this level of activity was observed in the presence of the indicated concentrations of NaCl or KCl. Therefore, the presence of a monovalent cation was dispensable in the ATPase sustained by r*Ph*GshB; nevertheless, in the following experiments 150 mM KCl was present in the reaction buffer, for a better comparison with the data referred to GshB from other sources.

The affinity of r*Ph*GshB for its three substrates, γ-Glu-Cys, glycine and ATP was evaluated at 15 °C, the optimum growth temperature of *P. haloplanktis*.[41] To this aim, the effect of various concentrations of each substrate on the activity was determined in the presence of a fixed concentration of the other substrates. In the resulting Lineweaver–Burk plots the three straight lines extrapolated to an almost identical *y*-axis intercept, thus indicating that the same maximum rate of ATP hydrolysis (V_{max}) was reached under the three different conditions (Fig. 6). This finding also proves that the reaction always depended on a single substrate, and that the other substrates were present at a saturating concentration. In particular, the value of k_{cat} calculated from the extrapolated V_{max} was 1.85, 1.93 and 2.03 s^{-1} for the steady-state measurement depending on ATP, γ-Glu-Cys and glycine, respectively. Concerning the affinity for the different substrates, the values of K_m for ATP and γ-Glu-Cys were quite similar (0.26 and 0.25 mM, respectively), whereas a higher K_m (0.75 mM) was determined for glycine. These data prove that the psychrophilic r*Ph*GshB displays a good catalytic efficiency at 15 °C, as also evaluated through the k_{cat}/K_m ratios.

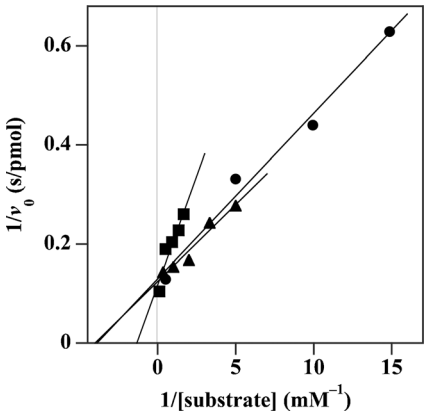

Fig. 6 Kinetic parameters of r*Ph*GshB. For the evaluation of the affinity of r*Ph*GshB for each substrate, Lineweaver–Burk plots were drawn under the following experimental conditions. The reaction mixture for measuring the affinity for ATP contained 0.17 μM r*Ph*GshB, 10 mM glycine and 2.5 mM γ-Glu-Cys in 250 μL final volume of buffer C. In this case the reaction started with the addition of the indicated concentrations of [γ-^{32}P]ATP (●) (specific radioactivity 3.98–166.4 cpm pmol^{-1}). For measuring the affinity for glycine or γ-Glu-Cys, the reaction mixture contained the same concentration of r*Ph*GshB, 2.5 mM γ-Glu-Cys and the indicated concentration of glycine (■), or 10 mM glycine and the indicated concentration of γ-Glu-Cys (▲), in 250 μL final volume of buffer C, respectively. Under these two experimental conditions the reaction started with the addition of 2 mM [γ-^{32}P]ATP (specific radioactivity 3.08 cpm pmol^{-1}). All reactions were carried out at 15 °C and followed kinetically, by analysing the amount of $^{32}P_i$ released on aliquots withdrawn at appropriate times. The values of v_0 (pmol ATP hydrolysed s^{-1}) were calculated from the slope of linear kinetics.

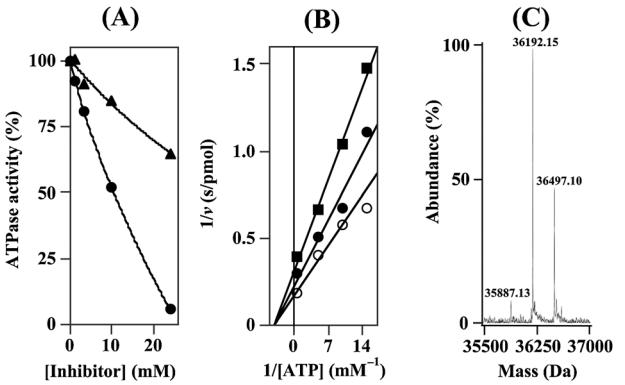

Fig. 7 Effect of glutathione forms on r*Ph*GshB. (A) Dose-dependent inhibition profile. The reaction mixture for measuring the r*Ph*GshB ATPase in the presence of the indicated concentrations of GSSG (●) or GSH (▲) contained 0.12 μM r*Ph*GshB, 10 mM glycine and 2.5 mM γ-Glu-Cys in 250 μL final volume of buffer C. The reaction, carried out at 15 °C, started with the addition of 2 mM [γ-^{32}P]ATP (specific radioactivity 1.73 cpm pmol^{-1}) and was followed kinetically, as indicated in Fig. 5. The ATPase activity was expressed as a percentage of that measured in the absence of the glutathione forms. (B) Effect of GSSG on the Lineweaver–Burk plot of the r*Ph*GshB ATPase. The reaction mixture, carried out in 250 μL final volume of buffer C, contained 0.12 μM r*Ph*GshB, 10 mM glycine, 2.5 mM γ-Glu-Cys in the absence (○) or in the presence of 3.2 mM GSSG (●) or 10 mM GSSG (■). The reaction started with the addition of the indicated concentrations of [γ-^{32}P]ATP (specific radioactivity 2.13–103.5 cpm pmol^{-1}). All reactions were carried out at 15 °C and followed kinetically, by analysing the amount of $^{32}P_i$ released on aliquots withdrawn at appropriate times. The values of v_0 (pmol ATP hydrolysed s^{-1}) were calculated from the slope of linear kinetics. (C) Electrospray mass spectrum of r*Ph*GshB treated with GSSG. A sample of r*Ph*GshB (55 μg in 250 μL final volume of buffer C) was treated with 24 mM GSSG and then analysed by ESI/Q-TOF mass spectrometry. The M_r values of the major peaks are indicated.

It has been reported that GSSG is an inhibitor of GshB from *E. coli*, whereas GSH is almost ineffective.[42] To investigate on the possible inhibition of r*Ph*GshB by GSSG or GSH, the enzyme activity was measured in the presence of increasing concentrations of these compounds (Fig. 7A). A marked dose-dependent inhibition was observed with GSSG; in particular, the concentration of this compound leading to 50% reduction of the activity (IC_{50}) was around 10 mM; moreover, an almost complete inhibition was obtained in the presence of 24 mM GSSG. On the other hand, only a moderate decrease in the activity was observed with GSH, the percentage of inhibition being far from 50% even at 24 mM GSH, a behavior indicating a lower inhibition power exerted by GSH compared to GSSG. To get an insight into the type of inhibition caused by GSSG, kinetic measurements of the r*Ph*GshB affinity for ATP were carried out in the absence or in the presence of two fixed GSSG concentrations (Fig. 7B). The V_{max} of the ATPase was reduced by GSSG in a dose-dependent way, whereas the K_m for ATP was essentially unaffected; the calculated K_i for this inhibitor was 10.7 mM. The behaviour of GSSG in the Lineweaver–Burk plots is consistent with that of an irreversible inhibitor of r*Ph*GshB. On the basis of the above-described reactivity of r*Ph*GshB cysteine residue(s) towards β-mercaptoethanol, the hypothesis was considered that GSSG acted through a covalent modification of the enzyme, such as the S-glutathionylation. To this aim, a sample of r*Ph*GshB was treated with 24 mM GSSG and then analysed by ESI/Q-TOF mass spectrometry. As shown in Fig. 7C, besides the less abundant peak with M_r 35 887.13, corresponding to the unmodified enzyme, other two more abundant peaks with M_r 36 192.15 and 36 497.10 indicated the presence of glutathionylated adducts on r*Ph*GshB. Indeed, the 305 Da and 610 Da extra masses are in perfect agreement with the presence of one or two mixed disulfides with glutathione, respectively. Therefore, r*Ph*GshB was the target of a covalent modification by GSSG, which could explain the irreversible inhibition of the enzyme.

Thermodependence and heat stability of r*Ph*GshB

In order to study the cold adaptation of r*Ph*GshB, the effect of temperature on the activity and stability was analysed. The kinetic parameters related to the affinity of r*Ph*GshB for ATP were determined in the 10–30 °C interval. As reported in Table 1, the enzyme was active even at 10 °C, a further prove of its cold adaptation; however, above 10 °C, a significant enhancement of the activity was observed. On the other hand, the effect of temperature on K_m for ATP was negligible, because the corresponding values ranged between 0.17 and 0.28 mM in the 10–30 °C interval. These data indicate that the catalytic efficiency of r*Ph*GshB significantly increased with temperature; for instance, a 3.3-fold enhancement of the

Table 1 Effect of temperature on the kinetic parameters of the ATPase activity of r*Ph*GshB

Temperature/°C	k_{cat}/s^{-1}	K_m for ATP/mM	$k_{cat}/K_m/s^{-1}$ mM^{-1}
10	0.87	0.17	5.1
15	1.85	0.26	7.1
20	2.42	0.18	13.4
25	4.72	0.28	16.9
28	4.99	0.21	23.8
30	5.32	0.18	29.6

Values of k_{cat} and K_m for ATP were calculated from Lineweaver–Burk plots realised on experiments carried out at the indicated temperatures as described in Fig. 6.

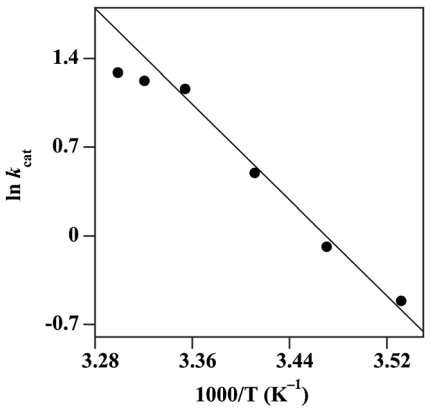

Fig. 8 Arrhenius plot of the ATPase activity of r*Ph*GshB. The k_{cat} values reported in Table 1 were analyzed according to the Arrhenius equation. A linear fit of the data was obtained in the 10–25 °C temperature interval.

k_{cat}/K_m ratio was calculated between 10 and 25 °C. The thermodependence of r*Ph*GshB was also evaluated through the Arrhenius plot of the k_{cat} values (Fig. 8). The plot was linear in the 10–25 °C interval and the calculated energy of activation (E_a) was 75.0 kJ mol^{-1}, a value unusually high for a psychrophilic enzyme. The other thermodynamic parameters of the ATPase reaction, calculated at 15 °C, are reported in Table 2.

The thermal stability of r*Ph*GshB was investigated through a heat inactivation profile. To this aim, aliquots of an enzyme sample were incubated for 10 min at different temperatures and then immediately cooled on ice. The residual ATPase activity of the treated samples was reported as a function of temperature and under these conditions the calculated temperature for half-inactivation ($T_{1/2}$) of r*Ph*GshB was 50.5 °C (Fig. 9). The heat stability of r*Ph*GshB was also investigated through inactivation kinetics realised at temperatures ranging between 45 °C and 54 °C. The heat inactivation of the enzyme followed first-order kinetics at each temperature and the corresponding inactivation rate constants (k_{in}) were treated according to the Arrhenius equation (Fig. 10). A linear plot was obtained in the chosen interval of temperature, thus allowing the determination of the energetic parameters of the heat inactivation process. The values of E_a, ΔH^*, ΔS^*, and ΔG^* are reported in Table 3. In particular, the value of E_a 208 kJ mol^{-1} is intermediate between those typically found for psychrophilic and mesophilic enzymes.

Table 2 Energy of activation and other thermodynamic parameters of the ATPase activity of r*Ph*GshB

Energetic parameters			
E_a/kJ mol^{-1}	ΔH^{*a}/kJ mol^{-1}	ΔS^{*a}/J mol^{-1} K^{-1}	ΔG^{*a}/kJ mol^{-1}
75.0	72.6	11.3	69.3

The energy of activation and the Arrhenius constant were derived from the experiment reported in Fig. 8. [a] Calculated at 15 °C.

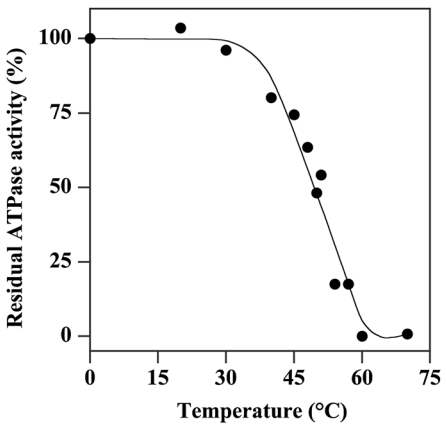

Fig. 9 Heat inactivation profile of r*Ph*GshB. A 1.0 μM solution of r*Ph*GshB in 20 mM Tris–HCl, pH 7.8 buffer, was incubated for 10 min at the indicated temperatures. After an ice-chilling for 30 min, the ATPase activity was measured at 15 °C in buffer C essentially as reported in Fig. 5 (specific radioactivity of [γ-^{32}P]ATP 3.30 cpm $pmol^{-1}$). The residual ATPase of the treated samples was expressed as a percentage of an untreated control kept at 0 °C.

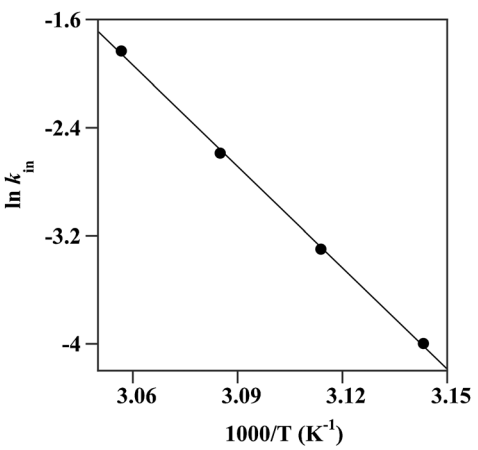

Fig. 10 Arrhenius plot of the heat inactivation process of r*Ph*GshB. The values of the rate constant of heat inactivation (k_{in}) were obtained from inactivation kinetics carried out at 45, 48, 51 or 54 °C on a 1.0 μM solution of r*Ph*GshB in 20 mM Tris–HCl, pH 7.8 buffer. At selected times aliquots were withdrawn from the incubation and immediately chilled on ice for 30 min. The residual ATPase activity was measured at 15 °C in buffer C essentially as reported in Fig. 5 (specific radioactivity of [γ-^{32}P]ATP 1.97–3.06 cpm $pmol^{-1}$). After data analysis according to first-order kinetics, the k_{in} values were treated according to the Arrhenius equation.

Table 3 Activation energetic parameters of the heat inactivation process of r*Ph*GshB

Energetic parameters			
E_a/kJ mol^{-1}	ΔH^{*a}/kJ mol^{-1}	ΔS^{*a}/J mol^{-1} K^{-1}	ΔG^{*a}/kJ mol^{-1}
208.0	205.2	366.2	86.9

The energy of activation and the Arrhenius constant were derived from the experiment reported in Fig. 10. [a] Calculated at 50 °C.

Discussion

The psychrophile *P. haloplanktis* was chosen as a model source for the investigation on the enzyme mechanism leading to the GSH synthesis in a cold-adapted microorganism. Among the two steps leading to the GSH biosynthesis in *P. haloplanktis*, the present work deals with the reaction converting γ-Glu-Cys and glycine into GSH in the presence of ATP. The enzyme involved in this reaction is *Ph*GshB and therefore, its recombinant form was purified and characterised.

The ESI/Q-TOF mass spectrometry data on r*Ph*GshB purified under non-reducing or reducing conditions suggested the presence of reactive cysteine residues(s) in the enzyme, which underwent a covalent modification by β-mercaptoethanol. Interestingly, similar findings were reported for other enzymes involved in the control of the oxidative metabolism of *P. haloplanktis*, such as superoxide dismutase, modified by either β-mercaptoethanol[37] or oxidised glutathione,[27] and thioredoxin reductase modified by oxidised glutathione.[28]

Concerning the molecular organization of r*Ph*GshB, the elution profiles on gel filtration chromatography under non-denaturing conditions suggested that the enzyme was apparently organised as a homotetramer or a homodimer at high or low protein concentration, respectively. This behaviour suggests that the assemblage of four subunits into a homotetramer is a two-step process: in the first one, strong interactions between subunits lead to stable homodimers, whereas in the second one weak interactions between homodimers allow the assemblage of poorly stable homotetramers. It has been reported that the corresponding GshB from *E. coli* is organised as a stable homotetramer.[43–45] However, it cannot be excluded that the poorly stable homotetramer of r*Ph*GshB at room temperature could become stable in the cold habitat of *P. haloplanktis*.

The study on the functional properties of r*Ph*GshB was faced with a convenient assay system, which measured the activity of the psychrophilic enzyme in the absence of other enzymes. The ATPase catalysed by r*Ph*GshB, likely coupled to the GSH synthesis, required the presence of both substrates, glycine and γ-Glu-Cys. The pH optimum ranged between 7.4 and 8.6, similarly to what found for the corresponding enzyme from *E. coli*.[42,45] Furthermore, the psychrophilic enzyme absolutely needed a divalent cation, such as Mg^{2+} or Mn^{2+}, a feature typical for ATP hydrolysing enzymes and observed also in *Ec*GshB;[42] among the two cations, Mg^{2+} was 2.4-fold more effective than Mn^{2+} at the respective optimal concentration. On the other hand, the monovalent cations Na^+ or K^+ were dispensable for the activity of r*Ph*GshB. Therefore, the halotolerance reported for other enzymes isolated from *P. haloplanktis*, such as α-amylase[46] or polynucleotide phosphorylase,[47] cannot be extended to r*Ph*GshB.

Table 4 Affinity of GshB for its substrates in various sources

	K_m/mM			
Source	ATP	γ-Glu-Cys	Gly	Ref.
Pseudoalteromonas haloplanktis	0.26	0.25	0.75	This work
Escherichia coli	0.24	0.24	0.91	49
Schizosaccharomyces pombe	0.45	0.27	0.67	50
Arabidopsis thaliana	0.057	0.039	1.51	51
Homo sapiens	0.07	0.66[a]	1.75	52

[a] The K_m was determined for γ-glutamyl-α-aminobutyrate, an analogue of γ-Glu-Cys.

In the fulfillment of its function, GshB interacts with three substrates, *i.e.* γ-Glu-Cys, glycine and ATP. The kinetic parameters of the r*Ph*GshB activity determined at 15 °C proved the catalytic efficiency of this enzyme at the optimum growth temperature of *P. haloplanktis*. For instance, the calculated k_{cat}/K_m referred to the steady-state measurement depending on the substrate ATP was 7.1 s^{-1} mM^{-1}, a value in the range of those reported for the corresponding enzyme from other sources at the respective working temperatures.[48–51] Concerning the affinity of r*Ph*GshB for its three substrates, the enzyme showed a higher K_m for glycine compared to γ-Glu-Cys or ATP. A comparison with the data from the corresponding enzyme from other sources is shown in Table 4. A noticeable similarity was found with the data from the mesophile *E. coli*[48] or the lower eukaryote *S. pombe*,[49] including the lower affinity for glycine. In higher eukaryotes, such as *A. thaliana*[50] or humans,[51] an improvement of the affinity for ATP and a small reduction of that for glycine made more evident the different affinities among these substrates.

The studies on the effects of GSH and GSSG on the activity of r*Ph*GshB indicated a significantly higher inhibition by GSSG compared to that exerted by GSH, a feature somehow similar to that reported for GshB from *E. coli*, even though in that case GSH was essentially ineffective.[42] Also the comparison of the K_i for GSSG pointed to a moderate similarity between the psychrophilic and mesophilic enzyme, the corresponding values being 10.7 mM and 4.4 mM, respectively. Our studies demonstrate that GSSG is as an irreversible inhibitor of r*Ph*GshB acting through the covalent modification of the enzyme; in particular, one or even two glutathionylated adducts were found on the enzyme, a finding confirming the sulfhydryl reactivity of the *P. haloplanktis* enzymes involved in the redox regulation of this psychrophile. The high reactivity of the cysteine residues is relevant for the regulation of the properties of the target proteins. In the case of Fe-SOD from *P. haloplanktis*, the covalent modification attenuated the sensitivity of the enzyme to peroxynitrite inactivation, without a significant variation of the enzyme activity;[27] in this work, the formation of covalent adducts by GSSG on r*Ph*GshB led to its irreversible inhibition.

The investigation on the thermodependence of r*Ph*GshB proved that the enzyme had a significant activity already at 10 °C, a property required for its cold-adaptation. When evaluating the effect of temperature on the kinetic parameters of r*Ph*GshB, the affinity for ATP remained essentially unchanged,

whereas the rate of ATP hydrolysis underwent a significant improvement up to 25 °C. This led to an unusual high value of E_a, a finding suggesting that the psychrophilic enzymes involved in the response to stress conditions display a thermal behaviour characterised by a high thermodependence. Interestingly, a similar finding was reported for another enzyme involved in the response to stress conditions, such as polynucleotide phosphorylase from *P. haloplanktis*.[47] This observation makes these macromolecules different from the other cold-adapted enzymes, as these latter are generally characterised by a low thermodependence.

The reduced improvement of the ATPase activity above 25 °C prompted an evaluation on the heat stability of r*Ph*GshB. The heat inactivation profile of r*Ph*GshB indicated that the enzyme possesses a discrete heat resistance, as evaluated from its $T_{1/2}$ value well above 25 °C, a behaviour already reported for other psychrophilic enzymes involved in the control of the redox homeostasis.[37,39,52] Therefore, other explanations must be invoked for the loss of linearity in the Arrhenius plot at temperatures higher than 25 °C. The enzyme interacts with three substrates during its catalytic mechanism; therefore, a temperature-dependence of the rate for the accommodation of the three substrates in the active site of the enzyme, or for the expulsion of the products, cannot be excluded. The enzyme could have a lower heat resistance, when measuring its catalysis rate at increasing temperatures, even considering the high flexibility usually displayed by psychrophilic enzymes.[53] Another explanation resides in the possible conversion from an active homotetramer to a less active homodimer, a process eventually more evident at temperatures higher than 25 °C. The moderate heat resistance of the psychrophilic enzyme was further investigated with the determination of the energetic parameters of the heat inactivation process. The calculated E_a is intermediate between the values typically found for psychrophilic and mesophilic enzymes. The thermodynamic parameters of the heat inactivation process point to a low enthalpic barrier accompanied to a significantly favourable entropic factor.

Conclusions

To our knowledge, this work represents the first contribution to the characterization of an enzyme involved in the GSH biosynthesis from a cold-adapted source. The studies on the psychrophilic glutathione synthetase from *P. haloplanktis* have been focused on some biochemical properties, such as pH, ionic strength, thermodependence, which are relevant to the growth habitat of this microorganism. Another enzyme, glutamyl-cysteine ligase, participates in GSH biosynthesis and future research will be devoted to the characterization of this activity in *P. haloplanktis*. The reconstitution of the complete system for the synthesis of this cellular thiol in *P. haloplanktis* will represent an essential tool in studies concerning its possible involvement in the regulation of growth and survival of this microorganism. Furthermore, the genome of this psychrophile contains the putative genes encoding other enzymes involved in the glutathione metabolism, such as glutathione peroxidase (ID 3710067), glutathione reductase (ID 3707989), glutathione *S*-transferase (ID 3708685) and γ-glutamyl transpeptidase (ID 3709451). Concerning this latter enzyme, its activity in thermophilic sources was already demonstrated.[54,55] It would be interesting to establish if the whole γ-glutamyl cycle, including biosynthesis and hydrolysis of glutathione, works also in sources adapted from cold to hot temperatures. Finally, the high reactivity of some cysteine residues possessed by GshB and other key enzymes controlling the redox homeostasis of *P. haloplanktis* opens the question on a possible common cold adaptation strategy of this psychrophile based on the modification of specific cysteine residues.

Acknowledgements

This work was supported by grants from PRIN 2009, Rome (Italy), awarded to Mariorosario Masullo and Emmanuele De Vendittis.

References

1 A. Meister and M. E. Anderson, *Annu. Rev. Biochem.*, 1983, **52**, 711–760.
2 R. C. Fahey, G. L. Newton, B. Arrick, T. Overdank-Bogart and S. B. Aley, *Science*, 1984, **224**, 70–72.
3 M. J. May, T. Vernoux, C. Leaver, M. Van Montagu and D. Inzé, *J. Exp. Bot.*, 1998, **49**, 649–667.
4 M. E. Anderson, *Chem.-Biol. Interact.*, 1998, **111–112**, 1–14.
5 I. Rahaman and W. MacNee, *Eur. Respir. J.*, 2000, **16**, 534–554.
6 R. C. Fahey, W. C. Brown, W. B. Adams and M. B. Worsham, *J. Bacteriol.*, 1978, **133**, 1126–1129.
7 R. C. Fahey and A. R. Sundquist, *Adv. Enzymol. Relat. Areas Mol. Biol.*, 1991, **64**, 1–53.
8 M. J. Penninckx and M. T. Elskens, *Adv. Microb. Physiol.*, 1993, **34**, 239–301.
9 G. L. Newton, K. Arnold, M. S. Price, C. Sherrill, S. B. Delcardayre, Y. Aharonowitz, G. Cohen, J. Davies, R. C. Fahey and C. Davis, *J. Bacteriol.*, 1996, **178**, 1990–1995.
10 L. Masip, K. Veeravalli and G. Georgiou, *Antioxid. Redox Signaling*, 2006, **8**, 753–762.
11 J. A. Thomas, B. Poland and R. Honzatko, *Arch. Biochem. Biophys.*, 1995, **319**, 1–9.
12 P. Klatt and S. Lamas, *Eur. J. Biochem.*, 2000, **267**, 4928–4944.
13 I. Dalle Donne, R. Rossi, G. Colombo, D. Giustarini and A. Milzani, *Trends Biochem. Sci.*, 2009, **34**, 85–96.
14 B. E. Janowiak and O. W. Griffith, *J. Biol. Chem.*, 2005, **280**, 11829–11839.
15 S. Gopal, I. Borovok, A. Ofer, M. Yanku, G. Cohen, W. Goebel, J. Kreft and Y. Aharonowitz, *J. Bacteriol.*, 2005, **187**, 3839–3847.
16 B. Vergauwen, D. De Vos and J. J. Van Beeumen, *J. Biol. Chem.*, 2006, **281**, 4380–4394.
17 O. W. Griffith and R. T. Mulcahy, *Adv. Enzymol. Relat. Areas Mol. Biol.*, 1999, **73**, 209–267.
18 P. G. Richman and A. Meister, *J. Biol. Chem.*, 1975, **250**, 1422–1426.
19 S. R. Soltaninassab, K. R. Sekhar, M. J. Meredith and M. L. Freeman, *J. Cell. Physiol.*, 2000, **182**, 163–170.
20 J. J. Abbott, J. Pei, J. L. Ford, Y. Qi, V. N. Grishin, L. A. Pitcher, M. A. Phillips and N. V. Grishin, *J. Biol. Chem.*, 2001, **276**, 42099–42107.
21 B. S. Kelly, W. E. Antholine and O. W. Griffith, *J. Biol. Chem.*, 2002, **277**, 50–58.
22 M. Orlowski and A. Meister, *Biochemistry*, 1971, **10**, 372–380.
23 J. A. Chesney, J. W. Eaton and J. R. Mahoney, Jr., *J. Bacteriol.*, 1996, **178**, 2131–2135.
24 J. T. Greenberg and B. Demple, *J. Bacteriol.*, 1986, **168**, 1026–1029.
25 C. Sherrill and R. C. Fahey, *J. Bacteriol.*, 1998, **180**, 1454–1459.
26 C. Medigue, E. Krin, G. Pascal, V. Barbe, A. Bernsel, P. N. Bertin, F. Cheung, S. Cruveiller, S. D'Amico, A. Duilio, G. Fang, G. Feller, C. Ho, S. Mangenot, G. Marino, J. Nilsson, E. Parrilli, E. P. Rocha, Z. Rouy, A. Sekowska, M. L. Tutino, D. Vallenet, G. von Heijne and A. Danchin, *Genome Res.*, 2005, **15**, 1325–1335.

27 I. Castellano, M. R. Ruocco, F. Cecere, A. Di Maro, A. Chambery, A. Michniewicz, G. Parlato, M. Masullo and E. De Vendittis, *Biochim. Biophys. Acta*, 2008, **1784**, 816–826.
28 P. Falasca, G. Evangelista, R. Cotugno, S. Marco, M. Masullo, E. De Vendittis and G. Raimo, *Extremophiles*, 2012, **16**, 539–552.
29 M. Masullo, P. Arcari, B. de Paola, A. Parmeggiani and V. Bocchini, *Biochemistry*, 2000, **39**, 15531–15539.
30 J. Sambrook, E. F. Fritsch and T. Maniatis, *Molecular cloning: a laboratory manual*, Cold Spring Harbor, Laboratory Press, New York, 2nd edn, 1989.
31 A. Merlino, I. Russo Krauss, A. Albino, A. Pica, A. Vergara, M. Masullo, E. De Vendittis and F. Sica, *Int. J. Mol. Sci.*, 2011, **12**, 6312–6319.
32 G. Sander, R. C. Marsh, J. Voigt and A. Parmeggiani, *Biochemistry*, 1975, **14**, 1805–1814.
33 I. Castellano, F. Cecere, A. De Vendittis, R. Cotugno, A. Chambery, A. Di Maro, A. Michniewicz, G. Parlato, M. Masullo, E. V. Avvedimento, E. De Vendittis and M. R. Ruocco, *Biopolymers*, 2009, **91**, 1215–1226.
34 M. M. Bradford, *Anal. Biochem.*, 1976, **72**, 248–254.
35 U. K. Laemmli, *Nature*, 1970, **227**, 680–685.
36 R. Dosi, A. Di Maro, A. Chambery, G. Colonna, S. Costantini, G. Geraci and A. Parente, *Comp. Biochem. Physiol., Part B: Biochem. Mol. Biol.*, 2006, **145**, 230–238.
37 I. Castellano, A. Di Maro, M. R. Ruocco, A. Chambery, A. Parente, M. T. Di Martino, G. Parlato, M. Masullo and E. De Vendittis, *Biochimie*, 2006, **88**, 1377–1389.
38 T. E. Creighton, in *Protein structure a practical approach*, ed. T. E. Creighton, Oxford University Press, Oxford, UK, 1989, pp. 155–167.
39 R. Cotugno, M. R. Ruocco, S. Marco, P. Falasca, G. Evangelista, G. Raimo, A. Chambery, A. Di Maro, M. Masullo and E. De Vendittis, *Mol. BioSyst.*, 2009, **5**, 519–528.
40 G. F. Seelig and A. Meister, *Methods Enzymol.*, 1985, **113**, 379–390.
41 M. M. Corsaro, R. Lanzetta, E. Parrilli, M. Parrilli, M. L. Tutino and S. Ummarino, *J. Bacteriol.*, 2004, **186**, 29–34.
42 H. Gushima, T. Miya, K. Murata and A. Kimura, *J. Appl. Biochem.*, 1983, **5**, 210–218.
43 H. Yamaguchi, H. Kato, Y. Hata, T. Nishioka, A. Kimura, J. Oda and Y. Katsube, *J. Mol. Biol.*, 1993, **229**, 1083–1100.
44 T. Hara, H. Kato, Y. Katsube and J. Oda, *Biochemistry*, 1996, **35**, 11967–11974.
45 K. Matsuda, K. Mizuguchi, T. Nishioka, H. Kato, N. Go and J. Oda, *Protein Eng.*, 1996, **9**, 1083–1092.
46 S. Srimathi, G. Jayaraman, G. Feller, B. Danielsson and P. R. Narayanan, *Extremophiles*, 2007, **11**, 505–515.
47 G. Evangelista, P. Falasca, I. Ruggiero, M. Masullo and G. Raimo, *Protein Pept. Lett.*, 2009, **16**, 999–1005.
48 T. Tanaka, T. Nishioka and J. Oda, *Arch. Biochem. Biophys.*, 1997, **339**, 151–156.
49 C. W. Nakagawa, N. Mutoh and Y. Hayashi, *Biochem. Cell Biol.*, 1993, **71**, 447–453.
50 J. M. Jez and R. E. Cahoon, *J. Biol. Chem.*, 2004, **279**, 42726–42731.
51 A. Dinescu, T. R. Cundari, V. S. Bhansali, J. L. Luo and M. E. Anderson, *J. Biol. Chem.*, 2004, **279**, 22412–22421.
52 A. Merlino, I. Russo Krauss, I. Castellano, E. De Vendittis, B. Rossi, M. Conte, A. Vergara and F. Sica, *J. Struct. Biol.*, 2010, **172**, 343–352.
53 A. D'Amico, T. Collins, J. C. Marx, G. Feller and C. Gerday, *EMBO Rep.*, 2006, **7**, 385–389.
54 I. Castellano, A. Merlino, M. Rossi and F. La Cara, *Biochimie*, 2010, **92**, 464–474.
55 I. Castellano, A. Di Salle, A. Merlino, M. Rossi and F. La Cara, *Extremophiles*, 2011, **15**, 259–270.

Extremophiles (2012) 16:539–552
DOI 10.1007/s00792-012-0453-0

ORIGINAL PAPER

Properties of the endogenous components of the thioredoxin system in the psychrophilic eubacterium *Pseudoalteromonas haloplanktis* TAC 125

Patrizia Falasca · Giovanna Evangelista · Roberta Cotugno · Salvatore Marco · Mariorosario Masullo · Emmanuele De Vendittis · Gennaro Raimo

Received: 29 April 2011 / Accepted: 2 April 2012 / Published online: 22 April 2012

Abstract The endogenous components of the thioredoxin system in the Antarctic eubacterium *Pseudoalteromonas haloplanktis* have been purified and characterised. The temperature dependence of the activities sustained by thioredoxin (*Ph*Trx) and thioredoxin reductase (*Ph*TrxR) pointed to their adaptation in the cold growth environment. *Ph*TrxR was purified as a flavoenzyme and its activity was significantly enhanced in the presence of molar concentration of monovalent cations. The energetics of the partial reactions leading to the whole electron transfer from NADPH to the target protein substrate in the reconstituted thioredoxin system was also investigated. While the initial electron transfer from NADPH to *Ph*TrxR was energetically favoured, the final passage to the heterologous protein substrate enhanced the energetic barrier of the whole process. The energy of activation of the heat inactivation process essentially reflected the psychrophilic origin of *Ph*TrxR. Vice versa, *Ph*Trx possessed an exceptional heat resistance (half-life, 4.4 h at 95 °C), ranking this protein among the most thermostable enzymes reported so far in psychrophiles. *Ph*TrxR was covalently modified by glutathione, mainly by its oxidised or nitrosylated forms. A mutagenic analysis realised on three non catalytic cysteines of the flavoenzyme allowed the identification of C_{303} as the target for the S-glutathionylation reaction.

Keywords Thioredoxin system · Psychrophile · *Pseudoalteromonas haloplanktis* · Temperature adaptation · S-glutathionylation · Energetic parameters

Abbreviations

Ap	*Aeropyrum pernix*
Ec	*Escherichia coli*
Ph	*Pseudoalteromonas haloplanktis*
DTNB	5,5′-dithiobis-2-nitrobenzoic acid
DTT	Dithiothreitol
GSH	Reduced glutathione
GSSG	Oxidised glutathione
GSNO	Nitrosylated glutathione
PMSF	Phenylmethanesulphonyl fluoride
TNB	2-nitro-5-thiobenzoate
Trx	Thioredoxin
TrxR	Thioredoxin reductase
Trx-S_2 and Trx-$(SH)_2$	Oxidised and reduced form of Trx, respectively
k_{in}	Heat inactivation rate constant

Introduction

Proteins outside the cell or located on its surface are rich in disulphides, reflecting the oxidising conditions of the

Communicated by F. Robb.

Authors P. Falasca and G. Evangelista equally contributed to this work.

P. Falasca · G. Evangelista · G. Raimo (✉)
Dipartimento di Scienze e Tecnologie dell'Ambiente e del Territorio, Università del Molise, Contrada Fonte Lappone, 86090 Pesche, IS, Italy
e-mail: raimo@unimol.it

R. Cotugno · S. Marco · M. Masullo · E. De Vendittis (✉) · G. Raimo
Dipartimento di Biochimica e Biotecnologie Mediche, Università di Napoli Federico II, Via S. Pansini 5, 80131 Naples, Italy
e-mail: devendittis@dbbm.unina.it

M. Masullo
Dipartimento di Studi delle Istituzioni e dei Sistemi Territoriali, Università di Napoli "Parthenope", Via Medina 40, 80133 Naples, Italy

extracellular environment. In contrast, intracellular proteins containing disulphide bridges are rare because of the reducing properties of the cytosol (Gilbert 1990). The redox state of cysteine residues in intracellular proteins is controlled through thiol-disulphide exchange reactions triggered by specific enzyme systems displaying a fast and readily reversible activity (Holmgren 1985). This thiol redox control becomes crucial when the target cysteines have a specific role; indeed, this system is emerging as a major regulatory mechanism in either signal transduction or preservation of the reduced state of cytosolic proteins (Gilbert 1990). The thioredoxin system, composed by thioredoxin (Trx), thioredoxin reductase (TrxR) and NADPH is a key thiol-disulphide exchanger involved in maintaining target cytoplasmic proteins in their reduced state (Arnér and Holmgren 2000; Holmgren 1989). Both Trx and TrxR possess a conserved sequence with two neighbouring cysteines forming a reversible disulphide bridge essential for their functioning as redox exchangers. Indeed, TrxR catalyses the NADPH-dependent electrons transfer to the active disulphide of the oxidised form of Trx (Trx-S_2) to form a dithiol (reaction 1 in the mechanism shown below); then, the reduced form of Trx (Trx-$(SH)_2$) reduces the disulphide bridges eventually formed in target proteins (reaction 2).

$$\text{Trx-S}_2 + \text{NADPH} + \text{H}^+ \xrightarrow{\text{TrxR}} \text{Trx-(SH)}_2 + \text{NADP}^+ \quad \text{(reaction 1)}$$

$$\text{Trx-(SH)}_2 + \text{Protein-S}_2 \rightarrow \text{Trx-S}_2 + \text{Protein-(SH)}_2. \quad \text{(reaction 2)}$$

Trx, conserved among all organisms, is a small protein, with a typical CXXC active-site motif. The first target proteins of the Trx activity, identified in bacterial and eukaryotic cells, are ribonucleotide reductase, 3′-phosphoadenosine-5′-phosphosulphate reductase and methionine-sulphoxide reductase (Tsang and Schiff 1976; Ejiri et al. 1979). Furthermore, it has been shown that Trx is involved in the activation of DNA binding activity of transcription factors (Matthews et al. 1992) and that a dimeric form of Trx binds to and improves the high processivity of T7 DNA polymerase (Huber et al. 1987).

TrxR is a homodimeric enzyme containing an active-site motif similar to that of Trx. The enzyme binds one molecule of FAD in each subunit and uses NADPH as electron donor (Moore et al. 1964). The activity of TrxR is essential for ribonucleotide metabolism (Holmgren 1989), regulation of transcriptional activity (Schenk et al. 1994) and protein folding (Kern et al. 2003). On the basis of the differences in size, structure and catalytic mechanism, TrxR is usually grouped in two classes (Arscott et al. 1997): type I high molecular mass TrxR (55–58 kDa per subunit), isolated from higher eukaryotes (Gasdaska et al. 1999; Kanzok et al. 2001), and type II low molecular mass TrxR (around 35 kDa per subunit), isolated from lower eukaryotes (Chae et al. 1994) and prokaryotes (Williams 1995). Both types of TrxR are members of the large family of pyridine nucleotide disulphide oxidoreductases, including lipoamide dehydrogenase, glutathione reductase and mercuric reductase (Ghisla and Massey 1989).

In recent years, the mechanisms leading to the formation/breakdown of disulphide bridges in proteins have been examined also in extremophilic organisms (Jeon and Ishikawa 2002; Kashima and Ishikawa 2003; Ruocco et al. 2004; Ladenstein and Ren 2006; Grimaldi et al. 2008; Hernandez et al. 2008; Cotugno et al. 2009). In particular, the components of the thioredoxin system have been characterised in some (hyper)thermophilic archaea, such as *Sulfolobus solfataricus* (Ruocco et al. 2004; Grimaldi et al. 2008), *Aeropyrum pernix* (Jeon and Ishikawa 2002), *Pyrococcus horikoshii* (Kashima and Ishikawa 2003) and *Thermoplasma acidophilum* (Hernandez et al. 2008). The information available for the thioredoxin system in cold-adapted microorganisms is limited to a recent paper, describing the properties of recombinant forms of Trx and TrxR from the psychrotolerant eubacterium *Pseudoalteromonas haloplanktis* TAC 125 (r*Ph*Trx and r*Ph*TrxR, respectively; Cotugno et al. 2009). It is known that this microorganism, isolated from the Antarctic sea and able to grow in a broad range of temperatures (4–20 °C), adapts its biochemical machinery to functioning either in the cold or in moderate temperature conditions (Birolo et al. 2000; Medigue et al. 2005). In particular, *P. haloplanktis* is adapted to fast growth, because the marine habitat, which is full of plankton debris, represents a rich medium; furthermore, in laboratory conditions, it grows to very high density in the presence of sufficient nutrients and high aeration, thus indicating that respiration is particularly efficient in this bacterium and that protection against reactive oxygen species must be ensured (Medigue et al. 2005). *P. haloplanktis* is also well adapted to salts because of its marine habitat, and some enzymes isolated from this bacterium show a marked halophilicity (Srimathi et al. 2007; Evangelista et al. 2009). All these findings make *P. haloplanktis* a valuable model to study the environment-driven adaptation mechanisms. Concerning the thioredoxin system in *P. haloplanktis*, the analysis of the effect of temperature on the structure–function relationships of r*Ph*Trx and r*Ph*TrxR indicated a differential cold adaptation among these enzymes (Cotugno et al. 2009). A structural reason for cold adaptation of psychrophilic proteins was suggested on the basis of their amino acid composition, as psychrophilic proteins use smaller-size and less hydrophobic amino acid residues, compared to the corresponding mesophilic counterparts (De Vendittis et al. 2008).

To further investigate the cold adaptation of the thioredoxin system, this work describes the properties of the components of this system isolated from *P. haloplanktis* cell extracts. The different psychrophilic character of the purified proteins (*Ph*Trx and *Ph*TrxR) has been assessed. In addition, the study was focused on the effect of different monovalent cations on the activity of *Ph*TrxR. Furthermore, it was found that this enzyme is the target of a S-glutathionylation reaction, which, however, does not greatly affect its activity. Finally, a mutagenic analysis allowed the identification of the cysteine residue target of the S-glutathionylation reaction.

Materials and methods

Materials

The chromatographic columns MonoQ™ 5/50 GL, Hi Prep™ Phenyl FF 16/10, Superdex™ 75 10/30 HR and Superdex™ 200 10/300 GL were from GE Healthcare. The Q-Sepharose chromatographic media, phenylmethanesulphonyl fluoride (PMSF), 5,5′-dithiobis-2-nitrobenzoic acid (DTNB), $NADP^+$, NADPH, dithiothreitol (DTT), human insulin (10 mg mL^{-1} solution) and molecular weight protein standards for gel filtration were from Sigma-Aldrich. Electrophoretic materials were from Bio-Rad. All other chemicals were of analytical grade. Oligonucleotide synthesis and nucleotide sequencing were carried out by Primm (Italy).

The following buffers were used: buffer A, 20 mM Tris–HCl, pH 7.8; buffer B, 100 mM Tris–HCl, pH 7.8; buffer C, 100 mM potassium phosphate, pH 7.6, 10 mM EDTA; buffer D, 5 mM $MgCl_2$, 10 % glycerol in buffer A; buffer PBS, phosphate buffer saline containing 10 mM sodium phosphate, pH 7.2 and 150 mM NaCl.

Purification of thioredoxin reductase and thioredoxin from *Pseudoalteromonas haloplanktis*

P. haloplanktis cells (50 g wet weight), grown in Luria–Bertani medium at 4 °C for 3 days (Masullo et al. 2000), were collected by centrifugation at 3000×*g* for 60 min at 4 °C and then resuspended in 150 mL buffer D supplemented with 1 mM PMSF. Cells were then disrupted by two passages through a Constant cell disruption system (Constant Systems Ltd., UK) at 1.5 MPa and the suspension was centrifuged at 30,000×*g* for 60 min at 4 °C to obtain the cell extract (S-30). This sample was ultra-centrifuged at 100,000×*g* for 2.5 h at 4 °C to obtain the soluble protein fraction (S-100). After extensive dialysis against buffer A, the S-100 was applied to a Q-Sepharose Fast-Flow column (1.6 × 60 cm) equilibrated with the same buffer. The column was washed with buffer A to remove unbound proteins; afterwards, bound proteins were eluted by a linear 0–450 mM NaCl gradient in buffer A (total volume 1200 mL) at a flow rate of 2 mL min^{-1}. Fractions were checked for Trx and TrxR activity, which eluted at a different NaCl concentration; in particular, the endogenous TrxR and Trx from *P. haloplanktis* (*Ph*TrxR and *Ph*Trx, respectively) eluted at 250–280 mM and 350–400 mM NaCl, respectively. To evaluate protein purity, the active fractions were also analysed by SDS-PAGE.

In order to purify *Ph*TrxR, fractions containing this activity were pooled together and dialysed against buffer A supplemented with 600 mM $(NH_4)_2SO_4$ and then applied to a Hi Prep™ Phenyl FF 16/10 column, equilibrated with the same buffer. Bound proteins were eluted by a linear 600–20 mM $(NH_4)_2SO_4$ inverse gradient in buffer A (total volume 480 mL) at a flow rate of 2 mL min^{-1}. Active fractions were dialysed against buffer A supplemented with 150 mM NaCl and loaded onto a Mono Q™ 5/50 GL, equilibrated with the same buffer. *Ph*TrxR was eluted by a linear 150–500 mM NaCl gradient in buffer A (70 mL total volume) at a flow rate of 1 mL min^{-1}.

For the purification of *Ph*Trx, fractions from the Q-Sepharose chromatography containing this activity were pooled together, concentrated and then loaded onto a Superdex 200 10/300 GL column equilibrated with buffer A supplemented with 100 mM NaCl, at a flow rate of 0.75 mL min^{-1}. The fractions displaying *Ph*TrxR or *Ph*Trx activity in the respective last chromatographic step, and showing a single protein band on SDS-PAGE, were pooled together, concentrated, dialysed against buffer A supplemented with 50 % glycerol and stored at −20 °C until use. Following this procedure, nearly 3 mg of pure *Ph*TrxR and 2 mg of pure *Ph*Trx from 50 g of wet cells were obtained.

Enzymatic assays

Enzymatic assays were carried out using a Cary 50 spectrophotometer (Varian), equipped with an electronic temperature controller. The activity of *Ph*TrxR was determined by the DTNB reduction method (Luthman and Holmgren 1982). Briefly, the reaction mixture contained 5 mM DTNB and appropriate amounts of *Ph*TrxR in 1 mL final volume buffer C. Unless otherwise indicated, the assay was carried out at 20 °C and started by the addition of 250 μM final concentration of NADPH. The reaction was followed kinetically by measuring the increase of the absorbance at 412 nm, due to the formation of TNB ($\varepsilon_M = 13.6$ mM^{-1} cm^{-1}). Blanks run in the absence of *Ph*TrxR were subtracted. One unit (U) of *Ph*TrxR activity was defined as the amount of enzyme that caused the conversion of 1 μmol DTNB in 1 min. The specific activity of *Ph*TrxR was expressed as U mg^{-1}.

The activity of the *Ph*Trx was determined by the insulin precipitation method (Holmgren 1979a). The standard assay mixture contained 0.13 mM human insulin and 0.5–15 μM *Ph*Trx in 700 μL final volume buffer C. The reaction was carried out at 20 °C and began with the addition of DTT at 0.5 mM final concentration. The increase of absorbance, due to precipitation of the reduced *β*-chain of insulin, was monitored at 650 nm up to 60 min, to determine the rate of insulin reduction in the linear part of the increase. The activity of *Ph*Trx was expressed as arbitrary units, corresponding to the value of ΔE_{650} min^{-1}.

In order to evaluate the combined activity of *Ph*TrxR and *Ph*Trx in the reconstituted thioredoxin system, 1μM *Ph*TrxR was added to a reaction mixture containing 1–20 μM *Ph*Trx and 0.13 mM human insulin in 700 μL final volume buffer C. The reaction started by the addition of NADPH at 200 μM final concentration and was followed at 20 °C monitoring the insulin precipitation at 650 nm and, when indicated, also the NADPH consumption at 340 nm (Holmgren 1979b; Spyrou et al. 1997); the values of ΔE_{340} min^{-1} were measured in the linear range of the reaction, where no interference occurred by the insulin precipitation (ΔE_{650} min^{-1}).

The kinetic parameters of the *Ph*TrxR reaction were derived at different temperatures from either the DTNB reduction or the insulin precipitation method in the reconstituted thioredoxin system. In the first assay the DTNB concentration ranged between 0.15 and 5 mM, whereas in the second one the *Ph*Trx concentration varied between 0.5 and 15 μM; a fixed *Ph*TrxR concentration of 0.12 or 1.03 μM was used in the first and second assay, respectively. The activity data were analysed by the Lineweaver–Burk method.

To determine the redox potential of the *P. haloplanktis* thioredoxin system, the reversibility of the NADPH-dependent reduction of *Ph*Trx catalysed by *Ph*TrxR in the absence of insulin was evaluated according to reaction 1. The assay was carried out at 25 °C as previously described (Krause et al. 1991; Jeon and Ishikawa 2002). In particular, the reaction mixture contained 60 μg *Ph*Trx (in its initial *Ph*Trx-S_2 form) and 50 μM NADPH in 500 μL final volume buffer A. The value of the redox potential ($E^{0\prime}_{(PhTrx)}$) was calculated according to the Nernst equation upon the sequential addition of 50 nM *Ph*TrxR and 1.2 mM $NADP^+$. The detailed procedure was previously reported (Cotugno et al. 2009). A value of −0.315 V was used for the $E^{0\prime}_{(NADP^+)}$ (Clark 1960).

Temperature-dependence studies on *Ph*TrxR and *Ph*Trx

The study of the temperature dependence of the reactions catalysed by *Ph*TrxR and *Ph*Trx, tested individually or in combination, was realised by determining the initial rate of the corresponding reactions from kinetics carried out at different temperatures, using the same protocol described in the previous paragraph. Data were analysed through the Arrhenius equation to obtain the activation energetic parameters of the reactions.

The thermal stability of *Ph*TrxR was evaluated by measuring the residual DTNB reduction activity after the incubation of enzyme samples at different temperatures. The rate constants of heat inactivation (k_{in}) were derived from a first order analysis of the residual activity. The k_{in} values (s^{-1}) were then analysed according to the Arrhenius equation to obtain the energetic parameters of the heat inactivation process.

Fluorescence-melting curves were obtained in the temperature interval 5–75 °C, using a computer-assisted Cary Eclipse Spectrofluorimeter (Varian) equipped with an electronic temperature controller. The increase in temperature was set at 0.2 °C min^{-1}, and the emission in the aromatic region was monitored at every degree centigrade, using 280 and 345 nm for excitation and emission wavelength, respectively. Excitation and emission slits were both set at 10 nm and the samples were analysed in 500 μl stoppered cuvettes. Values of fluorescence intensity were subtracted for blanks run in the absence of the protein, corrected for temperature quenching, normalised between 0 and 100 %, and plotted versus temperature (Ruocco et al. 2004).

The heat stability of *Ph*Trx was investigated through inactivation kinetics carried out at 95 °C. The residual *Ph*Trx activity was determined at 20 °C by the insulin reduction method, using DTT as electron donor. The rate of insulin precipitation was compared to that measured on untreated *Ph*Trx samples kept at 0 °C.

Parameters related to the amino acid composition of Trx and TrxR

The Trx and TrxR sequences were obtained (http://www.ncbi.nlm.nih.gov or http://www.expasy.ch) from microorganisms belonging to the eubacterial or archaeal kingdom and covering optimum growth temperatures from 7 to 103 °C; the list, including 42 microbial sources, was identical to that described in a previous work (De Vendittis et al. 2008). The number of proteins analysed (71 Trx and 45 TrxR) considered putative redundant isoforms, mainly for Trx; on the other hand, in some of the sources a canonic Trx or TrxR was apparently absent. The data of average mass and hydrophobicity per amino acid residue were obtained as previously reported (De Vendittis et al. 2008). The dependence of the average parameter on the growth temperature was evaluated as a linear curve fit of the data ($y = a + b\ x$) obtained with the least-squares method in which y represents the value of the average parameter,

a the intercept at 0 °C, *b* the slope of the equation and *x* the optimum growth temperature of the source. The correlation of the data was estimated from the correlation coefficient *r*; the significance test included the calculation of the *t* Student parameter and the level was estimated by *p*.

Production of Cys → Ser mutants of *Ph*TrxR

The production of a recombinant form of *Ph*TrxR (r*Ph*TrxR) through the expression vector v*Ph*TrxR was previously described (Cotugno et al. 2009). Besides the two cysteine residues (C_{136} and C_{139}) engaged in the disulphide bridge of its active site, *Ph*TrxR possesses three other cysteines (C_7, C_{106} and C_{303}) as free thiols. In order to replace each of these residues with Ser, a site-directed mutagenesis was conducted on the vector v*Ph*TrxR, using the following pairs of oligonucleotides, in which the base mismatch introduced to create the desired amino acid replacement is italicised. In particular, primers for C_7S substitution were 5′-d-G_7AA·GCA·AAA·CAT·*A*GT·AAG·TTA·CTT·ATT·TTA·GGC_{39}-3′ and 5′-d-G_{39}CC·TAA·AAT·AAG·TAA·CTT·AC*T*·ATG·TTT·TGC·TTC_7-3′; primers for $C_{106}S$ substitution were 5′-d-G_{340}GC·ACT·TAC·ACC·*A*GT·GAC·GCA·CTA·ATC·ATT·GC_{372}-3′ and 5′-d-G_{372}C·AAT·GAT·TAG·TGC·GTC·AC*T*·GGT·GTA·AGT·GCC_{340}-3′; primers for $C_{303}S$ substitution were 5′-d-G_{892}CC·GGA·ACA·GGT·*A*GT·ATG·GCA·GCA·TTA·GAT·GC_{923}-3′ and 5′-d-G_{923}C·ATC·TAA·TGC·TGC·CAT·AC*T*·ACC·TGT·TCC·GGC_{892}-3′. The PCR, containing the v*Ph*TrxR as template, the specific primers and the *PfuTurbo*™ DNA polymerase, was carried out according to the protocol of the QuikChange™ Site-Directed Mutagenesis Kit (Stratagene). The correct substitutions and the absence of other undesired mutations were confirmed by sequence analysis. After transformation of BL21(DE3) with the mutant plasmids, purification of the corresponding heterologous products, named C_7S-*Ph*TrxR, $C_{106}S$-*Ph*TrxR and $C_{303}S$-*Ph*TrxR, was obtained as described for r*Ph*TrxR (Cotugno et al. 2009).

S-glutathionylation reaction

The reaction of S-glutathionylation was carried out as previously described (Castellano et al. 2008). Briefly, a 6.6-μM solution of *Ph*TrxR or its recombinant and mutated forms in buffer A was incubated at room temperature for 1 h with increasing concentration of reduced glutathione (GSH), oxidised glutathione (GSSG) or S-nitrosoglutathione (GSNO) up to 10 mM. After incubation, the unbound glutathione forms were removed by ultrafiltration on Microcon-3 (Amicon) and the protein concentration of each sample was determined; aliquots were then run on SDS-PAGE under non reducing conditions. After SDS-PAGE, the protein samples were blotted onto an Immobilon P membrane (Millipore) and analysed by Western blotting using anti-glutathione monoclonal antibodies (Chemicon), as previously reported (Castellano et al. 2008).

Other methods

Protein purity was evaluated by SDS-PAGE according to standard protocols (Laemmli 1970). The molecular mass of *Ph*TrxR and *Ph*Trx under denaturing conditions was determined by SDS-PAGE on 12 and 15 % polyacrylamide gels, respectively. The molecular mass under non denaturing conditions was estimated by gel filtration on Superdex™ 75 10/30 HR connected to a computer-assisted FPLC apparatus (GE Healthcare). The column was equilibrated at 4 °C with buffer A supplemented with 100 mM NaCl at a flow rate of 0.5 mL min^{-1}. Protein concentration was determined by the method of Bradford (1976), using bovine serum albumin as standard. Fluorimetric measurements for the determination of the amount of FAD bound to *Ph*TrxR were realised on a Cary Eclipse fluorescence spectrophotometer (Varian), according to the protocol previously described (Cotugno et al. 2009).

Results

Molecular properties of *Ph*TrxR and *Ph*Trx

The endogenous components of the thioredoxin system, *Ph*TrxR and *Ph*Trx, were isolated from a cell extract of *P. haloplanktis*. Under denaturing conditions, the molecular mass of *Ph*TrxR and *Ph*Trx was 34 and 12 kDa, respectively (not shown). These values are in good agreement with the theoretical values deduced from the amino acid sequence of *Ph*TrxR (33.8 kDa) and *Ph*Trx (11.9 kDa), respectively (Medigue et al. 2005). In order to get information on their structural organisation, the molecular mass of the psychrophilic proteins was also determined by gel filtration under non-denaturing conditions. Both *Ph*TrxR and *Ph*Trx eluted as single symmetric peaks and the molecular mass of *Ph*TrxR was 68 kDa (not shown), thus clearly indicating that *Ph*TrxR has a homodimeric organisation, as usually observed for other members of class II TrxR (Hirt et al. 2002; Windle et al. 2000); the molecular mass of *Ph*Trx was 14 kDa, a value roughly similar to that obtained under denaturing conditions. Therefore, *Ph*Trx should act as a monomeric protein, a feature typically observed for most of the Trx known to date (Jeon and Ishikawa 2002; Windle et al. 2000).

In the recombinant *Ph*TrxR (r*Ph*TrxR) it has been reported that a stoichiometric FAD/r*Ph*TrxR ratio, ranging between 0.92 and 0.98, is essential for full activity of

r*Ph*TrxR (Cotugno et al. 2009). However, this ratio was reached only upon the addition of exogenous FAD. The amount of flavin cofactor bound to the endogenous *Ph*TrxR was measured and the calculated molar ratio was 0.67. Although understoichiometric, the FAD/*Ph*TrxR ratio was sufficient for evaluating the enzyme functionality; on the other hand, the flavin content reflected the FAD uptake during the *P. haloplanktis* growth. Therefore, the addition of exogenous FAD during purification of *Ph*TrxR was not considered, to avoid a possible alteration of the functionality assay.

Functionality of the endogenous components of the thioredoxin system in *P. haloplanktis*

The functionality of *Ph*TrxR and *Ph*Trx was analysed in different assays, to assess that each endogenous component of the thioredoxin system from *P. haloplanktis* was purified in its active native form. The activity of *Ph*TrxR was first measured with the synthetic substrate DTNB, using a reaction temperature of 20 °C, corresponding to the maximum growth temperature tolerated by *P. haloplanktis*. In particular, the kinetic parameters of the reduction reaction (k_{cat}, 3 s^{-1}; K_M for DTNB, 2.6 mM), although not coincident with those previously reported for the recombinant *Ph*TrxR (k_{cat}, 6.9 s^{-1}; K_M for DTNB, 1.9 mM; Cotugno et al. 2009), indicate that the enzyme was purified in its active form. The difference could be explained with the understoichiometric FAD/*Ph*TrxR ratio found in the endogenous flavoenzyme.

Concerning *Ph*Trx, its activity was measured at 20 °C with the insulin precipitation method in the presence of DTT as electron donor. The rate of insulin reduction progressively increased upon addition of increasing amounts of *Ph*Trx (Fig. 1); concomitantly, the lag phase in the insulin precipitation progressively decreased. Under these conditions, the apparent maximum rate of the reaction was 0.040 ΔE_{650} min^{-1} and the *Ph*Trx concentration leading to half maximal rate was 5 μM. These values indicate that also *Ph*Trx was purified in its active form.

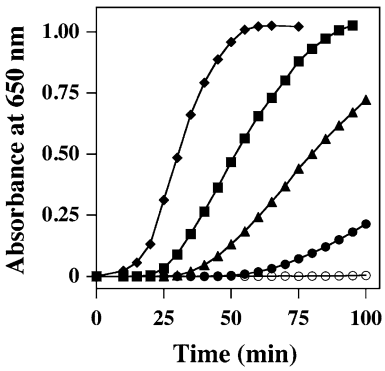

Fig. 1 Thiol-disulphide oxidoreductase activity of *Ph*Trx at 20 °C. The activity was measured with a continuous monitoring of the absorbance at 650 nm either in the absence (*open circle*) or in the presence of 0.9 μM *Ph*Trx (*filled circle*), 2.2 μM *Ph*Trx (*filled triangle*), 4.4 μM *Ph*Trx (*filled square*), 8.9 μM *Ph*Trx (*filled diamond*)

The availability of both endogenous components of the thioredoxin system of *P. haloplanktis* allowed an evaluation of their combined functionality in a reconstituted assay containing *Ph*TrxR, *Ph*Trx, NADPH as electron donor and human insulin as the thioredoxin substrate. The K_M found for *Ph*Trx was 2 μM, a value indicating the efficient interaction between the two thioredoxin components.

The full reversibility of the electron transfer between *Ph*TrxR and *Ph*Trx in the presence of NADPH/$NADP^+$ was evaluated at 25 °C in the reconstituted thioredoxin system without insulin (not shown). The reaction was fully reversible and then associable to a cyclic process, thus confirming both the functionality and the composition of the thioredoxin system in *P. haloplanktis*. Moreover, this procedure allowed the evaluation of the redox potential of the *Ph*Trx$(SH)_2$/*Ph*TrxS_2 pair through the Nernst equation and the calculated $E^{0\prime}_{(PhTrx)}$ was −289 mV, a value indicating the reducing power of the psychrophilic thioredoxin system.

Effect of monovalent cations on the *Ph*TrxR activity

The effect of chloride salts of selected monovalent cations on the DTNB reduction activity of *Ph*TrxR was investigated. As shown in Fig. 2, all these salts were able to stimulate the activity of *Ph*TrxR, although to a different extent. Among the salts used, NaCl at 0.5-M final

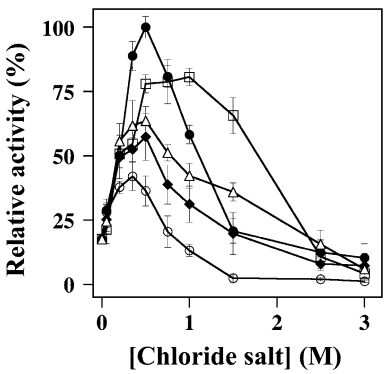

Fig. 2 Effect of monovalent cations on the activity of *Ph*TrxR. The DTNB reduction activity at 20 °C of 0.15 μ M *Ph*TrxR was measured in the absence or in the presence of the indicated concentration of chloride salts of the following monovalent cations: Na^+ (*filled circle*), K^+ (*open square*), NH_4^+ (*open triangle*), Li^+ (*filled diamond*) and Cs^+ (*open circle*). The activity data were reported as a percentage of that measured in the presence of 0.5 M NaCl and represent mean values of three different determinations; the corresponding *error bars* are shown

concentration was the most effective, as it caused a fivefold increase in the activity measured in the absence of salt. The determination of the kinetic parameters of the DTNB reduction activity of *Ph*TrxR in the presence of 0.5 M NaCl pointed to an improvement of both the affinity for the substrate and the catalytic constant of the reaction. Indeed the K_M for DTNB was lowered to 1.3 mM, whereas the k_{cat} increased to 7.6 s^{-1}; therefore, a sixfold increase of the catalytic efficiency of *Ph*TrxR was observed upon the addition of 0.5 M NaCl.

Temperature dependence of *Ph*TrxR and *Ph*Trx activity

The temperature dependence of the reactions sustained by *Ph*TrxR and *Ph*Trx was investigated (Fig. 3). The activities promoted by the two isolated enzymes, namely the insulin precipitation by *Ph*Trx (Fig. 3a) and the DTNB reduction by *Ph*TrxR (Fig. 3b), were first evaluated. Both *Ph*Trx and *Ph*TrxR showed the maximum activity at around 30 °C, a value at least 15 °C higher than the optimal growth temperature of *P. haloplanktis*. The following decrease of activity was more evident in the DTNB reduction assay catalysed by *Ph*TrxR. The temperature dependence of combined *Ph*TrxR and *Ph*Trx was also evaluated in the reconstituted system. This activity was followed by the insulin precipitation (Fig. 3c) and NADPH consumption (Fig. 3d). In the first case, the maximum activity shifted towards a higher temperature, around 40 °C, and remained almost constant up to 60 °C; only above this temperature, a significant lower activity was observed. In the second case, the fast NADPH reduction observed at temperatures higher than 20 °C impaired a correct determination of the activity above this temperature.

The studies on the effect of temperature included the determination of the energetic parameters of the enzymatic reactions promoted by *Ph*Trx and *Ph*TrxR. To this aim, the previously described data of activity were analysed according to the Arrhenius equation in the 5–20 °C temperature interval. As shown in Fig. 4, the linearity of the plots excluded temperature-dependent conformational changes in the range of temperature considered. This circumstance allowed the calculation of the energy of activation (E_a) of the reactions. The lowest value of E_a, 18.7 kJ mol^{-1}, was measured with the reconstituted thioredoxin system, when the reaction was followed by the NADPH consumption; however, the E_a raised to 47.1 kJ mol^{-1} when the insulin precipitation was used for activity measurements. Notably, a similar E_a of 53.1 kJ mol^{-1} was

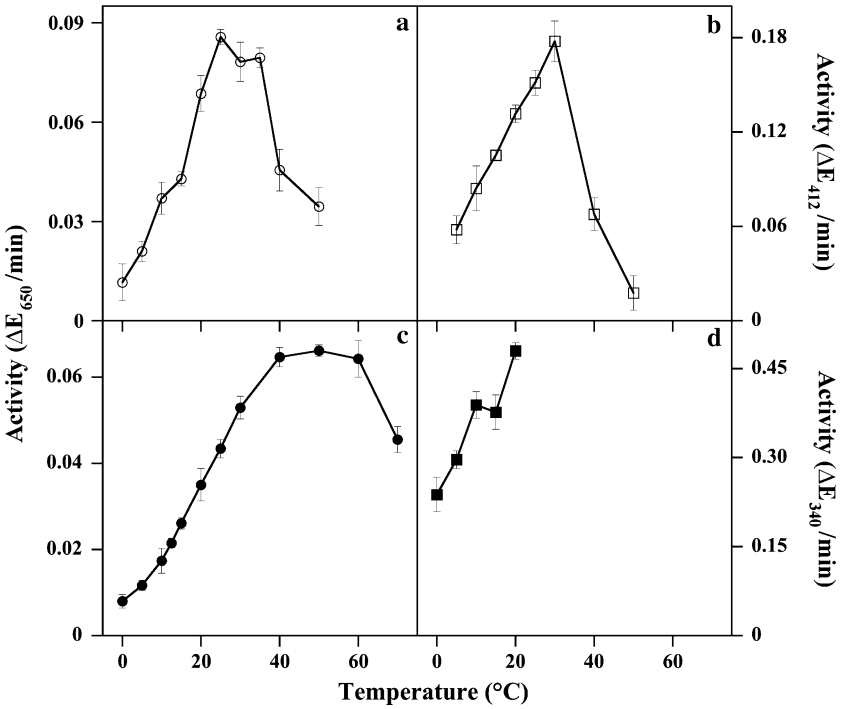

Fig. 3 Effect of temperature on *Ph*TrxR and *Ph*Trx activities in different experimental conditions. **a** Activity of *Ph*Trx measured through the insulin precipitation method. The reaction was carried out at the indicated temperatures and the final concentration of *Ph*Trx was 10.1 μM. **b** Activity of *Ph*TrxR measured through the DTNB reduction assay. The final concentration of *Ph*TrxR was 0.014 μM. **c** Combined activity of *Ph*Trx and *Ph*TrxR measured through the insulin precipitation method. The final concentration of *Ph*Trx and *Ph*TrxR was 10.0 and 1.0 μM, respectively. **d** Same conditions as in **c**, with the exception that the activity was followed through the NADPH consumption. In all the experimental conditions the data were reported as mean values of three determinations with the corresponding *error bars*. Other details are indicated in "Materials and methods"

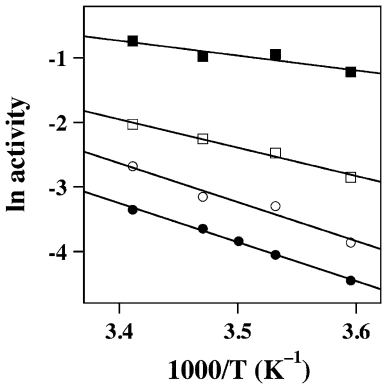

Fig. 4 Arrhenius analysis of the activities sustained by *Ph*TrxR and *Ph*Trx in different experimental conditions. The data referred to the different activities reported in Fig. 3 were analysed according to the Arrhenius equation in the 5–20 °C temperature interval. *Symbols* as in Fig. 3. The squared correlation coefficient of data fitting ranged between 0.85 and 0.99

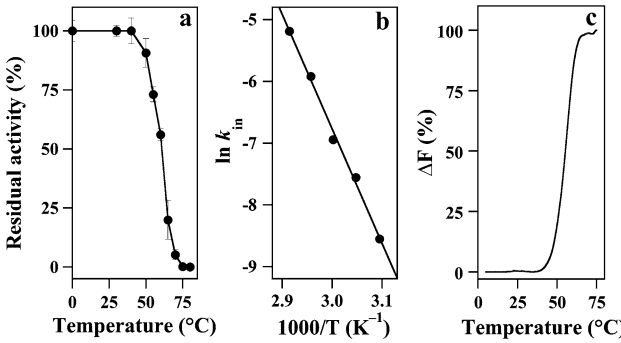

Fig. 5 Heat stability of *Ph*TrxR. **a** Heat inactivation profile. A 0.62-μM solution of *Ph*TrxR in buffer A was incubated for 10 min at the indicated temperatures. The residual activity of the treated samples was determined after ice-chilling for 30 min, and expressed as a percentage of the untreated control kept at 0 °C. The data were reported as mean values of three determinations with the corresponding *error bars*. **b** Arrhenius plot of the heat inactivation process. Inactivation kinetics of *Ph*TrxR were realised at temperatures ranging from 50 to 70 °C. To this aim, a 0.62-μM solution of the enzyme in buffer A was incubated at the indicated temperatures and, at selected times depending on the temperature chosen, an aliquot was withdrawn and assayed for the residual DTNB reduction activity. All kinetics were linear and the squared correlation coefficient of data fitting ranged between 0.87 and 0.99. The first-order k_{in} values were used to draw the Arrhenius plot. **c** Fluorescence-melting curve of a 2-μM solution of *Ph*TrxR in buffer A. Other details are indicated in "Materials and methods"

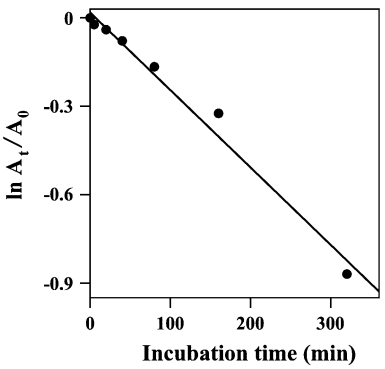

Fig. 6 Heat inactivation kinetics of *Ph*Trx at 95 °C. A 16.5-μM *Ph*Trx solution in buffer A was incubated at 95 °C. At the times indicated, aliquots were withdrawn and immediately chilled on ice for at least 30 min. The residual activity was measured through the insulin precipitation at a final *Ph*Trx concentration of 2.8 μM. A_t and A_0 represent the activities determined at the time *t* and *zero*, respectively. The squared correlation coefficient of data fitting was 0.98

obtained with the insulin precipitation method, when the activity of isolated *Ph*Trx was evaluated. An intermediate value of 30.9 kJ mol^{-1} was calculated in the DTNB reduction assay. Therefore, the energetics of the various steps of the whole electron transfer from the initial donor NADPH to the final acceptor human insulin are affected by the interaction between *Ph*TrxR and *Ph*Trx and by the usage of a synthetic or heterologous electron acceptor/donor.

Effect of temperature on the stability of *Ph*TrxR and *Ph*Trx

The thermostability of *Ph*TrxR was investigated by heat inactivation studies and fluorescence-melting curves. In a first approach to evaluate the heat resistance of *Ph*TrxR, a heat inactivation profile was determined from enzyme samples incubated for 10 min at temperatures ranging from 30 to 80 °C (Fig. 5a); the extrapolated half-inactivation temperature of *Ph*TrxR was approximately 60 °C. The heat inactivation of *Ph*TrxR was also followed kinetically and the process followed a first order kinetics at each temperature, thus allowing the calculation of the corresponding kinetic constants of heat inactivation (k_{in}). The values of k_{in} obtained in the 50–70 °C interval were analysed according to the Arrhenius equation (Fig. 5b) to obtain the energy of activation (E_a) of the heat inactivation process, whose value was 154 kJ mol^{-1}.

In the 5–75 °C interval the heat denaturation process of *Ph*TrxR was also followed by fluorescence-melting curves, evaluating the increase of intrinsic fluorescence of the enzyme. The results reported in Fig. 5c indicate that the temperature for half denaturation of *Ph*TrxR was approximately 55 °C, a value 5 °C lower than that determined through the heat inactivation profile. These data indicate that *Ph*TrxR exhibits discrete heat resistance in spite of its psychrophilic origin.

Much more pronounced was the thermostability of the other component of the thioredoxin system in *P. haloplanktis*. This behaviour is clearly evident in the inactivation kinetics of *Ph*Trx carried out at 95 °C and shown in

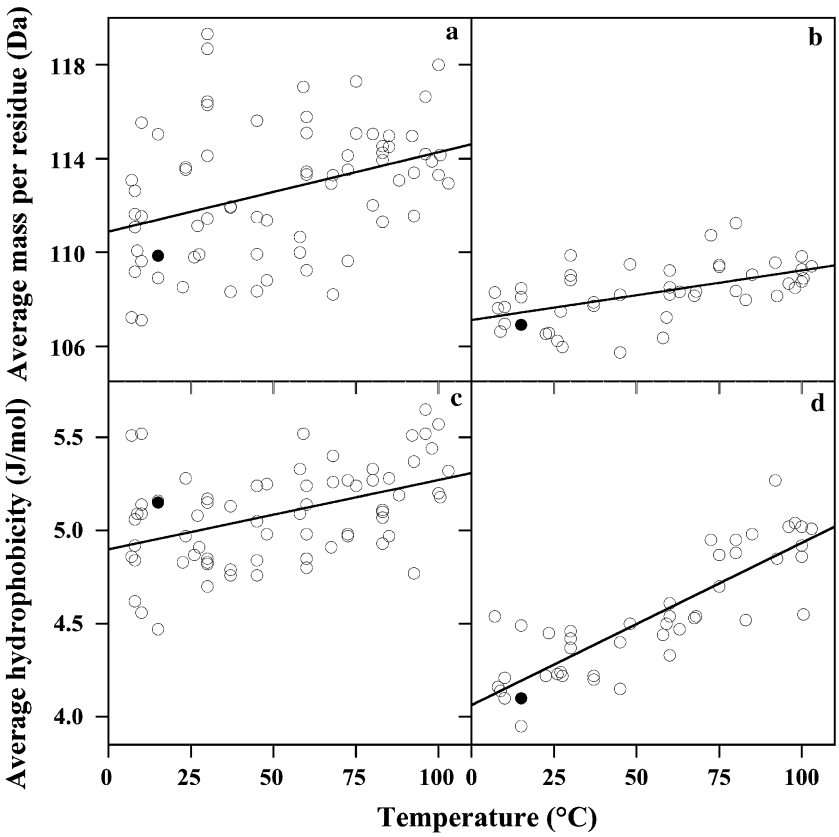

Fig. 7 Temperature dependence of average parameters related to the amino acid composition of Trx and TrxR form sources adapted from cold to hot environments. **a** Effect of growth temperature on the average mass per residue of Trx. Values of the linear fit: $a = 110.89$ Da; $b = 0.03385$ Da °C^{-1}; $r = 0.3644$; $t = 3.25$; $p < 0.005$. **b** Effect of growth temperature on the average mass per residue of TrxR. Values of the linear fit: $a = 107.12$ Da; $b = 0.02109$ Da °C^{-1}; $r = 0.5432$; $t = 4.24$; $p < 0.001$. **c** Effect of growth temperature on the average hydrophobicity per residue of Trx. Values of the linear fit: $a = 4.90$ kJ mol^{-1}; $b = 0.003722$ kJ mol^{-1} °C^{-1}; $r = 0.4491$; $t = 4.17$; $p < 0.001$. **d** Effect of growth temperature on the average hydrophobicity per residue of TrxR. Values of the linear fit: $a = 4.06$ kJ mol^{-1}; $b = 0.008703$ kJ mol^{-1} °C^{-1}; $r = 0.8468$; $t = 10.44$; $p < 0.001$. In each panel the *filled circle* indicates the actual value referred to the *P. haloplanktis* enzyme

Fig. 6. The calculated half-life of the psychrophilic protein was 263 min, a value pointing to the exceptional heat resistance of *Ph*Trx in spite of its psychrophilic origin. The great heat resistance of *Ph*Trx was also confirmed by the lack of any detectable effect in the fluorescence of this enzyme in the aromatic region of the spectrum, remaining constant between 20 and 99 °C (not shown).

Amino acid composition of *Ph*Trx and *Ph*TrxR and correlation with cold adaptation

The different temperature dependence and heat resistance of the two thioredoxin components prompted a phylogenetic analysis among the corresponding enzymes from other sources adapted at various growth temperatures in order to shed light on the behaviour of these psychrophilic enzymes. In particular, the evolutionary relationships were focused on the possible identification of specific structural requirements possessed by *Ph*Trx and *Ph*TrxR, which could explain their different cold adaptation. A previous study carried out on six model proteins covering various functional roles played by these macromolecules, showed that adaptation from cold to hot environments involved continuous and small adjustments of average parameters related to the amino acid composition (De Vendittis et al. 2008). Indeed, in all model proteins the average value per residue of mass and hydrophobicity almost linearly increased with the growth temperature of the host microorganism, even though some differences emerged in the "ideal proportion" of bulky and hydrophobic residues required for the adaptation to a selected temperature of each model protein. To this aim, parameters related to the amino acid composition of *Ph*Trx and *Ph*TrxR were compared to those of the corresponding enzymes from the same microorganisms analysed previously. As shown in Fig. 7, the average mass per residue in Trx (Fig. 7a) and TrxR (Fig. 7b) almost linearly increased with the growth temperature of the microorganism and a similar behaviour

was also observed for the average hydrophobicity per residue of Trx (Fig. 7c) and TrxR (Fig. 7d). Therefore, the cold-adapted Trx and TrxR show a tendency towards smaller-sized and less hydrophobic residues in comparison to the mesophilic and the (hyper)thermophilic counterparts. However, significant differences emerged in the behaviour of the thioredoxin components, when considering the specific values of average mass and hydrophobicity of Trx or TrxR and the temperature-dependent increase of these parameters. The main difference resided in the significantly higher values of either average mass or hydrophobicity obtained for Trx with respect to TrxR. Moreover, at increasing temperatures, the distance between the average mass of Trx and TrxR slightly increased with temperature, whereas an opposite trend was observed for the average hydrophobicity. The extrapolated ideal values of average mass and hydrophobicity for the adaptation at 15 °C, the optimum growth temperature of *P. haloplanktis*, were 111.40 Da and 4.95 kJ mol^{-1} for Trx and 107.44 Da and 4.19 kJ mol^{-1} for TrxR. Interestingly, these figures are not far from the actual values calculated for *Ph*Trx (109.87 Da and 5.15 kJ mol^{-1}) and *Ph*TrxR (106.92 Da and 4.10 kJ mol^{-1}). The significant differences of these parameters between the two enzymes are likely related to their different cold adaptation and point to an increased usage of bulky and hydrophobic residues by *Ph*Trx compared to *Ph*TrxR.

S-glutathionylation of *Ph*TrxR

Previous reports on superoxide dismutase from *P. haloplanktis* (*Ph*SOD) proved that this enzyme has a highly reactive cysteine residue, forming disulphide adducts with either β-mercaptoethanol (Castellano et al. 2006) or cellular thiols, such as glutathione in its oxidised or nitrosylated form (Castellano et al. 2008). This covalent modification of *Ph*SOD regulates the functions of this key anti-oxidant enzyme, thus suggesting that the S-glutathionylation reaction acts as a sensor of the cellular redox state of *P. haloplanktis*. Concerning *Ph*TrxR, besides the two cysteines (C_{136} and C_{139}) engaged in its active-site disulphide bridge, three other cysteines (C_7, C_{103} and C_{303}) are present as free thiols in the amino acid sequence of this flavoenzyme (Cotugno et al. 2009). These findings promoted an evaluation on the possible reactivity of *Ph*TrxR towards glutathione. Therefore, *Ph*TrxR was incubated with increasing concentrations of the oxidised form of glutathione (GSSG) and then analysed by Western blotting using anti-glutathione antibodies. As shown in Fig. 8a, the formation of a mixed disulphide between glutathione and *Ph*TrxR was demonstrated by the presence of an immunoreactive band, which was already detectable in the sample treated with 0.1 mM GSSG; moreover, the

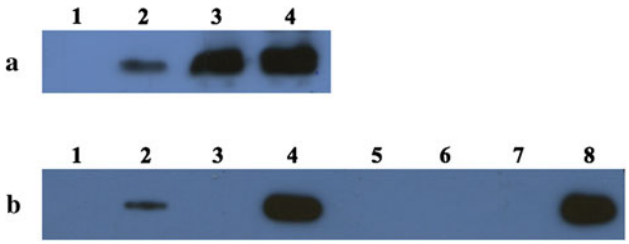

Fig. 8 S-glutathionylation of *Ph*TrxR and its mutated forms. **a** Dose-dependent glutathionylation of endogenous *Ph*TrxR. *Ph*TrxR in buffer A was incubated at 25 °C in the absence (*lane 1*) or in the presence of 0.1 mM (*lane 2*), 1 mM (*lane 3*) or 10 mM (*lane 4*) GSSG. After removal of unbound glutathione, 0.9 µg of each protein sample was analysed by Western blotting. **b** Glutathionylation of recombinant mutated forms of *Ph*TrxR. C_7S-*Ph*TrxR (*lane 1*, *2*), C_{106}S-*Ph*TrxR (*lane 3*, *4*), C_{303}S-*Ph*TrxR (*lane 5*, *6*), or r*Ph*TrxR (*lane 7*, *8*) in buffer A was incubated at 25 °C in the absence (*lane 1*, *3*, *5*, *7*) or in the presence of 10 mM GSSG (*lane 2*, *4*, *6*, *8*). After removal of unbound glutathione, 0.9 µg of each protein sample was analysed by Western blotting. Other details are reported in "Materials and methods"

immunoreactivity increased with the concentration of the modifying reagent. The glutathionylation by the nitrosylated (GSNO) or reduced (GSH) form of glutathione was also evaluated (not shown); however, immunoreactivity was evident starting from 1 mM GSNO or 10 mM GSH. These results suggest that, as already observed for *Ph*SOD, *Ph*TrxR is also the target of a S-glutathionylation reaction. The GSSG-treated samples were also assayed for DTNB reduction activity; however, the presence of the S-glutathionyl adduct did not apparently affect this catalytic property of *Ph*TrxR (not shown).

In order to identify the cysteine residue(s) target of the covalent modification by glutathione, three mutated forms of the flavoenzyme were obtained, in which each of the three free cysteines was replaced by a serine residue. The analysis by Western blotting of r*Ph*TrxR and its mutated forms (C_7S-r*Ph*TrxR, C_{106}S-r*Ph*TrxR or C_{303}S-r*Ph*TrxR), untreated or treated with 1 mM GSSG, is shown in Fig. 8b. In the GSSG-treated samples, the immunoreactive band was present in r*Ph*TrxR, C_{106}S-r*Ph*TrxR and C_7S-r*Ph*TrxR, although with different intensity; on the other hand, no reactivity at all was observed in the C_{303}S-r*Ph*TrxR sample. These data clearly suggest that C_{303} should be the target residue in the S-glutathionylation reaction of r*Ph*TrxR.

Discussion

The molecular and functional properties of the purified endogenous components of the thioredoxin system isolated from the psychrophile *Pseudoalteromonas haloplanktis* have been investigated. The activity of this system,

restoring the reduced state of cellular proteins after an oxidation reaction, is crucial for the survival of *P. haloplanktis*. Indeed, this microorganism is likely more exposed to the reactive oxygen species for both the increased oxygen solubility in the cold Antarctic sea and the enhanced stability of these toxic compounds at cold temperatures (Medigue et al. 2005; Pörtner et al. 2007). Previous work showed the different cold adaptation of the recombinant components of the thioredoxin system in *P. haloplanktis* (Cotugno et al. 2009). In this work, the biochemical characterisation of the purified endogenous *Ph*Trx and *Ph*TrxR confirmed the different temperature dependence and heat stability of the psychrophilic proteins and extended the study to the comparison of the energetic parameters of the reactions catalysed by these factors either alone or in combination. Moreover, the study included the effect of monovalent cations on the activity of *Ph*TrxR, as well as the sensitivity of the flavoenzyme to the cellular thiol glutathione.

The study of the molecular properties of the purified endogenous components of the thioredoxin system in *P. haloplanktis* confirmed the previous data obtained on the recombinant counterparts (Cotugno et al. 2009). In particular, while *Ph*TrxR is organised as a homodimer, *Ph*Trx functions as a small monomeric protein, as usually found for most eubacterial components of the thioredoxin system. Furthermore, *Ph*TrxR was purified as a flavoenzyme and the amount of FAD bound to the enzyme, although slightly understoichiometric, allowed the evaluation of the activity of the endogenous *Ph*TrxR. Indeed, this FAD/*Ph*TrxR ratio could reflect the required functionality of the enzyme, which activity is related to the FAD content. However, it cannot be excluded that the understoichiometric ratio was the consequence of the purification procedure.

*Ph*Trx and *Ph*TrxR were purified in their active oxidised form, as they catalysed the typical reactions sustained by these factors either alone or in combination. Indeed, when analysed alone, *Ph*TrxR reduced the synthetic substrate DTNB using NADPH as electron donor, whereas *Ph*Trx transferred the reducing equivalents from DTT to the heterologous substrate insulin. The kinetic parameters of these reactions were similar to those previously reported for the recombinant counterparts (Cotugno et al. 2009). When the combined activity of *Ph*TrxR and *Ph*Trx was analysed in a reconstituted thioredoxin system, the electron passage from the initial donor NADPH to the final acceptor insulin was demonstrated. Under these conditions, the K_M of *Ph*TrxR for its natural substrate *Ph*Trx (2 μM) was similar to those reported for the mesophilic TrxR isolated from *Escherichia coli* (*Ec*) towards its two natural substrates, *Ec*Trx1 (1.9 μM) and *Ec*Trx2 (2.4 μM) (Miranda-Vizuete et al.1997). On the other hand, a higher K_M (12.3 μM) was reported for the hyperthermophilic TrxR from *Aeropyrum pernix* (*Ap*) towards *Ap*Trx (Jeon and Ishikawa 2002). Finally, the reversibility of the electron transfer in the reconstituted thioredoxin system allowed the determination of the $E^{0\prime}_{(PhTrx)}$, whose value (−289 mV) was similar to that recently reported for the recombinant system of *P. haloplanktis* ($E^{0\prime}_{(rPhTrx)} = -276$ mV; Cotugno et al. 2009). Furthermore, no great differences were found with the corresponding parameters related to the mesophile *E. coli* ($E^{0\prime}_{(EcTrx)} = -270$ mV; Krause et al. 1991) or the hyperthermophile *A. pernix* ($E^{0\prime}_{(ApTrx)} = -262$ mV; Jeon and Ishikawa 2002). Therefore, all these data prove the interaction and functionality of the endogenous components of the thioredoxin system in *P. haloplanktis*.

The temperature dependence of the reactions associated to the electron transfer from the initial NADPH donor to the final acceptor human insulin was also investigated. In particular, a comparison was made among the values of E_a found for each reduction step. The lowest E_a (18.7 kJ mol^{-1}) measured in the complete thioredoxin system, when the reaction was followed through the NADPH consumption, suggests that the first electron transfer from NADPH to the flavoenzyme is an energetically favoured process. Vice versa, when the activity of the complete thioredoxin system was followed through the insulin precipitation, the significant increase of E_a (47.1 kJ mol^{-1}) suggests that the final electron passage to the heterologous insulin could enhance the energetic barrier of the whole process. This suggestion is confirmed by the similar E_a (53.1 kJ mol^{-1}) obtained when the activity of *Ph*Trx alone was evaluated through the insulin precipitation, using DTT as electron donor. The intermediate E_a value (30.9 kJ mol^{-1}) measured in the DTNB reduction assay catalysed by *Ph*TrxR indicates that the energetic barrier of the electron passage from the flavoenzyme to the synthetic substrate DTNB, although higher than that measured in the first passage from NADPH to the flavoenzyme, remains lower than that obtained through the insulin precipitation assay. When a natural substrate for the psychrophilic *Ph*Trx will be available, the redetermination of the E_a value could be helpful for understanding the mechanism of the whole electron transfer, at least from the energetic point of view.

The studies on the thermostability of *Ph*TrxR and *Ph*Trx indicated that both psychrophilic proteins could tolerate temperatures significantly higher than those of the growth environment of *P. haloplanktis*. In the case of *Ph*TrxR, the half-inactivation temperature of the flavoenzyme (60 °C) is well above the maximum growth temperature of 20 °C tolerated by *P. haloplanktis*. The energetics of the heat inactivation process of *Ph*TrxR was also investigated and the calculated value of E_a (154 kJ mol^{-1}), although higher than that reported for polynucleotide phosphorylase (96.7 kJ mol^{-1}), another enzyme isolated from *P. haloplanktis* (Evangelista et al. 2009), still reflects the

psychrophilic origin of the source, as it is lower than the values usually reported for mesophilic and thermophilic enzymes, showing an average E_a value of 278 ± 60 kJ mol^{-1} (Masullo et al. 1993; Grimaldi et al. 2008; Castellano et al. 2009; De Vendittis et al. 2010). Furthermore, since the denaturation profile of the flavoenzyme determined through fluorescence-melting curves is roughly similar to the heat inactivation profile, it is possible to conclude that heat inactivation and protein denaturation occur in the same temperature interval. These data, in agreement with the previous results obtained with the recombinant flavoenzyme (Cotugno et al. 2009) point to the discrete heat stability of *Ph*TrxR.

In the case of *Ph*Trx, the exceptional half-life measured in the inactivation kinetics at 95 °C (263 min) ranks this protein as the most thermostable from a psychrophilic origin. To our knowledge, the enzymes isolated from *P. haloplanktis* display a higher heat resistance compared to other psychrophiles. However, the half-life of other *P. haloplanktis* enzymes is significantly lower compared to *Ph*Trx. Indeed, besides *Ph*TrxR (half-life 10 min at 60 °C, this work), superoxide dismutase, another antioxidant enzyme (Castellano et al. 2006), and the elongation factor Ts (Raimo et al. 2004) display a lower heat resistance (half-life 10 min at 54 and 57 °C, respectively). Interestingly, *Ph*Trx possesses a greater resistance to heat inactivation even in comparison to the mesophilic recombinant *Ec*Trx2; in fact, 40 % of the insulin-reducing activity of *Ec*Trx2 was lost after 5 min of incubation at 85 °C (Miranda-Vizuete et al. 1997). Moreover, the heat resistance of *Ph*Trx is not very distant from that of Trx from a hyperthermophilic microorganism. For instance, at 92 °C the half-life of recombinant Trx-A1 and Trx-A2 from *Sulfolobus solfataricus* was 20.5 and 56.6 h, respectively (Grimaldi et al. 2008).

The analysis of some parameters related to the amino acid composition of *Ph*Trx and *Ph*TrxR gave a possible explanation on the different thermodependence and thermostability of the two psychrophilic thioredoxin components. Indeed, the significantly higher proportion of bulky and hydrophobic residues possessed by *Ph*Trx made this protein intrinsically more compact compared to *Ph*TrxR, a finding suggesting a structural basis for the exceptional thermostability of *Ph*Trx. On the other hand, the consequent lower flexibility of *Ph*Trx was not dramatic for its cold adaptation, probably because of its small size and the absence of large conformational changes during catalysis. Concerning *Ph*TrxR, its lower proportion of bulky and hydrophobic residues ensured an appropriate flexibility of the flavoenzyme, which underwent a large conformational change during catalysis (Lennon et al. 2000), although reducing its thermostability compared to *Ph*Trx.

The biochemical characterisation of *Ph*TrxR included the effect of some monovalent cations on the DTNB reduction reaction catalysed by the flavoenzyme. The results showed that all monovalent cations enhance the activity of *Ph*TrxR and that the highest stimulation, nearly sixfold increase, was reached upon the addition of 0.5 M NaCl. Therefore, *Ph*TrxR could be classified as a polyextremophilic protein. A similar behaviour was already observed for other enzymes isolated from *P. haloplanktis* (Srimathi et al. 2007; Evangelista et al. 2009). Furthermore, the stimulation of the activity by monovalent cations is common to other psychrophilic proteins, thus indicating a possible common regulatory role exerted by these cations on the mechanism of action in psychrophiles.

Another interesting feature emerging from this work concerns the reactivity of *Ph*TrxR towards the cellular thiol glutathione. In particular, the flavoenzyme was S-glutathionylated by the oxidised form of glutathione in a dose-dependent way; a reactivity was also observed with the nitrosylated and even the reduced form of this thiol, even though at tenfold and 100-fold higher doses, respectively. A similar behaviour was already observed for the *Ph*SOD and in that case the covalent modification regulated the functions of the anti-oxidant enzyme (Castellano et al. 2008). Vice versa, in the case of *Ph*TrxR the S-glutathionylation of the enzyme did not apparently cause a significant alteration of the DTNB reduction activity. In any case, the S-glutathionylation reaction must play a key role in controlling the cellular redox state of *P. haloplanktis*, because it was demonstrated that this covalent modification is induced by cellular oxidative stress conditions (Castellano et al. 2008). The mutagenic analysis of the three free cysteines possessed by *Ph*TrxR allowed the identification of C_{303} as the target residue of the S-glutathionylation reaction on the basis of the lack of reactivity towards glutathione upon the $C_{303}S$ replacement. Indeed, the S-glutathionylation reaction was evident, even though to a different extent, with either C_7S or $C_{106}S$ replacement. A clear explanation for the significant lower reactivity observed with the C_7S-r*Ph*TrxR mutant compared to wild type is unavailable at moment; when the 3D structure of the enzyme will be available, it will be interesting to evaluate if the C_7S amino acid replacement could reduce the accessibility of the C_{303} residue of *Ph*TrxR to the modification reaction by glutathione. However, on the basis of a 3D model, the residue C_{303}, target of the covalent modification by glutathione, appears more exposed to solvent than other non catalytic cysteines.

Conclusions

The results reported in this paper indicate that the efficiency of the thioredoxin system is crucial for the preservation of the reduced state of cellular proteins in

P. haloplanktis, even considering the possible involvement of glutathione in the alteration of the redox state of the free cysteine residues possessed by the cellular proteins of this psychrophile and the activity of components of another thiol-disulphide oxidoreductase system aimed at the formation of disulphide bonds (*Ph*DsbA and *Ph*DsbA2) in the periplasmic space (Madonna et al. 2006). The most relevant finding of this work was the high thermal stability of both components of the thioredoxin system, mainly for *Ph*Trx. It is likely that the exceptional heat resistance of the thioredoxin system in *P. haloplanktis* reflects an adaptation mechanism of this psychrophile, considering its growth under oxidative stress conditions caused by the increased oxygen solubility in the cold environment.

Acknowledgments This work was supported by grants from MIUR, PRIN 2009 (Rome) awarded to MM, EDV, GR.

References

Arnér ESJ, Holmgren A (2000) Physiological functions of thioredoxin and thioredoxin reductase. Eur J Biochem 267:6102–6109

Arscott LD, Gromer S, Schirmer RH, Becker K, Williams CH Jr (1997) The mechanism of thioredoxin reductase from human placenta is similar to the mechanisms of lipoamide dehydrogenase and glutathione reductase and is distinct from the mechanism of thioredoxin reductase from *Escherichia coli*. Proc Natl Acad Sci 94:3621–3626

Birolo L, Tutino ML, Fontanella B, Gerday C, Mainolfi K, Pascarella S, Sannia G, Vinci F, Marino G (2000) Aspartate aminotransferase from the Antarctic bacterium *Pseudoalteromonas haloplanktis* TAC 125. Cloning, expression, properties, and molecular modelling. Eur J Biochem 267:2790–2802

Bradford M (1976) A rapid and sensitive method for the quantitation of microgram quantities of protein utilizing the principle of protein-dye binding. Anal Biochem 72:248–254

Castellano I, Di Maro A, Ruocco MR, Chambery A, Parente A, Di Martino MT, Parlato G, Masullo M, De Vendittis E (2006) Psychrophilic superoxide dismutase from *Pseudoalteromonas haloplanktis*: biochemical characterization and identification of a highly reactive cysteine residue. Biochimie 88:1377–1389

Castellano I, Ruocco MR, Cecere F, Di Maro A, Chambery A, Michniewicz A, Parlato G, Masullo M, De Vendittis E (2008) Glutathionylation of the iron superoxide dismutase from the psychrophilic eubacterium *Pseudoalteromonas haloplanktis*. Biochim Biophys Acta 1784:816–826

Castellano I, Cecere F, De Vendittis A, Cotugno R, Chambery A, Di Maro A, Michniewicz A, Parlato G, Masullo M, Avvedimento EV, De Vendittis E, Ruocco MR (2009) Rat mitochondrial manganese superoxide dismutase: amino acid positions involved in covalent modifications, activity, and heat stability. Biopolymers 91:1215–1226

Chae HZ, Chung SJ, Rhee SG (1994) Thioredoxin-dependent peroxide reductase from yeast. J Biol Chem 269:27670–27678

Clark WM (1960) Oxidation-reduction potentials of organic systems. The Williams & Wilkins Co., Baltimore

Cotugno R, Ruocco MR, Marco S, Falasca P, Evangelista G, Raimo G, Chambery A, Di Maro A, Masullo M, De Vendittis E (2009) Differential cold-adaptation among protein components of the thioredoxin system in the psychrophilic eubacterium *Pseudoalteromonas haloplanktis* TAC 125. Mol BioSyst 5:519–528

De Vendittis E, Castellano I, Cotugno R, Ruocco MR, Raimo G, Masullo M (2008) Adaptation of model proteins from cold to hot environments involves continuous and small adjustments of average parameters related to amino acid composition. J Theor Biol 250:156–171

De Vendittis A, Amato M, Mickniewicz A, Parlato G, De Angelis A, Castellano I, Rullo R, Riccitiello F, Rengo S, Masullo M, De Vendittis E (2010) Regulation of the properties of superoxide dismutase from the dental pathogenic microorganism *Streptococcus mutans* by iron- and manganese-bound co-factor. Mol BioSyst 6:1973–1982

Ejiri SI, Weissbach H, Brot N (1979) Reduction of methionine sulfoxide to methionine by *Escherichia coli*. J Bacteriol 139: 161–164

Evangelista G, Falasca P, Ruggiero I, Masullo M, Raimo G (2009) Molecular and functional characterization of polynucleotide phosphorylase from the Antarctic eubacterium *Pseudoalteromonas haloplanktis*. Protein Pept Lett 16:999–1005

Gasdaska PY, Berggren MM, Berry MJ, Powis G (1999) Cloning, sequencing and functional expression of a novel human thioredoxin reductase. FEBS Lett 442:105–111

Ghisla S, Massey V (1989) Mechanisms of flavoprotein-catalyzed reactions. Eur J Biochem 181:1–17

Gilbert HF (1990) Molecular and cellular aspects of thiol-disulfide exchange. Adv Enzymol Relat Areas Mol Biol 63:69–172

Grimaldi P, Ruocco MR, Lanzotti MA, Ruggiero A, Ruggiero I, Arcari P, Vitagliano L, Masullo M (2008) Characterisation of the components of the thioredoxin system in the archaeon *Sulfolobus solfataricus*. Extremophiles 12:553–562

Hernandez HH, Jaquez OA, Hamill LJ, Elliot SJ, Drennan CL (2008) Thioredoxin reductase from *Thermoplasma acidophilum*: a new twist on redox regulation. Biochemistry 47:9728–9737

Hirt RP, Müller S, Embley TM, Coombs GH (2002) The diversity and evolution of thioredoxin reductase: new perspectives. Trends Parasitol 18:302–308

Holmgren A (1979a) Thioredoxin catalyzes the reduction of insulin disulfides by dithiothreitol and dihydrolipoamide. J Biol Chem 254:9627–9632

Holmgren A (1979b) Reduction of disulfides by thioredoxin. Exceptional reactivity of insulin and suggested functions of thioredoxin in mechanism of hormone action. J Biol Chem 254: 9113–9119

Holmgren A (1985) Thioredoxin. Annu Rev Biochem 54:237–271

Holmgren A (1989) Thioredoxin and glutaredoxin systems. J Biol Chem 264:13963–13966

Huber HE, Tabor S, Richardson CC (1987) *Escherichia coli* thioredoxin stabilizes complexes of bacteriophage T7 DNA polymerase and primed templates. J Biol Chem 262:16224–16232

Jeon SJ, Ishikawa K (2002) Identification and characterization of thioredoxin and thioredoxin reductase from *Aeropyrum pernix* K1. Eur J Biochem 269:5423–5430

Kanzok SM, Fechner A, Bauer H, Ulschmid JK, Müller HM, Botella-Munoz J, Schneuwly S, Schirmer R, Becker K (2001) Substitution of the thioredoxin system for glutathione reductase in *Drosophila melanogaster*. Science 291:643–646

Kashima Y, Ishikawa K (2003) A hyperthermostable novel protein-disulfide oxidoreductase is reduced by thioredoxin reductase from hyperthermophilic archaeon *Pyrococcus horikoshii*. Arch Biochem Biophys 418:179–185

Kern R, Malki A, Holmgren A, Richarme G (2003) Chaperone properties of *Escherichia coli* thioredoxin and thioredoxin reductase. Biochem J 371:965–972

Krause G, Lundstrom J, Barea JL, Pueyo de la Cuesta C, Holmgren A (1991) Mimicking the active site of protein disulfide isomerase by substitution of proline 34 in *Escherichia coli* thioredoxin. J Biol Chem 266:9494–9500

Ladenstein R, Ren B (2006) Protein disulfides and protein disulfide oxidoreductases in hyperthermophiles. FEBS J 273:4170–4185

Laemmli UK (1970) Cleavage of structural proteins during the assembly of the head of bacteriophage T4. Nature 227:680–685

Lennon BW, Williams CH Jr, Ludwig ML (2000) Twists in catalysis: alternating conformations of *Escherichia coli* thioredoxin reductase. Science 289:1190–1194

Luthman M, Holmgren A (1982) Rat liver thioredoxin and thioredoxin reductase: purification and characterization. Biochemistry 21:6628–6633

Madonna S, Papa R, Birolo L, Autore F, Doti N, Marino G, Quemeneur E, Sannia G, Tutino ML, Duilio A (2006) The thiol-disulfide oxidoreductase system in the cold-adapted bacterium *Pseudoalteromonas haloplanktis* TAC 125: discovery of a novel disulfide oxidoreductase enzyme. Extremophiles 10:41–51

Masullo M, Raimo G, Bocchini V (1993) Resistance of archaebacterial aEF-1alpha·GDP against denaturation by heat and urea. Biochim Biophys Acta 1162:35–39

Masullo M, Arcari P, de Paola B, Parmeggiani A, Bocchini V (2000) Psychrophilic elongation factor Tu from the Antarctic Moraxella s. Tac II25: biochemical characterization and cloning of the encoding gene. Biochemistry 39:15531–15539

Matthews JR, Wakasugi N, Virelizier JL, Yodoi J, Hay RT (1992) Thioredoxin regulates the DNA binding activity of NF-kappa B by reduction of a disulphide bond involving cysteine 62. Nucleic Acids Res 20:3821–3830

Medigue C, Krin E, Pascal G, Barbe V, Bernsel A, Bertin PN, Cheung F, Cruveiller S, D'Amico S, Duilio A, Fang G, Feller G, Ho C, Mangenot S, Marino G, Nilsson J, Parrilli E, Rocha EPC, Rouy Z, Sekowska A, Tutino ML, Vallenet D, von Heijne G, Danchin A (2005) Coping with cold: the genome of the versatile marine Antarctica bacterium *Pseudoalteromonas haloplanktis* TAC125. Genome Res 15:1325–1335

Miranda-Vizuete A, Damdimopoulos AE, Gustafsson J, Spyrou G (1997) Cloning, expression, and characterization of a novel *Escherichia coli* thioredoxin. J Biol Chem 272:30841–30847

Moore EC, Reichard P, Thelander L (1964) Enzymatic synthesis of deoxyribonucleotides. V. Purification and properties of thioredoxin reductase from *Escherichia coli* B. J Biol Chem 239:3445–3452

Pörtner HO, Peck L, Somero G (2007) Thermal limits and adaptation in marine Antarctic ectotherms: and integrative view. Phil Trans R Soc B 362:2233–2258

Raimo G, Lombardo B, Masullo M, Lamberti A, Longo O, Arcari P (2004) Elongation factor Ts from the Antarctic eubacterium *Pseudoalteromonas haloplanktis* TAC 125: biochemical characterization and cloning of the encoding gene. Biochemistry 43:14759–14766

Ruocco MR, Ruggiero A, Masullo L, Arcari P, Masullo M (2004) A 35 kDa NAD(P)H oxidase previously isolated from the archaeon *Sulfolobus solfataricus* is instead a thioredoxin reductase. Biochimie 86:883–892

Schenk H, Klein M, Erdbrügger W, Dröge W, Schulze-Osthoff K (1994) Distinct effects of thioredoxin and antioxidants on the activation of transcription factors NF-kappa B and AP-1. Proc Natl Acad Sci USA 91:1672–1676

Spyrou G, Enmark E, Miranda-Vizuete A, Gustaffson J (1997) Cloning and expression of a novel mammalian thioredoxin. J Biol Chem 272:2936–2941

Srimathi S, Jayaraman G, Feller G, Danielsson B, Narayanan PR (2007) Intrinsic halotolerance of the psychrophilic α-amylase from *Pseudoalteromonas haloplanktis*. Extremophiles 11:505–515

Tsang ML, Schiff JA (1976) Sulfate-reducing pathway in *Escherichia coli* involving bound intermediates. J Bacteriol 125:923–933

Williams CH Jr (1995) Mechanism and structure of thioredoxin reductase from *Escherichia coli*. FASEB J 9:1267–1276

Windle HJ, Fox A, Ni Eidhin D, Kelleher D (2000) The thioredoxin system of *Helicobacter pylori*. J Biol Chem 275:5081–5089

Properties of a Putative Cambialistic Superoxide Dismutase from the Aerotolerant Bacterium *Streptococcus thermophilus* Strain LMG 18311

Alberto De Vendittis[a], Salvatore Marco[a], Antimo Di Maro[b], Angela Chambery[b], Antonella Albino[a], Mariorosario Masullo[a,c], Andzelika Michniewicz[d], Giuseppe Parlato[d], Amalia De Angelis[a], Emmanuele De Vendittis[a,*] and Rosario Rullo[a,e,*]

[a]*Dipartimento di Biochimica e Biotecnologie Mediche, Università di Napoli Federico II, Via S. Pansini 5, 80131 Napoli, Italy;* [b]*Dipartimento di Scienze della Vita, II Università di Napoli, Via Vivaldi 43, 81100 Caserta, Italy;* [c]*Dipartimento di Studi delle Istituzioni e dei Sistemi Territoriali, Università di Napoli "Parthenope", Via Medina 40, 80133 Napoli, Italy;* [d]*Dipartimento di Medicina Sperimentale e Clinica "G. Salvatore", Università di Catanzaro "Magna Graecia", Via T. Campanella 115, 88100 Catanzaro, Italy;* [e]*Consiglio Nazionale delle Ricerche, Via Argine 1085, 80147 Napoli, Italy*

Abstract: The aerotolerance of the lactic–fermentative bacterium *Streptococcus thermophilus* is mainly based on the key antioxidant function of superoxide dismutase (*St*SOD). In this work, the comparison of recombinant *St*SOD (r*St*SOD) forms obtained from two different initiation triplets indicated that the enzyme from *S. thermophilus* strain LMG 18311 spans 201 residues. r*St*SOD is organised as a homodimer, even though protein aggregates are formed in concentrated solutions. The capability of binding and exchanging Fe or Mn in the active site classifies r*St*SOD as a putative cambialistic enzyme; the moderate preference for iron is counteracted by a 1.5–fold higher activity measured for the Mn–containing form. The enzyme is thermostable, being its half–inactivation time 10 min at 73.5°C; the energetic parameters of the heat inactivation process are regulated by the level of Mn cofactor. The effect of Mn content on the r*St*SOD sensitivity towards inhibitors and inactivators was also evaluated. Sodium azide acts as a weak inhibitor of r*St*SOD and its Mn content does not greatly affect this sensitivity. Concerning the physiological inactivator hydrogen peroxide, the Mn–enriched r*St*SOD displays a great resistance; a moderate sensitivity is instead observed in the presence of a low Mn content. Contrary to hydrogen peroxide, sodium peroxynitrite is a powerful inactivator, a behaviour enhanced in the Mn–enriched enzyme. All these results were compared with the corresponding data previously reported for the cambialistic SOD from the taxonomically related *S. mutans*. In *S. thermophilus* the regulation of the enzyme functions by the Mn content appears less relevant with respect to *S. mutans*.

Keywords: Aerotolerance, cambialistic, enzyme regulation, *Streptococcus thermophilus,* stress response, superoxide dismutase.

1. INTRODUCTION

Streptococcus salivarius subsp. *thermophilus*, hereafter called *Streptococcus thermophilus*, is a gram–positive facultative anaerobic microorganism, whose specific metabolic, growth and phylogenetic properties have been reviewed [1]. This lactic acid bacterium plays a fundamental role in the production of cheeses and fermented milk. Indeed, *S. thermophilus,* often in combination with *Lactobacillus delbrueckii* subsp. *bulgaricus* or *Lactobacillus helveticus*, is currently used for the manufacture of dairy products, such as yogurt or hard cooked cheeses, whose preparation takes advantage of the resistance to a moderate thermal treatment of the microorganisms [2–4]. *S. thermophilus* is closely related to *Lactobacillus*, but also to other streptococcal species including several human pathogens, such as *S. pneumoniae*, *S. pyogenes*, *S. agalactiae* or *S. mutans* [5,6]. The nucleotide sequence of the genome from four *S. thermophilus* strains (LMG 18311, LMD 9, CNRZ 1066, ND03) has become available in the NCBI database [7–9], thus allowing a comparison with that of other pathogenic streptococcal species [10–15]. The study revealed that the most important determinants of pathogenicity were absent or present as pseudogenes in the *S. thermophilus* genome [1,7]. Therefore, it is likely that the dairy *Streptococcus* has followed an evolutionary pathway divergent from that of the other pathogenic species, probably because of its adaptation to milk as ecological niche.

During growth in milk, curd or starter culture production, *S. thermophilus* is exposed to many stresses (low pH, low water activity, high and low temperatures, oxidative stress, starvation and competition with other species) that may affect growth, fermentative capabilities and consequently may have repercussion on texture and flavour of the final food product. Although *S. thermophilus* is one of the most important industrial dairy starters, only a limited number of studies was published on its stress response, considering that this

*Address correspondence to these authors at the Dipartimento di Biochimica e Biotecnologie Mediche, Università di Napoli Federico II, Via S. Pansini 5, 80131 Napoli, Italy; Tel: +39 081 7463118; Fax: +39 081 7463653; E-mail: devendittis@dbbm.unina.it
Consiglio Nazionale delle Ricerche, Via Argine 1085, 80147 Napoli, Italy; Tel.: +39 081 5966006; Fax: +39 081 7463653; E-mail: rosario.rullo@cnr.it

0929-8665/12 $58.00+.00

microorganism can grow in aerobic conditions and survive in the presence of low concentrations of hydrogen peroxyde [16]. For this reason, this study was focused on the characterization of superoxide dismutase (SOD), in order to get some information on the *S. thermophilus* response to the oxidative stress. Indeed, the activity of this key antioxidant enzyme is relevant for the aerobic tolerance of *S. thermophilus*, even considering that this microorganism lacks cytochromes and catalase [1,7].

SOD is a widely distributed metal enzyme catalysing the dismutation of two superoxide anions into molecular oxygen and hydrogen peroxide [17–19]. This anti–oxidant function of SOD, involved in the scavenging of the first ROS produced during the oxygen consumption, takes place through a catalytic mechanism conserved in aerobic and anaerobic organisms. In spite of this conserved function, SODs are usually grouped in structurally unrelated families on the basis of metal content and cellular localisation. For instance, mammals contain a cytosolic Cu/Zn–SOD, a mitochondrial Mn–SOD and an extracellular SOD; vice versa, most eubacteria and archaea usually contain only a Fe–SOD and/or a Mn–SOD, both belonging to the same group of mitochondrial Mn–SOD. Indeed, this ubiquitous SOD family displays the most crucial role in the defence against ROS. The presence of Fe or Mn in the active site of the enzyme is dictated by specific metal requirements and/or physiological conditions; moreover, the exchange between these two metal ions usually leads to loss of enzyme activity [17, 20–21]. On the other hand, some prokaryotes with facultative anaerobic growth conditions possess a cambialistic SOD belonging to the same group of this ubiquitous SOD family; the enzyme, able to bind and exchange Fe or Mn in the active site, displays substantial though different activity with each metal [22–27]. Previous reports described the presence of a single SOD in *S. thermophilus* strain AO54 [28] and analysed the functions of the corresponding gene [29]. The enzyme, whose expression depended on the growth phase, was insensitive to cyanide or H_2O_2 treatment, a behaviour suggesting that SOD from *S. thermophilus* (*St*SOD) was a Mn–containing enzyme. However, no direct metal detection was presented to rule out the possibility of a cambialistic *St*SOD, as already demonstrated for the corresponding enzyme from the taxonomically related source *S. mutans* (*Sm*SOD) [24,27], nor the characterization of the biochemical properties of the purified enzyme was carried out. Another unresolved question was the size of SOD from the *S. thermophilus* strain LMG 18311, as predicted from its putative encoding gene, because it presented a N–terminal extension absent in other bacterial SODs [7].

To address the exact size of *St*SOD from the *S. thermophilus* strain LMG 18311, as well as the type of metal cofactor in its active site, and the regulation of the biochemical properties, a recombinant *St*SOD (r*St*SOD) was produced and characterized. Evidence is presented that r*St*SOD, shorter than that annotated in its genome [7], is a putative cambialistic enzyme, able to bind and exchange Fe for Mn in its active site. The amount of metal cofactor never reached the predicted 1:1 stoichiometry, a finding already reported for other recombinant SODs, mainly those accepting the Mn cofactor [30,31]. However, a preference for Fe binding was found, counteracted by a moderately enhanced activity measured when the Mn content in the active site was increased. Interestingly, the biochemical properties of r*St*SOD, such as thermal resistance and sensitivity to inhibitors and inactivators were regulated by the Mn content of the enzyme. A similar behaviour was found in the cambialistic *Sm*SOD [27], even though the regulatory role exerted by the metal cofactor on the *S. thermophilus* enzyme was lower, mainly in the modulation of the enzymatic activity.

2. MATERIALS AND METHODS

2.1. Materials

Restriction and modifying enzymes were from GE Healthcare or Promega. Ampli*Taq* DNA polymerase from Perkin Elmer or *Taq* DNA polymerase from Takara were used in PCR experiments. Plasmid pGEM–T Easy was from Promega, whereas vector pET–22b(+) and the *Escherichia coli* BL21(DE3) strain were from Novagen. The genomic DNA from *S. thermophilus* strain LMG 18311 was purchased from the American Type Culture Collection. Purification of plasmids and DNA fragments was realised with Qiagen kits from M–Medical. Oligonucleotide synthesis and nucleotide sequencing was carried out at Primm (Italy). Ampicillin, isopropyl-β-thiogalactopiranoside (IPTG), xanthine, xanthine oxidase and cytochrome *c* were from Sigma-Aldrich. The stock solution of sodium peroxynitrite was prepared and used as previously described [32,33]. The chromatographic medium Ni–NTA agarose was from Qiagen. Aquacide IIA was from Calbiochem. HPLC–grade solvents for mass spectrometry were obtained from Carlo Erba. All other chemicals were of analytical grade. The following buffers were used: buffer A, 20 mM Tris•HCl, pH 7.8; buffer B, 20 mM Tris•HCl, pH 7.8, 150 mM KCl; buffer C, 100 mM potassium phosphate, pH 7.8, 0.1 mM Na–EDTA.

2.2. Heterologous Expression of the SOD Gene from *Streptococcus thermophilus*

Transformation of bacterial strains, preparation of plasmids and other details of DNA recombinant technology were as previously described [34]. To engineer a vector for the heterologous expression of the *StsodA* gene (ID: 3164641), the TTG starting codon indicated in the NCBI annotation was considered and a DNA segment was amplified by PCR, using the genomic DNA from *S. thermophilus* strain LMG 18311 as a template, and the following oligonucleotides as primers: 5'd–T_{-14}GTAAGCAAAA**CAT**•*ATG*•AAA•GCT•CTA_{12}–3' (forward primer) and 5'd–A_{662}TTCTAGAC**CTC**•**GAG**•AGC•TTC•TGC•GT_{637}–3' (reverse primer). Numbering in primers begins from the T_1TG starting codon mutagenised to *ATG* (italics), whereas bold letters indicate the base substitutions to create *Nde*I and *Xho*I cloning sites. The amplification product was sub–cloned in pGEM–T Easy, and after digestion of the recombinant plasmid with *Nde*I and *Xho*I, the resulting fragment containing the *StsodA* gene was cloned into the pET–22b(+) vector, previously digested with the same endonucleases. This construct was named v*St*SOD-$_{long}$. Also the downstream A_{58}TG triplet was considered as putative starting codon of the *StsodA* gene and a new vector was engineered by replacing the previous forward primer with the following 5'd–A_{42}AAGAGGACCTT **TCAT**•*ATG*•GCT•ATT•ATT_{69}–3'. The new construct was named

v*St*SOD. Both v*St*SOD$_{long}$ and v*St*SOD were checked by restriction analysis and nucleotide sequencing, to exclude the presence of undesired mutations. Both expression vectors were used for the purification of recombinant forms of *St*SOD fused to a His–tag, useful for the one–step purification of the expression product. In particular, in these heterologous products the C–terminal lysine residue of the endogenous *St*SOD was replaced by the extrapeptide LE(H)$_6$.

The vectors v*St*SOD$_{long}$ and v*St*SOD were then used to transform the *E. coli* BL21(DE3) strain. With this system the expression of the cloned heterologous *StsodA* gene takes place after induction by IPTG. A culture of the transformant grew at 37°C in 1 L of Luria–Bertani medium containing 0.1 mg mL^{-1} ampicillin up to 0.6 OD$_{600}$. The culture was then induced with 0.1 mg mL^{-1} IPTG and grown up for one additional hour, as established for the corresponding heterologous expression of *Sm*SOD [27]. Under these conditions the bacterial cells were collected by centrifugation, resuspended in 30 mL of buffer A, and then lysed with a French Press (Aminco). The sample was then centrifuged at 30,000x*g* for 1 hour and the supernatant (S–30) was used as starting material for the purification of the recombinant product. The His–tagged proteins were purified by Ni^{2+}–agarose affinity chromatography. To this aim, the S–30 (around 28 mL) was added in batch to 2 mL of Ni–NTA Agarose chromatographic medium equilibrated in buffer A. After an overnight incubation, the slurry was poured in a column and extensively washed with buffer A. For the purification of the recombinant *St*SOD forms, bound proteins were stepwise eluted with ten volumes of buffer A supplemented with 10 mM or 50 mM imidazole, respectively. The expected heterologous product was found in both elutions, even though with a different purification degree. In particular, most of the recombinant *St*SOD was eluted as a pure protein in fractions collected at 50 mM imidazole. These fractions were pooled together, concentrated with Aquacide IIA, and stored at –20°C in buffer A supplemented with 50% (v/v) glycerol. Under these conditions, the final yield was nearly 15 mg from a 1–L culture.

2.3. Metal Content and Activity of Recombinant *St*SOD

The iron and manganese content of different recombinant *St*SOD samples was determined by graphite furnace atomic absorption spectrometry, as previously indicated [33]. Metal substitution reactions were carried out as previously described [27]. SOD activity was measured at 25°C in buffer C by the inhibition of cytochrome *c* reduction caused by superoxide anions generated with the xanthine/xanthine oxidase method [17,35]. One unit of SOD activity was defined as the amount of enzyme causing 50% inhibition of cytochrome *c* reduction. The data were reported as mean values of three determinations with the indication of the standard error.

2.4. Other Methods

Protein concentration was determined by the method of Bradford, using bovine serum albumin as standard [36]. Purity of protein samples was assessed by 14% SDS–PAGE according to standard protocols [37]. The quaternary structure of recombinant *St*SOD was evaluated by gel–filtration on a Superdex 75 10/300 GL column (GE Healthcare) eluted with buffer B. The mass spectrometry analysis was realised on protein samples desalted by RP–HPLC, as previously reported [33,38]. The energy of activation E_a and the Arrhenius constant A of the heat inactivation process, and the related thermodynamic parameters of activation, namely enthalpy (ΔH^*), entropy (ΔS^*) and free energy (ΔG^*), were calculated at 70°C as reported elsewhere [30]. The immunoblotting analysis, using anti–nitrotyrosine monoclonal antibodies (Upstate), was carried out as previously described [39].

3. RESULTS

3.1. Size of Superoxide Dismutase from *Streptococcus thermophilus* Strain LMG 18311

The NCBI annotation on the coding sequence of the putative *StsodA* gene (ID: 3164641; *S. thermophilus* strain LMG 18311) [7] led to the prediction of a protein spanning 220 residues encoded by a DNA segment starting with an unusual T$_1$TG triplet. Curiously, this prediction would render *St*SOD longer than other bacterial SODs; indeed, the multiple alignment with other Fe– and Mn–SODs, including the enzyme isolated from the *S. thermophilus* strain AO54 [29] and the closely related bacterium *S. mutans* [10,27], indicated that *St*SOD would contain a N-terminal amino acid extension of 19 residues. Moreover, the position of the most conserved residues, such as those of the first and second coordination sphere, would shift ahead by 19 residues, a finding never reported for bacterial SODs. For these reasons, the assignment of the starting triplet was reconsidered. Indeed, the T$_1$TG starting triplet of the *StsodA* gene was followed by other two ATGs in frame with the coding sequence and located at +28 and +58 from the preceding T$_1$TG. The A$_{58}$TG triplet appeared the best candidate as start codon, because it predicted a shorter *St*SOD spanning 201 residues, which aligned with SOD from *S. thermophilus* strain AO54 [29], and other Fe– and Mn–SODs, without the N–terminal extension. In this way the conserved residues of this enzyme were located in their canonical sequence positions.

To address the question about the length of the amino acid sequence of *St*SOD strain LMG 18311, two vectors for the heterologous expression of the corresponding gene were realised. In particular, the cloned segment in v*St*SOD$_{long}$ and v*St*SOD started from T$_1$TG (mutagenised to A$_1$TG) or A$_{58}$TG, respectively. The purified expression products obtained from bacterial cultures of BL21(DE3) transformed with each vector were analysed by SDS–PAGE. As shown in Fig. (**1**), the sample from v*St*SOD$_{long}$ contained two major protein bands with electrophoretic mobilities corresponding to molecular masses of 26 kDa and 24 kDa, respectively. Vice versa, the sample from v*St*SOD was homogenous and contained a protein band with an apparent mass of 24 kDa, thus corresponding to the enzyme without the N–terminal extension. The identical migration possessed by the lighter protein band in the other enzyme sample allowed its identification as the mature enzyme without the N–terminal extension; therefore, the heavier protein band should represent the enzyme containing its N–terminal extension. Interestingly, in the sample from v*St*SOD$_{long}$, the amount of the heavier band, essentially coincident with the theoretical mass of the expected product (M_r 25686.98, including His tail), was lower

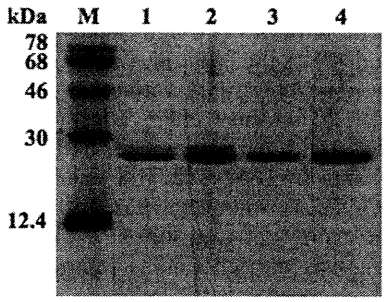

Fig. (1). SDS–PAGE of purified r*St*SOD samples. The migration of 2 and 5 μg of the purified expression product from v*St*SOD$_{long}$ (*lanes* 1 and 2) and v*St*SOD (*lanes* 3 and 4) on a 14% polyacrilamide gel was compared with that of protein standards (*lane* M). The protein standards used were: human transferrin (M_r 78,000); bovine serum albumin (M_r 68,000); albumin from chicken egg (M_r 46,000); carbonic anhydrase from bovine erythrocyte (M_r 30,000); cytochrome *c* from horse heart (M_r 12,400).

than that of the lighter band; moreover, the mass of this lighter band, equal to that obtained from v*St*SOD expression, was coincident with the theoretical mass of the expected lighter product (M_r 23429.28, including His tail).

The M_r of both protein samples was also evaluated by mass spectrometry (Fig. (**2**)). The product obtained from the expression of v*St*SOD$_{long}$ contained five major peaks, the lighter of them with M_r 23298.59 (Fig. (**2A**)); vice versa, the sample obtained from the expression of v*St*SOD showed a single peak with M_r 23298.50 (Fig. (**2B**)). This latter mass was essentially coincident with the lighter peak in Fig. (**2A**) and corresponded to the theoretical M_r of 23298.09 assigned to the product expected from the expression of v*St*SOD, considering His–tail and the lack of initial methionine. Among the other peaks in Fig. (**2A**), the M_r 25687.07 corresponded to the intact product from the v*St*SOD$_{long}$ expression, because it was essentially coincident with the theoretical M_r 25686.98. Peak with M_r 25702.77 could be explained by the oxidation of a methionine residue (theoretical mass difference 16 Da); M_r 25725.56 was due to the combination of methionine oxidation together with the formation of sodium adduct (theoretical extra mass 39 Da), as frequently observed in the mass spectra of proteins. An explanation for the M_r 25156.92 is the possible internal proteolytic cleavage, occurring in the N-terminal extension of the product from v*St*SOD$_{long}$; indeed, the loss of the initial peptide MKALS led to the theoretical M_r 25156.30 for the protein. The instability of the product from the expression of v*St*SOD$_{long}$ led to its partial conversion into the smaller M_r of 23298.59. Furthermore, no peaks corresponding to the size of Mn– or Fe–SOD from the *E. coli* host strain were detected in the mass spectra, thus excluding the possibility of either protein contamination or formation of mixed heterodimers. The homogenous protein sample obtained from the expression of v*St*SOD was the recombinant form of *St*SOD (r*St*SOD) used in this work to characterise its molecular and biochemical properties.

3.2. Structural Organisation, Metal Content and Activity of r*St*SOD

To inspect its structural organization, a 0.11 mg mL^{-1} r*St*SOD sample was analysed by gel filtration chromatography under non–denaturing conditions. After comparison of its elution pattern (Fig. (**3**), ***black line*** **a**) with that of protein standards, a value of 53 kDa was evaluated for its molecular mass. Regardless of the difference from the theoretical mass of 46.6 kDa calculated for two assembled subunits, the finding suggests that the native r*St*SOD is organised as a homodimer, a typical behaviour of mesophilic bacterial SODs. However the mass discrepancy, already observed for the cambialistic *Sm*SOD [27], was further investigated through the gel–flitration of r*St*SOD samples having a concentration up to 8.1 mg mL^{-1}. As shown in Fig. (**3**), at increasing protein concentration, the elution pattern of r*St*SOD became broader with a moderate shift of the major peak and the appearance of a faster–eluting peak in the void volume of the column; furthermore, at the highest concentration tested, two poorly resolved peaks replaced the major peak present in the other elutions. These features were tentatively ascribed to a reversible formation of protein aggregates containing multiple homodimers of the enzyme. Therefore, the mass discrepancy with a theoretical homodimer is likely related to this phenomenon.

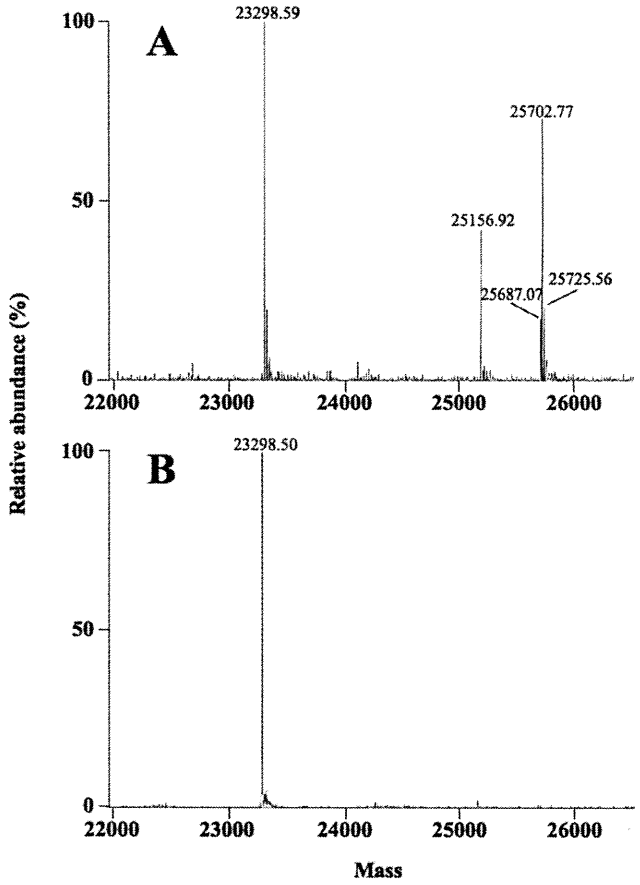

Fig. (2). Electrospray mass spectrum of a purified protein sample from the expression of v*St*SOD$_{long}$ (**A**) and v*St*SOD (**B**).

Some microaerophilic bacteria possess a cambialistic SOD, capable of functioning with Fe or Mn in the active site [22,27]. For instance, the enzyme from *S. mutans* is a cambialistic enzyme, because of its ability to undergo a metal

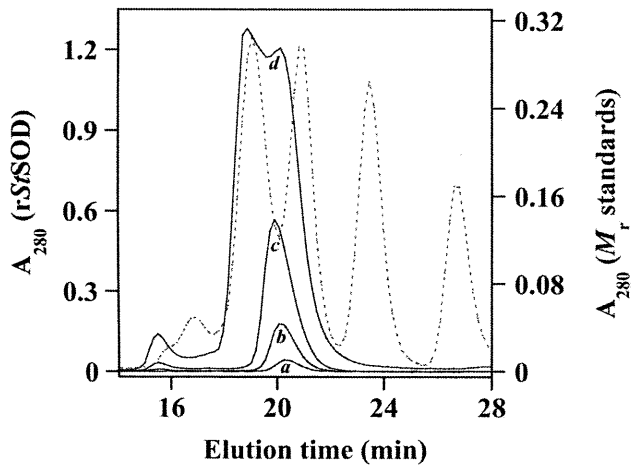

Fig. (3). Structural organization of r*St*SOD. Four dilutions of r*St*SOD in buffer B were analysed on a Superdex 75 10/300 GL column eluted with the same buffer at a flow rate of 0.5 mL min^{-1}. In particular, 100 µL of the following dilutions of r*St*SOD were analysed: 0.11 mg mL^{-1} (line ***a***), 0.44 mg mL^{-1} (line ***b***), 1.6 mg mL^{-1} (line ***c***), 8.1 mg mL^{-1} (line ***d***). The corresponding elution profiles were compared with that of a mixture of protein standards (dotted line), which contained 2.3 mg mL^{-1} bovine serum albumin (M_r 68000), 1.6 mg mL^{-1} albumin from chicken egg (M_r 46000), 0.6 mg mL^{-1} carbonic anhydrase from bovine erythrocite (M_r 30000), 0.4 mg mL^{-1} cytochrome *c* from horse heart (M_r 12400). Absorbance was continuously monitored at 280 nm.

exchange reaction [27]. To evaluate which metal was bound to r*St*SOD during its heterologous production in *E. coli*, the amount of iron and manganese bound to the purified enzyme was measured (Table **1**). The data show that the occupancy of active site by metal cofactor was incomplete, a finding observed also in other SODs belonging to the same family. Indeed, the predicted 1:1 stoichiometry was almost never reached, even when the enzyme was purified from its endogenous source. Furthermore, it has been reported that the Mn uptake in *E. coli* expression systems leads to a low content of this metal in recombinant Mn–SODs [30,31]. Indeed, the purified r*St*SOD sample contained both iron and manganese, even though to a different extent. In particular, the content of Fe (0.35 mol/mol subunit) was nearly 7–fold higher than that of Mn (0.047 mol/mol subunit). An improvement of the metal content of r*St*SOD was tried, by the preparation of a metal–free enzyme, which could then uptake Fe or Mn under selected conditions. However, previously described protocols for the preparation of the apoenzyme [40] were unseccessful for r*St*SOD, because of the occurrence of a massive protein precipitation during the treatment. Therefore, the metal exchange ability of r*St*SOD was investigated using the successful protocol described for the cambialistic *Sm*SOD [27] and was focused at improving the low Mn content of the enzyme. For this reason, a 1.2 mg mL^{-1} sample was incubated at 60°C for 30 min in buffer A in the absence or in the presence of 2 mM $MnCl_2$. After treatment and following extensive dialysis to remove the unbound metal, the amount of Fe and Mn was remeasured (Table **1**). In the sample treated with $MnCl_2$ (r*St*SOD–Mn_{high}) the Mn content improved to 0.49 mol/mol subunit and that of Fe decreased to 0.21 mol/mol subunit. Therefore, the total metal content underwent a significant improvement from 0.4 mol/mol subunit to 0.7 mol/mol subunit. On the other hand, in the control sample (r*St*SOD–Mn_{low}), content of Mn and Fe was essentially equal to that of the untreated sample. These data confirm that r*St*SOD was able to accomodate and exchange iron and manganese in its active site and suggest a moderate preference for iron binding, because a significant Fe content remained bound to the enzyme, even when the protein sample was treated with a high Mn concentration.

Table **1** also reports the specific activity of r*St*SOD before and after the metal exchange reaction. The data indicate that *in vitro* the activity of this crucial antioxidant enzyme from *S. thermophilus* is regulated by its metal cofactor. Indeed, an improvement of the specific activity was measured in r*St*SOD–Mn_{high}, the sample with a 10–fold increased Mn content with respect to r*St*SOD–Mn_{low} or untreated r*St*SOD. The specific activities of the enzyme due to 1 mol Mn or Fe per mol r*St*SOD subunit, called Act_{Mn} or Act_{Fe}, respectively, were extrapolated through the data obtained from r*St*SOD–Mn_{high} and r*St*SOD–Mn_{low}, according to the equation:

$$Act_{tot} = (R_{Mn} \times Act_{Mn}) + (R_{Fe} \times Act_{Fe})$$

where Act_{tot} is the specific activity measured on r*St*SOD–Mn_{high} or r*St*SOD–Mn_{low}, and R_{Mn} and R_{Fe} are the measured molar ratios of Mn and Fe, respectively. The calculated values of Act_{Mn} and Act_{Fe} were 4279 and 2807 U/mg, respectively. Therefore, the Mn–containing form of r*St*SOD is nearly 1.5–fold more active than the Fe–containing form. It is worth noting that the preference for a specific cation during metal uptake and the modulation of the activity upon different metal content are typical features of cambialistic

Table 1. Metal Content and Activity of r*St*SOD

Treatment at 60°C for 30 Min	R_{Mn}[a]	R_{Fe}[a]	Specific Activity[b]
	mol mol^{-1}		U mg^{-1}
None	0.047	0.35	1140
In buffer A	0.046	0.33	1123
In buffer A + 2 mM $MnCl_2$	0.49	0.21	2686

[a]The Mn and Fe content (R_{Mn} and R_{Fe}, respectively) were determined by graphite furnace atomic absorption spectrometry on three dilutions of each sample; variability of the data never exceeded 10%.

[b]Measured in triplicates through the inhibition of the cytochrome *c* reduction in the xanthine/xanthine oxidase system; variability of the data never exceeded 10%.

SODs, as already observed in *Sm*SOD [27]. However, in that case the regulation of SOD activity by metal cofactor was much more evident and thus relevant; indeed, the Mn–containing form of the *S. mutans* enzyme was nearly 71–fold more active than the Fe–containing form.

3.3. Thermal Inactivation of r*St*SOD

Because of the moderately thermophilic behaviour of *S. thermophilus* [1], the heat resistance of r*St*SOD was investigated through a thermal inactivation profile. To this aim, aliquots of a r*St*SOD solution were incubated for 10 min at different temperatures and then immediately cooled on ice. The residual SOD activity of the treated samples was reported as a function of temperature; a half–inactivation temperature ($T_{1/2}$) of 73.5°C was calculated from the resulting inactivation profile (Fig. (**4**)). The heat stability of r*St*SOD was also studied through inactivation kinetics realised at temperatures ranging between 64°C and 74°C. The analysis was carried out on r*St*SOD–Mn_{high} and r*St*SOD–Mn_{low} to study the effect of a different Mn content on the heat inactivation parameters of the enzyme. Both enzymes followed first–order kinetics at each temperature and the corresponding inactivation rate constants were treated according to the Arrhenius equation (Fig. (**5**)). Plots were linear in the 64–71°C temperature interval, thus allowing the determination of the energetic parameters of the heat inactivation process. The values of E_a, ΔH^*, ΔS^*, and ΔG^* calculated for r*St*SOD–Mn_{high} and r*St*SOD–Mn_{low} are reported in Table **2**. The differences found between the two enzyme samples were interpreted in terms of the different Mn content. Indeed, a higher content of this metal cofactor lowered the energy of activation and thus the enthalpic barrier of the heat inactivation process of the enzyme. Vice versa, an opposite trend was observed for the entropic factor, because a higher Mn level led to a less favourable ΔS^*. Therefore, the energetic parameters of the heat inactivation process of r*St*SOD were affected by the Mn content, as already observed for the cambialistic *Sm*SOD [27].

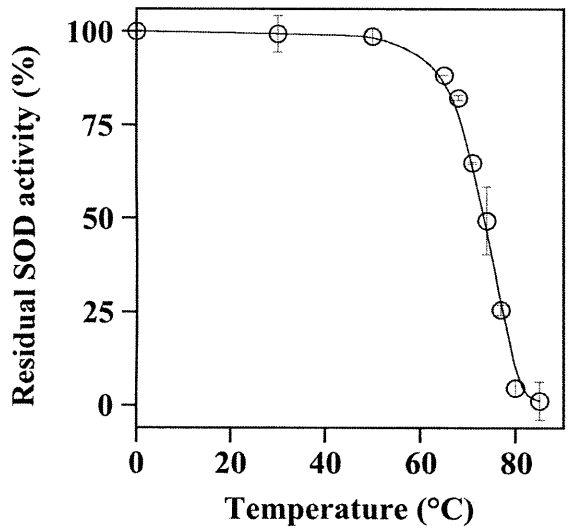

Fig. (4). Heat inactivation profile of r*St*SOD. Aliquots from a 50 μg mL^{-1} r*St*SOD solution in buffer A were incubated for 10 min at the indicated temperatures and then immediately cooled on ice for 30 min. The residual SOD activity, measured in triplicates on 25 μL aliquots withdrawn from the treated samples, was compared with that of an untreated sample kept at 0°C, taken as 100% activity.

3.4. Inhibition and Inactivation of r*St*SOD

The resistance of r*St*SOD to typical inhibitors and inactivators was investigated, focusing the attention on the effect of a different Mn content in the enzyme sensitivity. To this aim, the study was carried out on r*St*SOD–Mn_{high} and r*St*SOD-Mn_{low} and the first compound considered was sodium azide. Fig. (**6**) reports the dose–dependent inhibition profile obtained when the activity of the enzyme samples was measured in the presence of increasing sodium azide concentrations. In both cases the percentage of inhibition was less than 50% at 10 mM NaN_3, the highest concentration tested for this compound, a behaviour indicating the weak inhibition power of sodium azide. However, the comparison between r*St*SOD–Mn_{high} and r*St*SOD–Mn_{low} pointed to a moderately greater resistance of the enzyme when a higher Mn amount was bound to its active site.

Hydrogen peroxide is a physiological inactivator of SODs, mainly acting on the Fe–containing enzymes. The effect of this compound on the activity of the cambialistic r*St*SOD was studied through inactivation kinetics carried out at 30°C in the presence of 1 mM H_2O_2. As shown in Fig. (**7**), the r*St*SOD–Mn_{high} sample was essentially insensitive to this treatment, because its extrapolated half–life was 139 h. A noticeable resistance to hydrogen peroxide was observed also with r*St*SOD–Mn_{low}, even though with a significantly shorter half–life of 5.6 h. These data point to a marked resistance of r*St*SOD towards H_2O_2 inactivation, a feature mainly

Table 2. Energy of Activation and other Thermodynamic Parameters related to the Heat Inactivation Process of r*St*SOD Samples with a Different Mn Content

	Metal content		Energetic parameters			
Enzyme sample	Mn	Fe	E_a	$\Delta H^{*\,a}$	$\Delta S^{*\,a}$	$\Delta G^{*\,a}$
	mol mol^{-1}		kJ mol^{-1}	kJ mol^{-1}	J mol^{-1} K^{-1}	kJ mol^{-1}
r*St*SOD–Mn_{low}	0.046	0.33	240	237	416	94
r*St*SOD–Mn_{high}	0.49	0.21	207	204	317	95

[a]Calculated at 70°C.

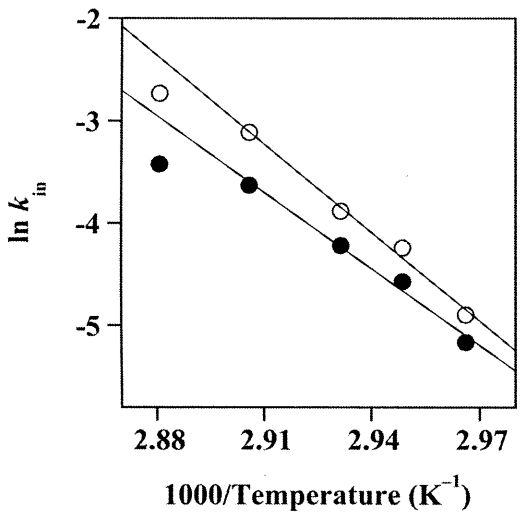

Fig. (5). Arrhenius plot of the heat inactivation process of r*St*SOD. The kinetic rate constants of inactivation (k_{in}) for r*St*SOD–Mn_{low} (○) and r*St*SOD–Mn_{high} (●) were obtained from heat inactivation kinetics realised at five temperatures, *i.e.* 64°C, 66°C, 68°C, 71°C and 74 °C. To this aim, a 50 μg mL^{-1} solution of each enzyme sample dissolved in buffer A was incubated at the indicated temperatures and, at five selected times depending on the temperature chosen, an aliquot was withdrawn from each kinetics, immediately cooled on ice for 1 h and then assayed for its residual SOD activity. In order to measure comparable values of activity, assays were realised on 15–μL or 8–μL aliquots from r*St*SOD–Mn_{low} or r*St*SOD–Mn_{high}, respectively. The activity data were treated according to the equation of a first order kinetics ($\ln A_t/A_0 = - k_{in} t$), where A_0 and A_t represent the activities measured at the time *zero* and *t*, respectively. All kinetics were linear in the selected time range and the squared correlation coefficient of data fitting ranged between 0.973 and 0.998. The calculated values of k_{in} (s^{-1}) were treated according to the Arrhenius equation; for a better fitting of the data, the k_{in} value at 74°C for both r*St*SOD–Mn_{low} and r*St*SOD–Mn_{high} was excluded. The squared coerrelation coefficient of data fitting was 0.991 and 0.989 for r*St*SOD–Mn_{low} and r*St*SOD–Mn_{high}, respectively.

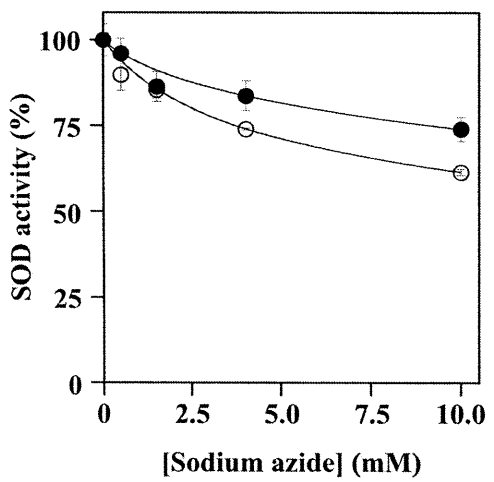

Fig. (6). Dose–dependent inhibition profile of r*St*SOD by sodium azide. The SOD activity of 0.58 μg mL^{-1} r*St*SOD–Mn_{low} (○) or 0.25 μg mL^{-1} r*St*SOD–Mn_{high} (●) was measured in triplicates in the presence of the indicated sodium azide concentration. The activity was expressed as a percentage of the activity measured in the absence of inhibitor.

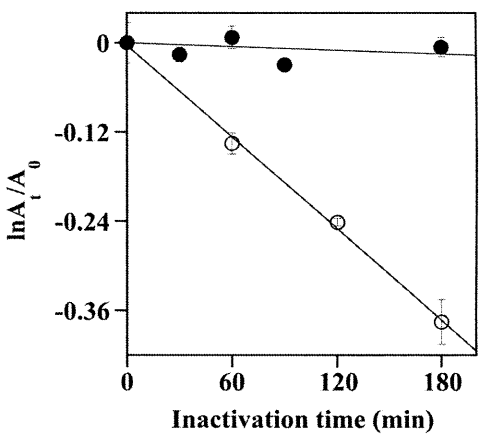

Fig. (7). Inactivation kinetics of r*St*SOD by hydrogen peroxide. A solution of 50 μg mL^{-1} r*St*SOD–Mn_{low} (○) or r*St*SOD–Mn_{high} (●) in buffer A was incubated at 30°C in the presence of 1 mM H_2O_2. At the times indicated, 15–μl or 8–μl aliquots were withdrawn from the incubation mixtures of r*St*SOD–Mn_{low} or r*St*SOD–Mn_{high}, respectively, and immediately assayed for SOD activity. A_0 and A_t represent the activities measured at the time *zero* and *t*, respectively.

evident for the enzyme containing a higher level of the Mn cofactor.

Another physiological inactivator of Fe– and Mn–SODs is peroxynitrite. This harmful ROS causes the covalent modification of a specific and conserved tyrosine residue of the enzyme located in the second coordination sphere of the metal [41,42]. To evaluate the effect of this compound, aliquots of r*St*SOD–Mn_{high} and r*St*SOD–Mn_{low} were incubated for 30 min at room temperature in the presence of increasing sodium peroxynitrite concentrations. The residual SOD activity of the treated samples was then measured and reported as a percentage with respect to untreated controls (Fig. (**8**)). The dose–dependent inactivation profiles indicate that peroxynitrite caused a moderate inactivation of the cambialistic enzyme; furthermore, differently from what was observed with the other tested compounds, r*St*SOD–Mn_{high} showed a higher sensitivity to peroxynitrite compared to r*St*SOD–Mn_{low}. Indeed, the concentration of inactivator leading to 50% reduction of activity (IC_{50}) was 94 μM for r*St*SOD–Mn_{high} and 269 μM for r*St*SOD–Mn_{low}. It is known that peroxynitrite leads to the formation of 3–nitrotyrosine [41–43], a modification usually revealed through the immunoblotting analysis [27,39]. For this reason, the peroxynitrite–treated samples were also probed with anti–nitrotyrosine antibodies and the results obtained are shown in Fig. (**9**). The immunoreactivity, already evident at the lowest concentration tested of peroxynitrite, increased in a dose–dependent manner for both r*St*SOD–Mn_{high} and r*St*SOD–Mn_{low}. Also in this case, a greater reactivity was evident in the enzyme sample containing the higher Mn level.

The results obtained with the *S. thermophilus* enzyme were compared with the data previously reported for the homologous enzyme from *S. mutans* [27]. All tested compounds displayed a lower inhibiting/inactivating power on r*St*SOD compared to the recombinant *Sm*SOD. Nevertheless, also in this case the content of bound Mn in the active site of

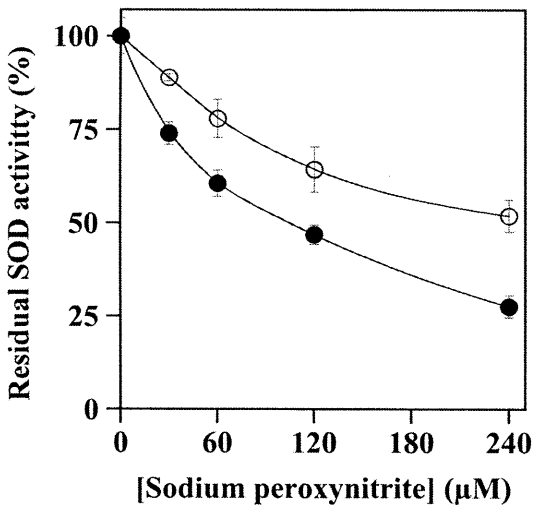

Fig. (8). Dose–dependent inactivation profile of r*St*SOD by sodium peroxynitrite. A solution of 50 μg mL^{-1} r*St*SOD–Mn_{low} (○) or r*St*SOD–Mn_{high} (●) in buffer A was incubated at 25°C for 30 min in the presence of the indicated sodium peroxynitrite concentration. After the treatment, 15–μl or 8–μl aliquots from r*St*SOD–Mn_{low} or r*St*SOD–Mn_{high}, respectively, were analysed for residual SOD activity. The results were expressed as a percentage of the activity measured in the absence of sodium peroxynitrite.

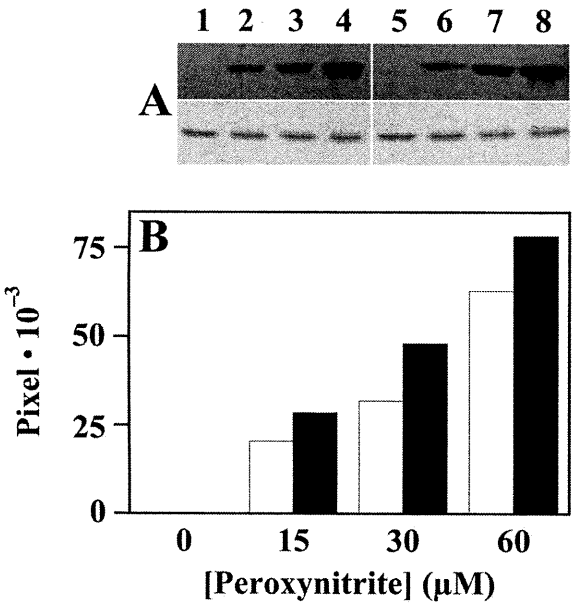

Fig. (9). Tyrosine nitration of r*St*SOD by sodium peroxynitrite. (**A**) Immunoblotting. A solution of 50 μg mL^{-1} r*St*SOD–Mn_{low} or r*St*SOD–Mn_{high} in buffer A was incubated at 25°C for 1 h in the presence of the indicated sodium peroxynitrite concentration. After the incubation, 15–μl aliquots were fractionated on SDS–PAGE and then analysed by Western blotting using anti–nitrotyrosine antibodies (upper panel) or Coomassie staining as loading control (lower panel). *Lanes* 1–4, r*St*SOD–Mn_{low} after treatment without (*lane* 1) or with 15 μM (*lane* 2), 30 μM (*lane* 3) or 60 μM (*lane* 4) sodium peroxynitrite; *lanes* 5–8, r*St*SOD–Mn_{high} after treatment without (*lane* 5) or with 15 μM (*lane* 6), 30 μM (*lane* 7) or 60 μM (*lane* 8) sodium peroxynitrite. (**B**) Scan densitometry of the immunoblotting referred to r*St*SOD–Mn_{low} (open columns) or r*St*SOD–Mn_{high} (filled columns).

the enzyme regulated the resistance towards each inhibitor/inactivator.

4. DISCUSSION

This work describes the characterisation of a recombinant SOD from *Streptococcus thermophilus*, a facultative anaerobic microorganism currently used as a starter in the manufacture of dairy products. The molecular properties of r*St*SOD were investigated and the first point addressed in this work regards the size of the enzyme, because of the existence of another possible starting codon in the *StsodA* gene, besides that annotated in the NCBI databases [7]. Indeed, when recombinant *St*SOD forms starting from two different initiation codons (the T_1TG triplet postulated in the NCBI databases and the downstream $A_{58}TG$ triplet) were produced and compared, the longer version of the enzyme was almost completely converted into the shorter one during its heterologous production in *E. coli*. The absence of the unusual N–termimal extension of 19 residues in r*St*SOD makes this enzyme essentially identical to the corresponding one from the *S. thermophilus* strain AO54 and similar to the other bacterial SODs. Furthermore, it has been reported that the primer extension realised on the 5'end transcript of the *sodA* gene from the *S. thermophilus* strain AO54 mapped the transcriptional start site on a G located 27 nucleotides upstream of the ATG start codon coincident with the $A_{58}TG$ triplet from *S. thermophilus* strain LMG 18311 [29]. Also the ribosomal binding site was located between the transcriptional start site and the ATG start codon. Notably, the nucleotide sequence at the 5' terminus of the *sodA* gene from *S. thermophilus* strains AO54 and LMG 18311 is identical. All these data strongly suggest that the starting codon preferentially used during the heterologous expression of the *StsodA* gene from the *S. thermophilus* strain LMG 18311 is $A_{58}TG$ and that the amino acid sequence of *St*SOD spans 201 residues.

The metal content of r*St*SOD revealed the presence of both Fe and Mn in the active site of the enzyme, even though with a higher amount of Fe with respect to Mn. However, a significant amount of enzyme was free of metal, a finding typically observed for recombinant SOD production. The presence of Fe and Mn in the active site of r*St*SOD prompted an investigation on the metal exchange reaction. In particular, we checked whether the small amount of Mn could increase upon a mild heat treatment of the enzyme in the presence of Mn^{++} ions. Indeed, part of the bound Fe was exchanged with Mn, and this led to a ten–fold improvement of the Mn level; nevertheless, a significant amount of Fe remained bound to r*St*SOD. Therefore, the total metal content of the enzyme significantly improved with respect to that measured in the untreated sample, thus approaching the theoretical 1:1 stoichiometry. These data suggest that r*St*SOD is able to bind either Fe or Mn, even though with a moderate preference for Fe binding.

The activity of samples of r*St*SOD with a different metal content was measured; indeed, a 1.5–fold increment of the specific activity was extrapolated in the Mn–containing with respect to the Fe–containing form of r*St*SOD. This behaviour, typically observed in cambialistic SODs, indicates that also the *S. thermophilus* enzyme belongs to this small group

of SODs. The cambialistic nature of r*St*SOD was compared with that of the homologous enzyme from *S. mutans* [27]. The most striking difference was observed in the regulation of the activity by metal cofactor. Indeed, the Mn–containing form of the *S. mutans* enzyme was much more active if compared to the corresponding one from *S. thermophilus*; an opposite trend was observed for the Fe–containing form. This feature becomes more evident when considering the ratios Act_{Mn}/Act_{Fe} of the two enzymes, because the values for *S. mutans* and *S. thermophilus* are 71 and 1.5, respectively. A smaller difference between the two enzymes resides in the metal uptake, because a greater Mn level was reached in the *S. thermophilus* compared to the *S. mutans* enzyme. All these findings could be related to the growth conditions of *S. thermophilus*, which for its ecological niche does not require a remarkable adaptation for tolerating strong and prolonged oxidative stress conditions. Vice versa, *S. mutans* is more adapetd to the oxidative stress, because it survives in the oral cavity in the presence of high oxygen concentrations.

The comparison of the molecular mass of r*St*SOD determined under denaturing and native conditions showed that the enzyme is structurally organised as a homodimer. Interestingly, when high concentrations of the enzyme were analysed by gel–filtration, higher–mass protein aggregates were observed, suggesting the possible formation of multiple homodimers of the enzyme. The formation of protein aggregates could be another interesting feature of cambialistic SODs, because a similar trend was observed with the cambialistic *Sm*SOD [27]. The functional analysis of these protein aggregates was complicated by the easy reversibility of the transition between aggregates and homodimers.

The thermostability of r*St*SOD was investigated, because *S. thermophilus* resists to the moderate thermal treatment of the industrial processes [2–4]. The half–inactivation temperature of the enzyme ($T_{1/2}$, 73.5°C), determined through its thermal inactivation profile, ranks r*St*SOD as a moderately heat resistant SOD. Curiously, in spite of the thermophilic character of *S. thermophilus*, the mesophlic mitochondrial Mn–SOD from rat mitochondria ($T_{1/2}$, 80°C) [30] is more resistant than r*St*SOD. The effect of the Mn cofactor content on the thermal inactivation process of r*St*SOD was evaluated through the determination of the energetic parameters of this process on two enzyme samples with a significantly different Mn level. Indeed, in the presence of a higher Mn content, the enthalpic barrier of the inactivation process of r*St*SOD is more favourable, whereas the entropic factor becomes less positive. This behaviour is similar to what was already reported for *Sm*SOD, even though in this latter case the differences in enthaplic and entropic parameters were much more significant [27], similarly to what was observed for the effect of Mn on the regulation of enzyme activity.

Inhibition/inactivation of the SOD activity is usually related to the type of metal bound in the active site [18,19], a feature particularly relevant in cambialistic SODs. Indeed, the data reported in this work show that the sensitivity of r*St*SOD to its typical inhibitors/inactivators was regulated by the Mn content of the enzyme. The results on the effect of sodium azide on the activity of r*St*SOD suggest that this compound is a weak inhibitor of the *S. thermophilus* enzyme, because the percentage of inhibition measured was modest even at high concentrations of NaN_3. Moreover, the r*St*SOD resistance to sodium azide was only hardly decreased in the enzyme sample with a lower Mn content. The comparison with the *S. mutans* system [27] points to a higher resistance for the *S. thermophilus* enzyme and to a possible inverted trend in the effect of the Mn cofactor; however, the significance of this latter observation is uncertain because of the low inhibitory effect by sodium azide. We could speculate that the low sensitivity to NaN_3 is in part due to the thermophilic character of the microorganism; in fact, the Fe–SOD from the hyperthermophilic archaeon *Sulfolobus solfataricus* displayed a full resistance to sodium azide [35,44].

The studies on the effects of two physiological inactivators, hydrogen peroxide and peroxynitrite, on the cambialistic r*St*SOD confirm a general lower sensitivity of this enzyme compared to that from *S. mutans* [27]; furthermore, the data point to the relevance of the metal cofactor in the r*St*SOD resistance to these inactivators. Indeed, the inactivation power of H_2O_2 was almost completely abolished in the enzyme sample with a higher Mn content, thus rendering *St*SOD very similar to a typical Mn–SOD. The *St*SOD resistance to hydrogen peroxide is functional to the *S. thermophilus* survival in the milk product [16]. Indeed, this bacterium cannot ensure a fast scavenging of the H_2O_2 produced by the SOD activity, because its genome lacks the catalase gene [7].

The inactivating power of peroxynitrite on r*St*SOD is more pronounced compared to H_2O_2, though lower than that observed on *Sm*SOD [27]. The immunoblotting analysis revealed that r*St*SOD inactivation takes place through the covalent modification of tyrosine residue(s) into 3–nitrotyrosine. Differently from the effect of H_2O_2, the sensitivity of the cambialistic enzyme to peroxynitrite was improved by the Mn content of r*St*SOD, a behaviour similar to what reported for *Sm*SOD [25]. Also this behaviour makes the *S. thermophilus* enzyme more similar to a Mn–SOD, rather than to a Fe–SOD. Indeed, it is known that the inactivating power of peroxynitrite is higher on Mn–SODs, such as the mitochondrial human enzyme [45], than on Fe–SODs, such as the iron–containing enzyme from *E. coli* [42].

The functional differences between *St*SOD and *Sm*SOD could be explained in terms of dissimilarities in the amino acid sequence. Under this concern, the enzymes share 87% amino acid identity (Fig. (**10**)). Among the amino acid dissimilarities, our attention was attracted by position 113, occupied by a Gln or Lys residue in *St*SOD or *Sm*SOD, respectively. When a Lys is present in this position (Lys_{107} in Fe–SOD from *E. coli*), a conserved cation–π interaction is evident in the core 3D–structure of SODs [46]. It is conceivable that this interaction is maintained in *Sm*SOD. However, the presence of a Gln residue in *St*SOD could destroy this interaction, thus leading to the observed differences in the biochemical properties between *St*SOD and *Sm*SOD.

5. CONCLUSIONS

The characterization of SODs from the taxonomically related aerotolerant microorganisms *S. thermophilus* and *S. mutans* allows an insight on the putative cambialistic behaviour of these enzymes. Indeed, the regulation of SOD func-

```
StSOD   AIILPDLPYA YDALEPYIDA ETMTLHHDKH HATYVANANA ALEKHPEIGE DLEALLADVE KIPADIRQAL  70
SmSOD   AILLPDLPYA YDALEPYIDA ETMTLHHDKH HATYVANANA ALEKHPEIGE NLEVLLADVE QIPADIRQSL  70

StSOD   INNGGGHLNH ALFWELLSPE KQEPTAEVAA AINEAFGSFE AFQEVFTTSA TTRFGSGWAW LVVNAEGKLE 140
SmSOD   INNGGGHLNH ALFWELLSPE KTKVTAEVAA AINEAFGSFD DFKAAFTAAA TTRFGSGWAW LVVDKEGKLE 140

StSOD   VVSTPNQDTP ISDGKKPILA LDVWEHAYYL KYRNVRPNYI KAFFEIINWN KVAELYAEA- -K 200
SmSOD   VTSTANQDTP ISQGLKPILA LDVWEHAYYL NYRNVRPNYI KAFFEVINWN TVARLYAEAL TK 202
```

Fig. (10). Sequence alignment between *St*SOD and *Sm*SOD. The initial methionine is absent in both enzymes. Amino acid position 113 is shaded.

tions by metal cofactor in cambialistic enzymes is likely related to the adaptation mechanisms that each microorganism adopts to face different environmental conditions. The most striking difference between *S. thermophilus* and *S. mutans* SOD is the significantly lower regulation of the activity of the former enzyme by the metal cofactor. This finding probably reflects the scarce adaptability of *S. thermophilus* to survive under prolonged and severe oxidative stress conditions.

ACKNOWLEDGEMENTS

Work supported by grants from PRIN 2007 and 2009. Alberto De Vendittis was recipient of a fellowship awarded from CEINGE Biotecnologie Avanzate, Naples.

ABBREVIATIONS

Act_{Fe} and Act_{Mn}	=	extrapolated specific activity of r*St*SOD due to 1 mol/mol of Fe or Mn cofactor, respectively
Act_{tot}	=	specific activity measured on r*St*SOD
IC_{50}	=	concentration of inhibitor/inactivator leading to 50% reduction of activity
IPTG	=	isopropyl-β-thiogalactopiranoside
R_{Fe} and R_{Mn}	=	molar ratio in r*St*SOD of Fe and Mn, respectively
ROS	=	reactive oxygen species
SOD	=	superoxide dismutase
*Sm*SOD	=	SOD from *Streptococcus mutans*
*St*SOD	=	SOD from *Streptococcus thermophilus*
r*St*SOD	=	recombinant *St*SOD
v*St*SOD$_{long}$ and v*St*SOD	=	vectors for the expression of the *StsodA* gene starting from T_1TG (mutagenised to A_1TG) or A_{58}TG, respectively
r*St*SOD–Mn$_{low}$ and r*St*SOD–Mn$_{high}$	=	r*St*SOD containing a high or low level of Mn, respectively
$T_{1/2}$	=	half–inactivation temperature

REFERENCES

[1] Hols, P.; Hancy, F.; Fontaine, L.; Grossiord, B.; Prozzi, D.; Leblond-Bourget, N.; Decaris, B.; Bolotin, A.; Delorme, C.; Dusko Ehrlich, S.; Guedon, E.; Monnet, V.; Renault, P.; Kleerebezem, M. New insights in the molecular biology and physiology of *Streptococcus thermophilus* revealed by comparative genomics. *FEMS Microbiol. Rev.*, **2005**, *29*, 435–463.

[2] Thunell, R.K.; Sandine, W.E. In: *Bacterial starter culture for foods*; Gilliland, S.E., Ed.; CRC Press Inc., Boca Raton, Fla, **1985**; pp. 127–144.

[3] Fox, P.F. *Cheese: chemistry, physics and microbiology*; Chapman & Hall: London, **1993**.

[4] Tamime, A.Y.; Deeth, H.C. Yogurt: technology and biochemistry. *J. Food Protect.*, **1980**, *43*, 939–977.

[5] Mitchell, T.J. The pathogenesis of streptococcal infections: from tooth decay to meningitis. *Nat. Rev. Microbiol.*, **2003**, *1*, 219–230.

[6] Tettelin, H. Streptococcal genomes provide food for thought. *Nat. Biotechnol.*, **2004**, *22*, 1523–1524.

[7] Bolotin, A.; Quinquis, B.; Renault, P.; Sorokin, A.; Dusko Ehrlich, S.; Kulakauskas, S.; Lapidus, A.; Goltsman, E.; Mazur, M.; Pusch, G.D.; Fonstein, M.; Overbeek, R.; Kyprides, N.; Purnelle, B.; Prozzi, D.; Ngui, K.; Masuy, D.; Hancy, F.; Burteau, S.; Boutry, M.; Delcour, J.; Goffeau, A.; Hols, P. Complete sequence and comparative genome analysis of the dairy bacterium *Streptococcus thermophilus*. *Nat. Biotechnol.*, **2004**, *22*, 1554–1558.

[8] Makarova, K.; Slesarev, A.; Wolf, Y.; Sorokin, A.; Mirkin, B.; Koonin, E.; Pavlov, A.; Pavlova, N.; Karamychev, V.; Polouchine, N.; Shakhova, V.; Grigoriev, I.; Lou, Y.; Rohksar, D.; Lucas, S.; Huang, K.; Goodstein, D.M.; Hawkins, T.; Plengvidhya, V.; Welker, D.; Hughes, J.; Goh, Y.; Benson, A.; Baldwin, K.; Lee, J.H.; Díaz-Muñiz, I.; Dosti, B.; Smeianov, V.; Wechter, W.; Barabote, R.; Lorca, G.; Altermann, E.; Barrangou, R.; Ganesan, B.; Xie, Y.; Rawsthorne, H.; Tamir, D.; Parker, C.; Breidt, F.; Broadbent, J.; Hutkins, R.; O'Sullivan, D.; Steele, J.; Unlu, G.; Saier, M.; Klaenhammer, T.; Richardson, P.; Kozyavkin, S.; Weimer, B.; Mills, D. Comparative genomics of the lactic acid bacteria. *Proc. Natl. Acad. Sci. USA*, **2006**, *103*, 15611–15616.

[9] Sun, Z.; Chen, X.; Wang, J.; Zhao, W.; Shao, Y.; Wu, L.; Zhou, Z.; Sun, T.; Wang, L.; Meng, H.; Zhang, H.; Chen, W. Complete genome sequence of *Streptococcus thermophilus* strain ND03. *J. Bacteriol.*, **2011**, *193*, 793–794.

[10] Ajdic, D.; McShan, W.M; McLaughlin, R.E.; Savic, G.; Chang, J.; Carson, M.B.; Primeaux, C.; Tian, R.; Kenton, S.; Jia, H.; Lin, S.; Qian, Y.; Li, S.; Zhu, H.; Najar, F.; Lai, H.; White, J.; Roe, B.A.; Ferretti, J.J. Genome sequence of *Streptococcus mutans* UA159, a cariogenic dental pathogen. *Proc. Natl. Acad. Sci. USA*, **2002**, *99*, 14434–14439.

[11] Ferretti, J.J.; McShan, W.M.; Ajdic, D.; Savic, D.J.; Savic, G.; Lyon, K.; Primeaux, C.; Sezate, S.; Suvorov, A.N.; Kenton, S.; Lai, H.S.; Lin, S.P.; Qian, Y.; Jia, H.G.; Najar, F.Z.; Ren, Q.; Zhu, H.; Song, L.; White, J.; Yuan, X.; Clifton, S.W.; Roe, B.A.; McLaughlin, R. Complete genome sequence of an M1 strain of *Streptococcus pyogenes. Proc. Natl. Acad. Sci. USA*, **2001**, *98*, 4658–4663.

[12] Glaser, P.; Rusniok, C.; Buchrieser, C.; Chevalier, F.; Frangeul, L.; Msadek, T.; Zouine, M.; Couvé, E.; Lalioui, L.; Poyart, C.; Trieu-Cout, P.; Kunst, F. Genome sequence of *Streptococcus agalactiae*, a pathogen causing invasive neonatal disease. *Mol. Microbiol.*, **2002**, *45*, 1499–1513.

[13] Hoskins, J.; Alborn, W.E. Jr; Arnold, J.; Blaszczak, L.C.; Burgett, S.; DeHoff, B.S.; Estrem, S.T.; Fritz, L.; Fu, D.J.; Fuller, W.; Geringer, C.; Gilmour, R.; Glass, J.S.; Khoja, H.; Kraft, A.R.; Lagace, R.E.; LeBlanc, D.J.; Lee, L.N.; Lefkowitz, E.J.; Lu, J.; Matsushima, P.; McAhren, S.M.; McHenney, M.; McLeaster, K.; Mundy, C.W.; Nicas, T.I.; Norris, F.H.; O'Gara, M.; Peery, R.B.; Robertson, G.T.; Rockey, P.; Sun, P.M.; Winkler, M.E.; Yang, Y.; Young-Bellido, M.; Zhao, G.; Zook, C.A.; Baltz, R.H.; Jaskunas, S.R.; Rosteck, P.R. Jr; Skatrud, P.L.; Glass, J.I. Genome of the bacterium *Streptococcus pneumoniae* strain R6. *J. Bacteriol.*, **2001**, *183*, 5709–5717.

[14] Tettelin, H.; Nelson, K.E.; Paulsen, I.T.; Eisen, J.A.; Read, T.D.; Peterson, S.; Heidelberg, J.; DeBoy, R.T.; Haft, D.H.; Dodson, R.J.; Durkin, A.S.; Gwinn, M.; Kolonay, J.F.; Nelson, W.C.; Peterson, J.D.; Umayam, L.A.; White, O.; Salzberg, S.L.; Lewis, M.R.; Radune, D.; Holtzapple, E.; Khouri, H.; Wolf, A.M.; Utterback, T.R.; Hansen, C.L.; McDonald, L.A.; Feldblyum, T.V.; Angiuoli, S.; Dickinson, T.; Hickey, E.K.; Holt, I.E.; Loftus, B.J.; Yang, F.; Smith, H.O.; Venter, J.C.; Dougherty, B.A.; Morrison, D.A.; Hollingshead, S.K.; Fraser, C.M. Complete genome sequence of a virulent isolate of *Streptococcus pneumoniae. Science*, **2001**, *293*, 498–506.

[15] Tettelin, H.; Masignani, V.; Cieslewicz, M.J.; Eisen, J.A.; Peterson, S.; Wessels, M.R.; Paulsen, I.T.; Nelson, K.E.; Margarit, I.; Read, T.D.; Madoff, L.C.; Wolf, A.M.; Beanan, M.J.; Brinkac, L.M.; Daugherty, S.C.; DeBoy, R.T.; Durkin, A.S.; Kolonay, J.F.; Madupu, R.; Lewis, M.R.; Radune, D.; Fedorova, N.B.; Scanlan, D.; Khouri, H.; Mulligan, S.; Carty, H.A.; Cline, R.T.; Van Aken, S.E.; Gill, J.; Scarselli, M.; Mora, M.; Iacobini, E.T.; Brettoni, C.; Galli, G.; Mariani, M.; Vegni, F.; Maione, D.; Rinaudo, D.; Rappuoli, R.; Telford, J.L.; Kasper, D.L.; Grandi, G.; Fraser, C.M. Complete genome sequence and comparative genomic analysis of an emerging human pathogen, serotype V *Streptococcus agalactiae. Proc. Natl. Acad. Sci. USA*, **2002**, *99*, 12391–12396.

[16] Thibessard, A.; Fernandez, A.; Gintz, B.; Leblond-Bourget, N.; Decaris, B. Hydrogen peroxide effects on *Streptococcus thermophilus* CNRZ368 cell viability. *Res. Microbiol.*, **2001**, *152*, 593–596.

[17] McCord, J.M.; Fridovich, I. Superoxide dismutase. An enzymic function for erythrocuprein (hemocuprein). *J. Biol. Chem.*, **1969**, *244*, 6049–6055.

[18] Bannister, J.V.; Bannister, W.H.; Rotilio, G. Aspects of the structure, function, and applications of superoxide dismutase. *CRC Crit. Rev. Biochem.*, **1987**, *22*, 111–180.

[19] Zelko, I.N.; Mariani, T.J.; Folz, R.J. Superoxide dismutase multigene family: a comparison of the CuZn–SOD (SOD1), Mn–SOD (SOD2), and EC–SOD (SOD3) gene structures, evolution, and expression. *Free Radic. Biol. Med.*, **2002**, *33*, 337–349.

[20] Yamakura, F.; Kobayashi, K.; Ue H.; Konno, M. The pH–dependent changes of the enzyme activity and spectroscopic properties of iron–substituted manganese superoxide dismutase. A study on the metal–specific activity of Mn–containing superoxide dismutase. *Eur. J. Biochem.*, **1995**, *227*, 700–706.

[21] Whittaker, M.M.; Whittaker, J.W. Mutagenesis of a proton linkage pathway in *Escherichia coli* superoxide dismutase. *Biochemistry*, **1997**, *36*, 8923–8931.

[22] Meier, B.; Barra, D.; Bossa, F.; Calabrese, L.; Rotilio, G. Synthesis of either Fe– or Mn–superoxide dismutase with an apparently identical protein moiety by an anaerobic bacterium dependent on the metal supplied. *J. Biol. Chem.*, **1982**, *257*, 13977–13980.

[23] Gregory, E.M.; Dapper, C.H. Isolation of iron–containing superoxide dismutase from *Bacteroides fragilis*: reconstitution as a Mn–containing enzyme. *Arch. Biochem. Biophys.*, **1983**, *220*, 293–300.

[24] Martin, M.E.; Byers, B.R.; Olson, M.O.J.; Salin, M.L.; Arceneaux, J.E.L.; Tolbert, C. A *Streptococcus mutans* superoxide dismutase that is active with either manganese or iron as a cofactor. *J. Biol. Chem.*, **1986**, *261*, 9361–9367.

[25] Amano, A.; Shizukuishi, S.; Tamagawa, H.; Iwakura, K.; Tsunasawa, S.; Tsunemitsu, A. Characterization of superoxide dismutase purified from either anaerobically maintained or aerated *Bacteroides gingivalis. J. Bacteriol.*, **1990**, *172*, 1457–1463.

[26] Tabares, L.C.; Bittel, C.; Carrillo, N.; Bortolotti, A.; Cortez, N. The single superoxide dismutase of *Rhodobacter capsulatus* is a cambialistic, manganese–containing enzyme, *J. Bacteriol.*, **2003**, *185*, 3223–3227.

[27] De Vendittis, A.; Amato, M.; Michniewicz, A.; Parlato, G.; De Angelis, A.; Castellano, I.; Rullo, R.; Riccitiello, F.; Rengo, S.; Masullo, M.; De Vendittis, E. Regulation of the properties of superoxide dismutase from the dental pathogenic microorganism *Streptococcus mutans* by iron– and manganese–bound co-factor. *Mol. BioSyst.*, **2010**, *6*, 1973–1982.

[28] Chang, S.K.; Hassan, H.M. Characterization of superoxide dismutase in *Streptococcus thermophilus. Appl. Environ. Microbiol.*, **1997**, *63*, 3732–3735.

[29] Andrus, J.M.; Bowen, S.W.; Klaenhammer, T.R.; Hassan, H.M. Molecular characterization and functional analysis of the manganese–containing superoxide dismutase gene (*sodA*) from *Streptococcus thermophilus* AO54. *Arch. Biochem. Biophys.*, **2003**, *420*, 103–113.

[30] Castellano, I.; Cecere, F.; De Vendittis, A.; Cotugno, R.; Chambery, A.; Di Maro, A.; Michniewicz, A.; Parlato, G.; Masullo, M.; Avvedimento, E.V.; De Vendittis, E.; Ruocco, M.R. Rat mitochondrial superoxide dismutase: amino acid positions involved in covalent modifications, activity, and heat stability. *Biopolymers*, **2009**, *91*, 1215–1226.

[31] Whittaker, J.W. The irony of manganese superoxide dismutase. *Biochem. Soc. Trans.*, **2003**, *31*, 1318–1321.

[32] Beckman, J.S.; Chen, J.; Ischiropoulos H.; Crow J.P. Oxidative chemistry of peroxynitrite, *Methods Enzymol.*, **1994**, *233*, 229–240.

[33] Castellano, I.; Di Maro, A.; Ruocco, M.R.; Chambery, A.; Parente, A.; Di Martino, M.T.; Parlato, G.; Masullo, M.; De Vendittis, E. Psychrophilic superoxide dismutase from *Pseudoalteromonas haloplanktis*: biochemical characterization and identification of a highly reactive cysteine residue. *Biochimie*, **2006**, *88*, 1377–1389.

[34] Sambrook, J.; Fritsch, E.F.; Maniatis, T. *Molecular cloning: a laboratory manual*, 2nd ed.; Cold Spring Harbor, Laboratory Press: New York, **1989**.

[35] Dello Russo, A.; Rullo, R.; Nitti, G.; Masullo, M.; Bocchini, V. Iron superoxide dismutase from the archaeon *Sulfolobus solfataricus*: average hydrophobicity and amino acid weight are involved in the adaptation of proteins to extreme environments. *Biochim. Biophys. Acta*, **1997**, *1343*, 23–30.

[36] Bradford, M.M. A rapid and sensitive method for the quantitation of microgram quantities of protein utilizing the principle of protein–dye binding. *Anal. Biochem.*, **1976**, *72*, 248–254.

[37] Laemmli, U.K. Cleavage of structural proteins during the assembly of the head of bacteriophage T4. *Nature*, **1970**, *227*, 680–685.

[38] Dosi, R.; Di Maro, A.; Chambery, A.; Colonna, G.; Costantini, S.; Geraci, G.; Parente, A. Characterization and kinetics studies of water buffalo (Bubalus bubalis) myoglobin. *Comp. Biochem. Physiol. B Biochem. Mol. Biol.*, **2006**, *145*, 230–238.

[39] Castellano, I.; Ruocco, M.R.; Cecere, F.; Di Maro, A.; Chambery, A.; Michniewicz, A.; Parlato, G.; Masullo, M.; De Vendittis, E. Glutathionylation of the iron superoxide dismutase from the psychrophilic eubacterium *Pseudoalteromonas haloplanktis. Biochim. Biophys. Acta*, **2008**, *1784*, 816–826.

[40] Whittaker, M.M.; Whittaker, J.W. Conformationally gated metal uptake by apomanganese superoxide dismutase. *Biochemistry*, **2008**, *47*, 11625–11636.

[41] MacMillan-Crow, L.A.; Crow, J.P.; Thompson, J.A. Peroxynitrite–mediated inactivation of manganese superoxide dismutase involves nitration and oxidation of critical tyrosine residues. *Biochemistry*, **1998**, *37*, 1613–1622.

[42] Soulere, L.; Claparols, C.; Perie, J.; Hoffmann, P. Peroxynitrite–induced nitration of tyrosine–34 does not inhibit *Escherichia coli* superoxide dismutase. *Biochem. J.*, **2001**, *360*, 563–567.

[43] Yamakura, F.; Taka, H.; Fujimura, T.; Murayama, K. Inactivation of human manganese–superoxide dismutase by peroxynitrite is caused by exclusive nitration of tyrosine 34 to 3–nitrotyrosine. *J. Biol. Chem.*, **1998**, *273*, 14085–14089.

[44] Yamano, S.; Maruyama, T. An azide–insensitive superoxide dismutase from a hyperthermophilic archaeon, *Sulfolobus solfataricus*. *J. Biochem. (Tokyo)*, **1999**, *125*, 186–193.

[45] MacMillan–Crow, L.A.; Crow, J.P.; Kerby, J.D.; Beckman, J.S.; Thompson, J.A. Nitration and inactivation of manganese superoxide dismutase in chronic rejection of human renal allografts. *Proc. Natl. Acad. Sci. USA*, **1996**, *93*, 11853–11858.

[46] Wintjens, R.; Noël, C.; May, A.C.W.; Gerbod, D.; Dufernez, F.; Capron, M.; Viscogliosi, E.; Rooman, M. Specificity and phenetic relationships of iron– and manganese–containing superoxide dismutases on the basis of structure and sequence comparisons. *J. Biol. Chem.*, **2004**, *279*, 9248–9254.

Received: February 21, 2011 **Revised: June 21, 2011** **Accepted: June 22, 2011**

Biochimie 94 (2012) 768–775

Contents lists available at SciVerse ScienceDirect

Biochimie

journal homepage: www.elsevier.com/locate/biochi

Research paper

Identification of an active dimeric intermediate populated during the unfolding process of the cambialistic superoxide dismutase from *Streptococcus mutans*

Antonello Merlino [a,b], Irene Russo Krauss [a], Bianca Rossi [a], Alessandro Vergara [a,b], Alberto De Vendittis [c], Salvatore Marco [c], Emmanuele De Vendittis [c], Filomena Sica [a,b,*]

[a] *Dipartimento di Chimica, Università di Napoli Federico II, Complesso Universitario Monte S. Angelo, Via Cinthia, I-80126 Naples, Italy*
[b] *Istituto di Biostrutture e Bioimmagini, CNR, Via Mezzocannone 16, I-80134 Naples, Italy*
[c] *Dipartimento di Biochimica e Biotecnologie Mediche, Università di Napoli Federico II, Via Pansini 5, I-80131 Napoli, Italy*

ARTICLE INFO

Article history:
Received 11 July 2011
Accepted 18 November 2011
Available online 28 November 2011

Keywords:
Superoxide dismutase
Thermal stability
Chemical stability
Dimeric intermediate
Unfolding

ABSTRACT

Superoxide dismutases are enzymes that protect biological systems against oxidative damage caused by superoxide radicals. In this paper, a detailed characterization is presented on the stability of *Sm*SOD, the dimeric cambialistic superoxide dismutase from the dental pathogenic microorganism *Streptococcus mutans*, towards temperature and guanidine hydrochloride. Thermal and chemical denaturations were investigated by means of circular dichroism, fourth-derivative UV spectroscopy and fluorescence measurements. Data indicate that *Sm*SOD is endowed with a significant thermostability and that both its thermal and guanidine hydrochloride-induced unfolding processes occur through a three-state model, characterized by a catalytically active dimeric intermediate species. To our knowledge, *Sm*SOD is the smallest known dimeric protein that populates a well-structured active dimeric rather than a monomeric intermediate during unfolding processes.

1. Introduction

The study of multi-subunit protein folding provides powerful information. Protein–protein interactions, which play crucial roles in the stabilization of oligomeric proteins, are indeed intrinsic to virtually every cellular process. A clear understanding of the self-organization mechanism can be achieved by structural stability analysis. Experimental studies on the folding mechanism of dimers, which can be considered as a stable complex of two subunits, provide key insights pertinent to understanding the biological assembly and regulation of protein–protein complexes [1,2].

In principle, the folding of dimeric proteins can occur via many different mechanisms, but the large majority of dimers can be essentially divided in two classes. The first corresponds to a group of proteins that folds following a simple two-state process, i.e. an *all-or-none* description of folding. Such a behaviour is typically observed in small globular proteins consisting of cooperatively hydrophobic units. The second class consists of proteins which follow a three-state process, characterized by an intermediate species [2,3]. The intermediate species is generally a monomeric chain, but proteins with relatively large subunits (chain lengths $>$ 250 residues) and with contact area between the monomers $>$1500 Å^2 have been found to populate dimeric rather than monomeric equilibrium intermediates [3]. Beside the fundamental importance in understanding protein folding problem [4], studying the nature of the intermediate structures on the folding/unfolding pathways of a protein may give an insight into the factors involved in the misfolding process. For these reasons, identification and characterization of intermediate states populated during the unfolding process of dimeric proteins have received considerable attention, and much effort is being spent on this objective (see for example [5–8]). A simple method for such studies involves the monitoring of conformational changes due to perturbation of various agents such as temperature and additives.

Superoxide dismutases (SODs) may represent an interesting class of enzymes to be studied through their unfolding process. These important antioxidant enzymes, present in many organisms, from bacteria to plants and animals, protect aerobic cells against the detrimental effects of superoxide radicals [9–11]. These proteins

Abbreviations: ANS, 1-anilino-8-naphthalene sulfonate; *Bs*SOD, superoxide dismutase (SOD) from *Bacillus subtilis*; $C_{1/2}$, concentration of denaturant at midpoint denaturation; *Ec*SOD, SOD from *Escherichia coli*; GdnHCl, guanidine hydrochloride; *Ph*SOD, SOD from *Pseudoalteromonas haloplanktis*; PDB, protein data bank; *Sm*SOD, SOD from *Streptococcus mutans*; T_m, melting temperature.

* Corresponding author. Department of Chemistry, University of Naples 'Federico II', Via Cinthia, I-80126 Naples, Italy. Tel.: +39 081674479; fax: +39 081674090.
E-mail address: filomena.sica@unina.it (F. Sica).

0300-9084/$ – see front matter © 2011 Elsevier Masson SAS. All rights reserved.
doi:10.1016/j.biochi.2011.11.008

catalyze the dismutation of superoxide ions in a cyclic redox reaction involving the active site metal ion by the following scheme:

$$SOD \bullet M^{3+} + O_2^{\cdot -} \rightarrow SOD \bullet M^{2+} + O_2$$

$$SOD \bullet M^{2+} + O_2^{\cdot -} + 2H^+ \rightarrow SOD \bullet M^{3+} + H_2O_2$$

SODs have been classified into structurally unrelated families on the basis of metal content and cellular location [12]. Mammals contain a cytosolic Cu/Zn-SOD (SOD1), a mitochondrial Mn-SOD (SOD2) and an extracellular SOD (SOD3), whereas most eubacteria and archaea usually contain only a Fe-SOD or a Mn-SOD, both belonging to the same group of SOD2 [13]. The folding mechanism of Cu/Zn-SODs has been extensively studied, because some cases of familial amyotrophic lateral sclerosis, a severe protein conformational disorder, have been associated with mutant protein misfolding [14]. Unfolding of Cu/Zn-SODs involves a three-state mechanism with the appearance of a monomeric intermediate [14–16]. Unfolding mechanism of Fe/Mn-SOD [17,18] has been also broadly studied, particularly in the case of thermostable enzymes which have attracted researchers' attention due to their industrial application potential [19–21]. Here we report the thermal and chemical stability of *Sm*SOD, the dimeric superoxide dismutase from the dental pathogenic microorganism *Streptococcus mutans*. A previous biochemical characterization indicated that *Sm*SOD is a cambialistic enzyme, able to bind and/or exchange Mn or Fe ions in its active site [22]. Even though the enzyme shows a marked preference for Fe binding, it is more active with Mn; furthermore, its half-inactivation occurs after 10 min exposure at more than 70 °C. In the present paper we show that *Sm*SOD has a high denaturation temperature, and transforms into a functional dimeric intermediate along its unfolding pathway.

2. Materials and methods

2.1. Biochemical analysis

The protein expression and purification were performed as previously reported [22]. Briefly, using a heterologous expression system constituted by v*Sm*SOD, a pET-28b(+) derivative, and the *Escherichia coli* BL21(DE3) strain, a recombinant His-tagged protein has been purified by Ni^{2+}–agarose affinity chromatography. Protein concentration was determined by the method of Bradford, using bovine serum albumin as standard [23]. The quaternary structure of recombinant *Sm*SOD was evaluated by gel-filtration on a Superdex 75 10/300 GL column (GE Healthcare). The iron and manganese content of purified *Sm*SOD was determined by graphite furnace atomic absorption spectrometry, as previously indicated [22]. In the sample used for all the experiments reported in this paper the iron content was 0.33 mol/mol subunit, whereas the Mn content was as low as 0.025 mol/mol subunit. However, even marked differences in metal content (0.86 and 0.11 mol/mol subunit for Fe and Mn, respectively) in a different lot of protein did not significantly affect both the spectroscopic properties and the thermal stability of *Sm*SOD (see next section). The activity of *Sm*SOD was measured by the inhibition of cytochrome *c* reduction caused by superoxide anions generated with the xanthine/xanthine oxidase method [9,24]. In particular, SOD activity was evaluated in three different reaction buffers, namely 100 mM potassium phosphate, pH 7.8, or 40 mM Tris HCl, pH 7.8, or 40 mM MOPS, pH 7.8, all of them supplemented with 0.1 mM Na–EDTA.

2.2. Circular dichroism

CD spectra were recorded at 20 °C using a Jasco J-710 spectropolarimeter equipped with a Peltier thermostatic cell holder (Model PTC-348WI). Molar ellipticity per mean residue, [θ] in deg cm^2 $dmol^{-1}$, was calculated from the equation: $[\theta] = [\theta]_{obs} \cdot mrw/(10 \cdot l \cdot C)$, where $[\theta]_{obs}$ is the ellipticity measured in degrees, mrw is the mean residue molecular weight, *C* is the protein concentration in g mL^{-1} and *l* is the optical path length of the cell in cm. Far-UV measurements (250–190 nm) were carried out using a 0.1 cm path length cell and protein concentration 0.3 mg mL^{-1} in various 10 mM buffers. Before measurements, the samples were pre-equilibrated at 10 °C for 5 min and the instrument was calibrated with an aqueous solution of D-10-(+)-camphorsulfonic acid at 290 nm. CD spectra were signal averaged over at least three scans and the baseline corrected by subtracting the buffer spectrum. Spectra analysis was performed by means of the SELCON3 method, as implemented in DICHROWEB [25]. Thermal unfolding curves were recorded in the temperature mode at 208 nm using a continuous heating protocol and various buffers (Tris HCl, Hepes, MOPS, sodium phosphate, pH 7.8). The thermal unfolding behaviour was confirmed by using a step heating procedure. In this case, the protein sample at 0.44 mg mL^{-1} in 10 mM Tris HCl buffer, pH 7.8, was equilibrated at the desired temperature for 15 min before measurements. The concentration dependence of thermal unfolding curves was also measured in the range 0.15–3.0 mg mL^{-1}, using 10 mM Tris HCl, pH 7.8 as a buffer.

The effect of metal content on *Sm*SOD behaviour was checked by comparing the CD spectra of two samples containing a different metal percentage (Fig. S1). Spectra analysis indicates that the samples have a comparable amount of α-helical and β-sheet structures (Table S1). Furthermore, the thermal unfolding curves of the two samples present inflection points at temperatures almost identical each other (Fig. S2).

2.3. Fluorescence studies

Steady-state fluorescence measurements were performed with a Perkin–Elmer spectrofluorimeter mod. LS50b equipped with thermostated cell holders. The emission spectra of *Sm*SOD were collected at 0.35 mg mL^{-1} protein concentration in 10 mM Tris HCl buffer, pH 7.8. Tryptophan was selectively excited at 295 nm, whereas excitation wavelength for both tyrosine and tryptophan fluorescence was 280 nm. The emission was recorded from 310 to 450 nm. The experiments were performed at different temperatures by using a 1 cm sealed cell and a 5 nm emission slit width, and corrected for background signal.

2.4. Fourth-derivative UV spectroscopy

UV absorption spectra were recorded using a Cary spectrophotometer (Cary 500) with a Peltier thermostated cell. The protein was dissolved at a concentration of 5.8 mg mL^{-1} in 10 mM Tris HCl buffer, pH 7.8. A 0.1 cm optical path-length quartz cell was used to record absorption spectra between 240 and 320 nm. All spectra were recorded in steps of 0.1 nm, and the time of data acquisition per step was 1 s at three temperatures: 20 °C, 50 °C and 98 °C. The protein absorption was recorded after a 3 min pause before each measurement. Cary Win UV software was used to control the system and to obtain the fourth-derivative spectra.

2.5. Guanidine hydrochloride-induced unfolding transition

The chemical-induced denaturation curves of *Sm*SOD were obtained at constant temperature (20 °C) by recording the CD signal at 222 nm and following the displacement of the emission maximum of intrinsic fluorescence spectra for each independent sample. The protein samples (0.35 mg mL^{-1}) were incubated overnight with increasing concentration of GdnHCl (0–6 M) at 20 °C.

2.6. ANS binding assay

Exposure of hydrophobic surface in the enzyme was detected by its ability to bind the fluorescent dye 1-Anilino-8-naphthalene sulfonate (ANS). A protein sample at 4 μM was incubated for 30 min at 20 °C with 100 μM ANS in 10 mM Tris HCl, pH 7.8 and the fluorescence emission of bound ANS was measured. The excitation wavelength was 380 nm and emission spectra were collected between 400 and 600 nm. Both slit widths of excitation and emission were set at 5 nm.

2.7. Molecular modelling

A starting model for the monomer of *Sm*SOD was obtained, using the structure of the superoxide dismutase from *Bacillus subtilis* (*Bs*SOD, PDB code 2RCV, 1.6 Å resolution, 62% sequence identity) as a template [26] and the SWISS-MODEL server (http://swissmodel.expasy.org/). The program "O" [27] was used to build the missing parts of the model, to include Fe or Mn ions in the active site pocket and to perform other manual adjustments of side chains in the vicinity of the active site.

The dimeric structure was assumed to be similar to that of *Bs*SOD. The dimer was thus obtained by manual superimposition of the monomer and its duplicated version on the two subunits of the template. Energy minimisation was then done through GROMACS [28] by using Steepest Descent and Conjugate Gradient Algorithms, following a well established procedure [29–33]. The final model was validated with PROSA web server [34]. Cartoons were generated using Pymol (www.pymol.org).

3. Results and discussion

3.1. Three-dimensional model of SmSOD

A model for the monomer of *Sm*SOD was obtained by homology modelling, using as a template the available 3D crystallographic structure of *Bs*SOD [26]. Positional sequence identity of *Bs*SOD and *Sm*SOD is 62%. The Z-score value of the combined statistical potential energy of the monomeric model used to build the dimeric form of *Sm*SOD is −8.26. This value is in the range of scores typically found in proteins of similar sequence length. The monomer was then used to build the *Sm*SOD dimer (Fig. 1), as described in the Methods section. The stereochemical analysis of the final model showed only two residues positioned in the generously allowed region and no residues in the disallowed regions of the Ramachandran plot. Overall comparison of the predicted structure of *Sm*SOD with that of *Bs*SOD revealed few differences. The superimposition of the two dimers gives a root mean square deviation of 0.90 Å for the main chain atoms. The first domain, of the typical two-domain fold of SODs, is composed of three α-helices, α1 (Ala20-Leu42), α2 (Leu52-Leu56) and α3 (Arg67-Glu85), with three connecting loops and three residues in β-strand (Leu86-Ser88). The other domain starts with helices α4 (Glu97-Ala105) and α5 (Phe109-Thr122), followed by a β-sheet formed by the three β-strands, β1 (Ser126-Asp134), β2 (Lys138-Asn146) and β3 (Lys156-Val163), and by two α-helices, α6 (Arg176-Phe184) and α7 (Arg189-Phe198). The inter-domain metal binding site, formed by residues His26, His80, Asp162 and His166, is also very well preserved. The dimer has a two-fold axis, and the extended symmetric interface of about 1700 Å^2 includes His30, Phe124, Gly125, Ser126, Trp164, Glu165, His166, Tyr169 and Leu170.

3.2. Thermal stability of SmSOD

The far-UV CD spectrum of *Sm*SOD at 20 °C, in 10 mM Tris HCl buffer, pH 7.8, presents a double minimum at 208 and 222 nm (Fig. 2), as expected for a protein with a large α-helical content. Indeed, the analysis of CD spectrum by means of DICHROWEB [25] indicates that *Sm*SOD has a folded structure with 53–55% helical structure and 17–19% β-sheet structure, in good agreement with the data obtained by the homology model of the protein (50% α-helix and 14% β-strand). Similar results have been obtained analyzing the CD spectra of *Sm*SOD collected at 20 °C in different buffers (10 mM MOPS, pH 7.8; 10 mM sodium phosphate, pH 7.8; 10 mM Hepes, pH 7.8; 10 mM CHES, pH 8.8 and pH 10.0 (data not shown). The temperature increase causes an appreciable modification in the spectrum, indicating a marked loss of secondary structure elements. In particular, for example, at 108 °C in Tris HCl buffer the spectrum shows a deep negative peak at about 205 nm and a shoulder at about 220 nm (Fig. S3). It is worth noting that these far-UV CD spectra are very similar to those obtained for SODs from *Pseudoalteromonas haloplanktis* (*Ph*SOD) and *E. coli* (*Ec*SOD) [21].

Thermal unfolding curves of *Sm*SOD samples at different concentrations in Tris HCl buffer were recorded in the temperature

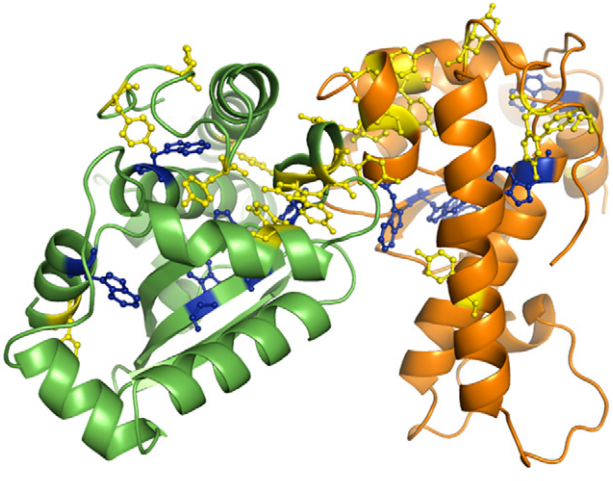

Fig. 1. Molecular model of *Sm*SOD. The two subunits are orange and green, respectively. The position of Tyr (yellow) and Trp (blue) residues is highlighted. (For interpretation of the references to colour in this figure legend, the reader is referred to the web version of this article.)

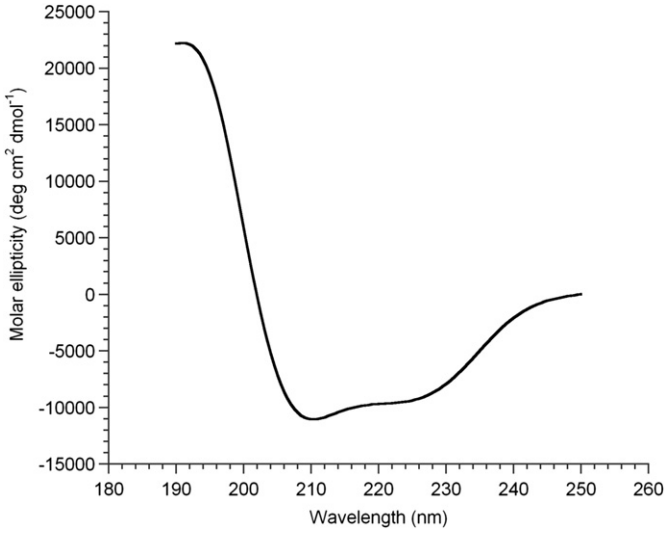

Fig. 2. Far-UV CD spectrum of *Sm*SOD. Spectrum was acquired at 20 °C using a protein concentration of 0.3 mg mL^{-1} in a 10 mM Tris HCl buffer, pH 7.8.

mode at 208 nm from 10 to 108 °C with a scan rate of 0.2 °C min^{-1} (Fig. 3). A visual inspection of the melting curves unequivocally indicates that the thermal unfolding is a biphasic transition: the curves present two inflection points (i.e., T_{m1} and T_{m2}) and a plateau region indicative of the presence of an intermediate along the denaturation pathway. The midpoints of the first (T_{m1}) and second transition (T_{m2}) of *Sm*SOD determined at 0.15 mg mL^{-1} were 46.2 °C and 95.4 °C, respectively (Fig. 3, green line). When the protein concentration is raised up to 3.0 mg mL^{-1}, a shift towards lower temperatures was observed for the second transition, whereas the first one was essentially concentration-independent (Fig. 3 yellow line and Table S1). These results indicate that the second transition is characterized by an aggregation phenomenon coupled to unfolding. These findings are in line with data obtained by gel filtration experiments performed on samples previously treated at 108 °C, indicating that *Sm*SOD unfolds forming high-weights oligomeric species. This led to complete irreversibility, as indicated by the lack of the CD and fluorescence signal recovery when temperature was decreased. Visual inspection of a heated sample (0.44 mg mL^{-1}) suggests that protein starts to aggregate between 70 °C and 75 °C.

Thermal unfolding studies performed in other buffers, such as MOPS (Fig. S4), confirmed the high heat stability of *Sm*SOD. However, when the unfolding curve in MOPS was compared with that observed in Tris HCl, some differences emerged at very high temperatures. Indeed, after an almost coincident first thermal transition, the second increase of the CD signal in MOPS started at significantly higher temperatures. Therefore, the T_{m1} value in MOPS was very close to that determined in Tris HCl; surprisingly, we were not able to determine the T_{m2}, because the second transition of *Sm*SOD did not yet practically start at 100 °C, on the basis of the recorded molar ellipticity values. This different behaviour could be due to the variation of pH with temperature that characterizes the sample in the Tris HCl buffer.

The oligomeric state of the protein in correspondence of the first thermal transition was analysed by gel filtration experiments carried out either in Tris or MOPS buffer. To this aim, the elution profile of *Sm*SOD samples incubated for 30 min at 55 °C was compared with that of untreated samples. The elution time of treated and untreated samples was identical and corresponded to that of a dimeric *Sm*SOD. As the column elution was carried out at room temperature, we cannot exclude that, after the heat treatment, a putative dissociated monomer of *Sm*SOD could reassemble to form a dimer at room temperature; however, this eventual reassembly should be immediate. As later stated on the basis of activity measurements, the presence of the dimeric state of *Sm*SOD was also inferred from the experiment described in Fig. 7, reporting the temperature dependence of the SOD assay, carried out with a real-time temperature control.

The comparison of the CD spectra recorded in Tris HCl at 20 °C and 55 °C reveals that the intermediate species observed at 55 °C (Fig. 4) retains a significant amount of secondary structure (48% of helical content, according to the spectra deconvolution by DICHROWEB [25]).

Since it is known that the use of different heating protocols can lead to different results, the thermal denaturation of *Sm*SOD in Tris HCl was also followed using a step heating procedure. The results obtained using this procedure are in full agreement with those described using the continuous heating protocol (Fig. S5). The thermal denaturation of *Sm*SOD was also investigated by steady-state fluorescence spectroscopy using the step heating protocol. Variations in the fluorescence emission intensity and shift in the emission maximum (λ_{max}) are sensitive measures of changes in solvent exposure of tyrosine and tryptophan residues, resulting from alterations of tertiary structure. Fluorescence was excited at the long-wave absorption spectrum edge (295 nm), where the contribution of tyrosine residues is negligible, and at 280 nm, where both tyrosine and tryptophan residues significantly contribute to the absorption. The spectra were recorded at five temperatures (20, 50, 65, 88, and 98 °C), which should correspond to the presence of native protein (20 °C), intermediate state (50 °C and 65 °C) and completely denaturated protein (88 °C and 98 °C). The fluorescence spectrum of *Sm*SOD at 20 °C exhibited a λ_{max} of 338 nm and 339 nm, upon excitation at 280 nm (Fig. 5A) and 295 nm (Fig. 5B), respectively. Spectra recorded at 50 °C and 65 °C upon excitation at 280 nm are characterized by a red-shift of λ_{max}

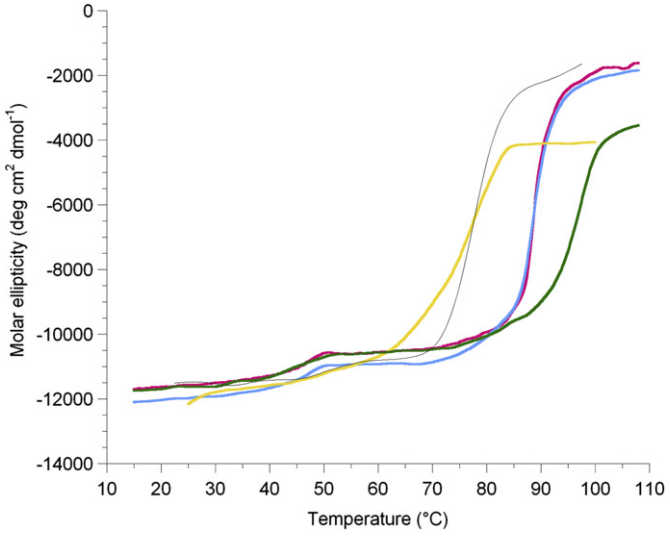

Fig. 3. Heat denaturation of *Sm*SOD as followed by CD spectroscopy at 208 nm, at a heating rate of 0.2 °C min^{-1}. Measurements were carried out in 10 mM Tris HCl buffer at pH 7.8, using an enzyme concentration of 0.15 mg mL^{-1} (green line), 0.25 mg mL^{-1} (pink line), 0.30 mg mL^{-1} (cyan line), 0.44 mg mL^{-1} (grey line) and 3.0 mg mL^{-1} (yellow line). T_{m2} significantly decreased from 95.4 °C at 0.15 mg mL^{-1} to 77.2 °C at 3.0 mg mL^{-1}, whereas T_{m1} only slightly increased at increasing protein concentration, passing from 46.2 °C at 0.15 mg mL^{-1} to 49.8 °C at 3.0 mg mL^{-1}. (For interpretation of the references to colour in this figure legend, the reader is referred to the web version of this article.)

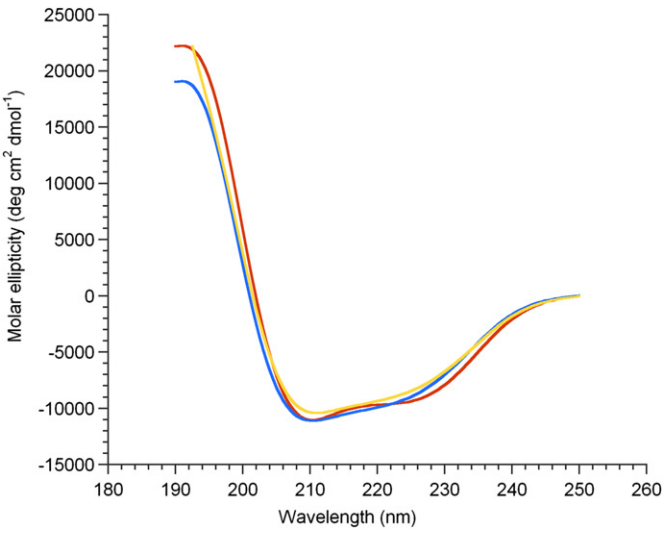

Fig. 4. Far-UV CD spectra of *Sm*SOD in 10 mM Tris HCl, pH 7.8. Spectra were acquired at 25 °C (native protein, coloured in red), at 55 °C (intermediate species, coloured in yellow) and at 25 °C after renaturation (cyan). (For interpretation of the references to colour in this figure legend, the reader is referred to the web version of this article.)

and by a net increase of the signal intensity, when compared to spectra recorded at 20 °C (Fig. 5A). This finding indicates that, in the putative dimeric intermediate species, a change of the microenvironment of aromatic residues occurs. Upon temperature increase from 65 °C to 88 °C, a further red-shift of the λ_{max} was observed; at higher temperatures, protein aggregation is no longer neglectable. The data collected upon excitation at 295 nm had a different behaviour (Fig. 5B). In this case, spectra recorded at different temperatures showed just a minor variation of λ_{max} (Fig. 5B). These data suggest that Trp residues are not involved in the temperature-driven protein conformational changes, although it cannot be excluded that the non-complete red-shift of λ_{max} is a consequence of the formation of aggregates.

To obtain further information about the specific environmental changes that take place around the aromatic residues of *Sm*SOD as a consequence of the thermal unfolding, fourth-derivative UV spectra of *Sm*SOD were collected at different temperatures (Fig. 6). Two are the regions of interest in the spectrum: the range 255–265 nm, where the absorption bands corresponding to Phe appear and the range 270–300 nm in which the bands arise from the electronic transitions of Tyr and Trp residues. In proteins with a Trp/Tyr content ratio value $\geq$ 0.25, the longest-wavelength minimum (λ_1) is mainly determined by the nature of the Trp environment [35,36]. A value of λ_1 close to 292 nm indicates hydrophobic surroundings for Trp residues. In *Sm*SOD, the Trp/Tyr content ratio is 0.56 and the values of λ_1 are close to 296 nm in both native and intermediate species. These data suggest that the native protein and the dimeric intermediate species have Trp residues trapped in an apolar environment, in agreement with the fluorescence data. The elevated number of aromatic residues in the sequence of *Sm*SOD does not allow to obtain a more detailed picture of the intermediate structure, but the presence of Trp residues at the dimeric interface (Fig. 1) suggests that intersubunit contacts are almost intact in the intermediate species. Strong contact interactions at the intersubunit interface that should contribute to the extra-stability of *Sm*SOD against temperature are depicted in Fig. S6. A list of hydrogen bonds and salt-bridges probably formed at the interface is reported in Table S3.

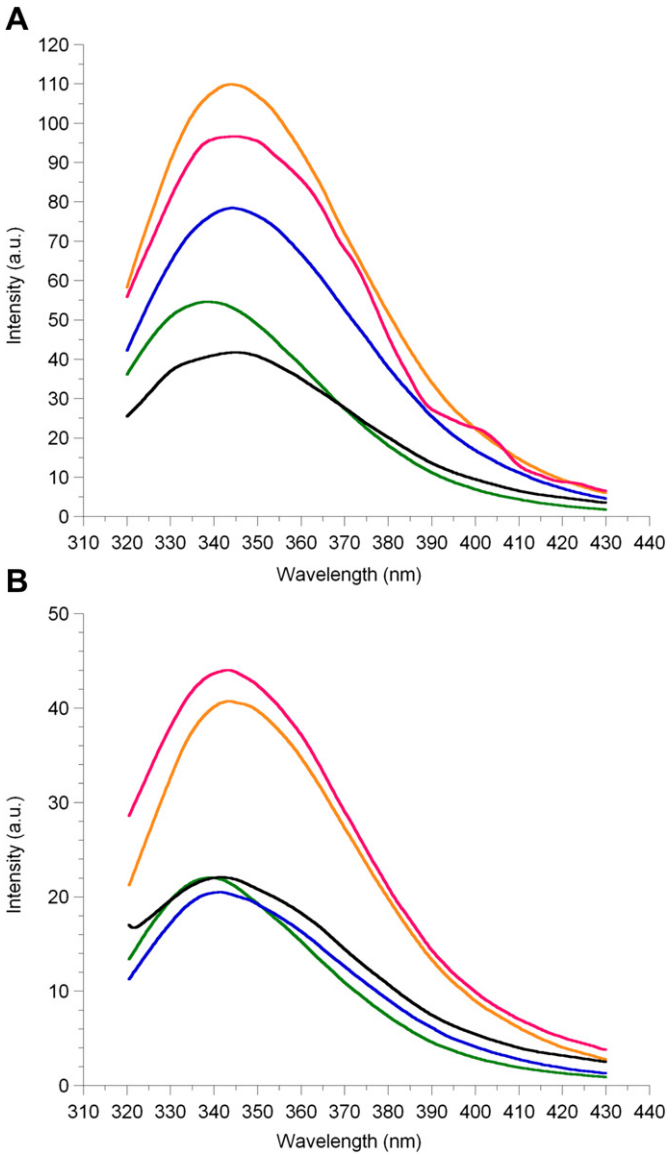

Fig. 5. Fluorescence spectra of 0.35 mg mL^{-1} *Sm*SOD in 10 mM Tris HCl buffer, pH 7.8 recorded at 20 °C (green), 50 °C (blue), 65 °C (yellow), 88 °C (red) and 98 °C (black). A) λ_{exc} = 280 nm; B) λ_{exc} = 295 nm. (For interpretation of the references to colour in this figure legend, the reader is referred to the web version of this article.)

3.3. Catalytic activity of the intermediate species observed during the thermal unfolding of SmSOD

We have hypothesized that during the first transition described in Fig. 3, *Sm*SOD keeps a dimeric structure. A previously reported heat inactivation profile of *Sm*SOD [22] suggested that this enzyme retained an almost full activity in the temperature range related to the first transition reported in Fig. 3. However, in that case, the activity of the heat-treated enzyme was measured after an ice-chilling, and therefore it is not possible to exclude that, in those experiments, a fraction of *Sm*SOD underwent a reversible transition from the intermediate to native state. To get an insight on the effect of temperature on *Sm*SOD activity and in particular to reveal if the intermediate species is still active at 45–50 °C (first transition), the catalytic activity of *Sm*SOD was measured in three different buffers and in the interval 25–80 °C with a real-time temperature control, using the xanthine/xanthine oxidase method [9,24]. This assay represents an indirect measurement of SOD activity, based on the inhibition of cytochrome *c* reduction caused by SOD. Therefore, the procedure includes a control of cytochrome *c* reduction in the absence of SOD. In the experiment reported in Fig. 7, carried out with the typical buffer constituted by potassium phosphate, the effect of temperature on this control activity (empty circles) followed the typical temperature-dependent curve. When SOD was added in the assay, a similar temperature-dependent curve was observed (filled circles), with the expected inhibition of cytochrome *c* reduction. Because of the presence of other enzymes in the assay, the method was unable to evaluate how the activity of SOD alone was affected by temperature. However, the assay clearly showed that SOD was active up to 55 °C, because it was able to inhibit the cytochrome *c* reduction at all temperatures investigated. A similar picture was obtained when the potassium phosphate was replaced by either Tris or MOPS buffer (data not shown). Furthermore, all these results are in line with the finding that thermal denaturation CD curves of cytochrome *c* in the same conditions used for the activity assay show that the enzyme retains its native structure at least up to 80 °C (data not shown). It is generally accepted that the oligomeric state of SOD (the so-called functional dimer) is essential for the mechanism of activity. Therefore, we can infer that the intermediate species of *Sm*SOD observed at 50 °C is populated by an active functional dimer. The finding that the dimeric intermediate is fully active up to 55 °C strongly suggests that the active site and the second coordination sphere around the active site (Fig. S7) should retain their native structure at this temperature.

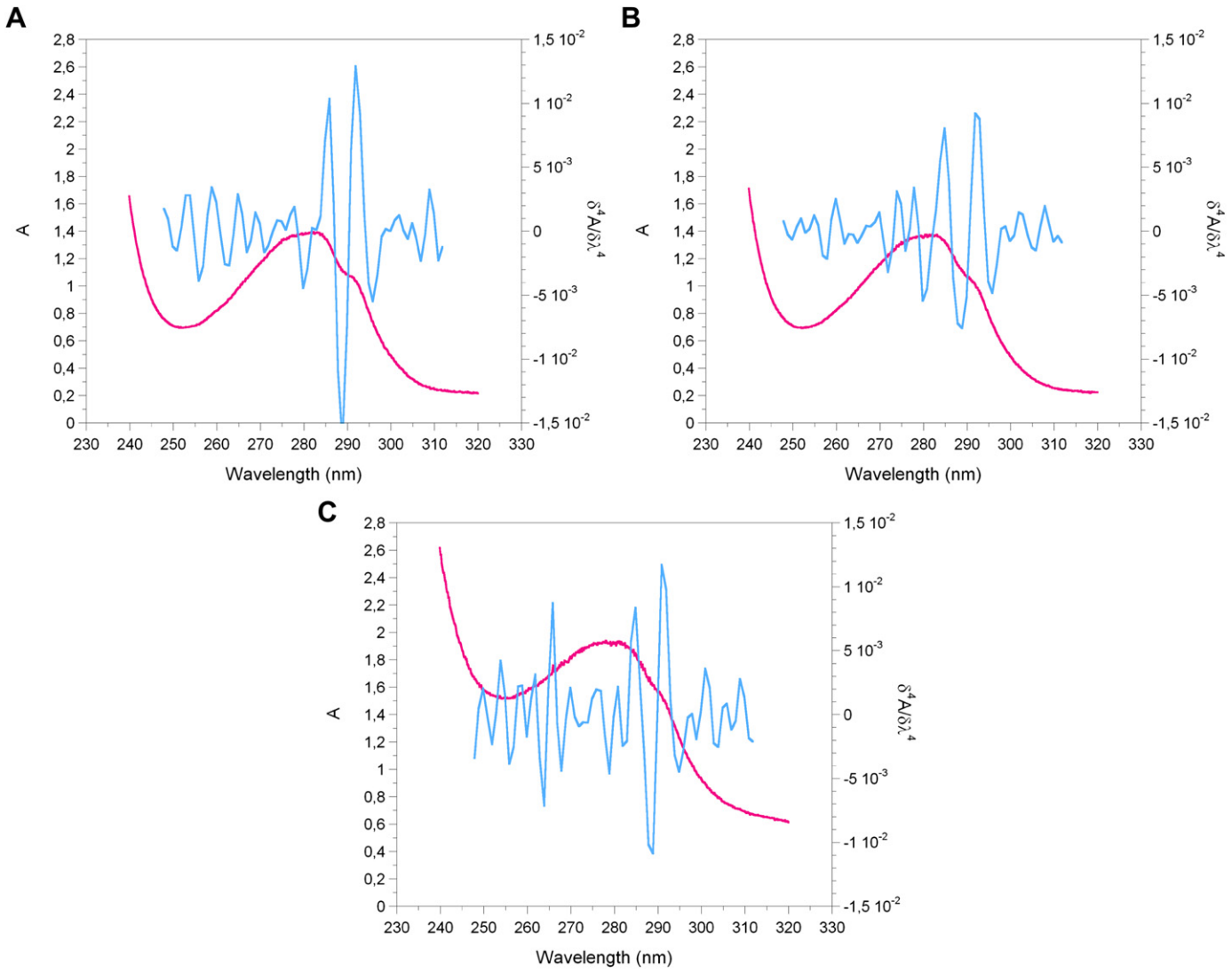

Fig. 6. UV absorbance (pink line) and fourth-derivative (blue line) spectra of *Sm*SOD at 20 °C (A), 50 °C (B) and 98 °C (C). The protein concentration was 5.8 mg mL^{-1} in 10 mM Tris HCl buffer, pH 7.8. (For interpretation of the references to colour in this figure legend, the reader is referred to the web version of this article.)

3.4. Chemical stability of SmSOD

In order to further characterize the unfolding of *Sm*SOD, the enzyme resistance to GdnHCl denaturation was investigated, following this chemical-induced denaturation by fluorescence and CD measurements. In the first approach, the red-shift of λ_{max} in the *Sm*SOD emission spectrum (Fig. 8A) and the fluorescence intensity at the λ_{max} (Fig. 8B) were followed as a function of denaturant concentration after excitation at 280 and 295 nm. At both excitation wavelengths, in the presence of increasing GdnHCl concentrations (up to 2 M) the emission maximum of *Sm*SOD raised from 338 nm to 346 nm (Fig. 8A), with an increase in the fluorescence intensity (Fig. 8B). Above 2 M GdnHCl, the fluorescence intensity began to decrease, reaching a minimum at 2.6 M GdnHCl (Fig. 8B). Increasing GdnHCl concentrations up to 6 M provoked a significant increase in fluorescence intensity (Fig. 8B), coupled to a further red-shift of the emission maximum from 346 to 355 nm (Fig. 8A). These data confirm the occurrence of a two-phase mechanism even in the GdnHCl-induced denaturation of *Sm*SOD. Furthermore, this overall behaviour is indicative of the transition towards an enzyme structure with tyrosine and tryptophan side chains exposed to a more hydrophilic environment.

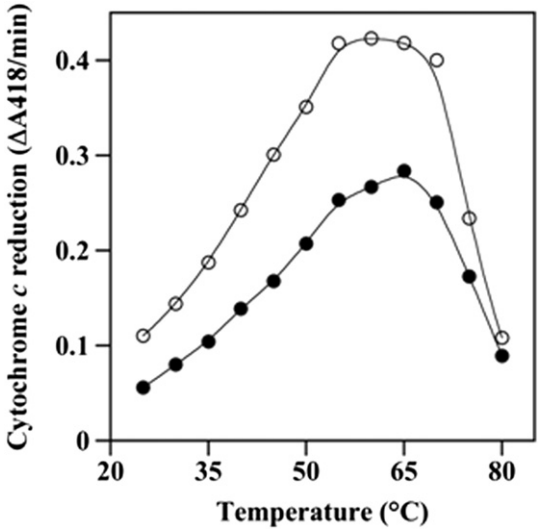

Fig. 7. Temperature dependence of the cytochrome *c* reduction assayed through the xanthine/xanthine oxidase method. The reduction was measured in phosphate buffer in the absence (open circles) or in the presence of *Sm*SOD (filled circles).

The CD measurements of *Sm*SOD were carried out at 20 °C and evaluated through the values of ellipticity at 222 nm obtained as a function of denaturant concentration. As shown in Fig. S8, the ellipticity moderately decreases in the GdnHCl concentration range from 0 to 1.5 M (first transition), thus indicating a slight decrease in the α-helical content of *Sm*SOD. In correspondence of the formation of the intermediate species (1.5–2.0 M GdnHCl), the ellipticity increases and becomes almost equal to that of the native protein. This finding suggests that this intermediate has an α-helix content similar to that of the native state (α-helix content about 50%). In the second transition of the denaturation profile above 2.0 M GdnHCl, a progressive loss of alpha helical structure was observed (Fig. S8).

Changes in the CD signals quite well correlate with fluorescence data. It should be also underlined that the chemical denaturation observed after the second transition is irreversible, while a full recovery of all the spectroscopic features of the native state was observed upon complete removal of the denaturant by ultrafiltration, just after the first transition (data not shown). Gel filtration experiments indicated that in the 1.5–2.0 M GdnHCl concentration range, the *Sm*SOD sample eluted as a dimer. Unfortunately, we cannot measure the catalytic activity of *Sm*SOD in the 1.5–2.0 M GdnHCl concentration range, since in this condition cytochrome *c* is fully denatured [40]. Summarizing all results, one can draw the conclusion that, as in the case of the thermal denaturation, the GdnHCl-induced unfolding involves an intermediate state of *Sm*SOD before it fully unfolds. However, in the presence of GdnHCl, the completely denatured state of the enzyme has Trp/Tyr residues in a hydrophilic microenvironment, whereas the thermally denatured protein has Trp/Tyr residues exposed to an apolar environment and is prone to aggregate.

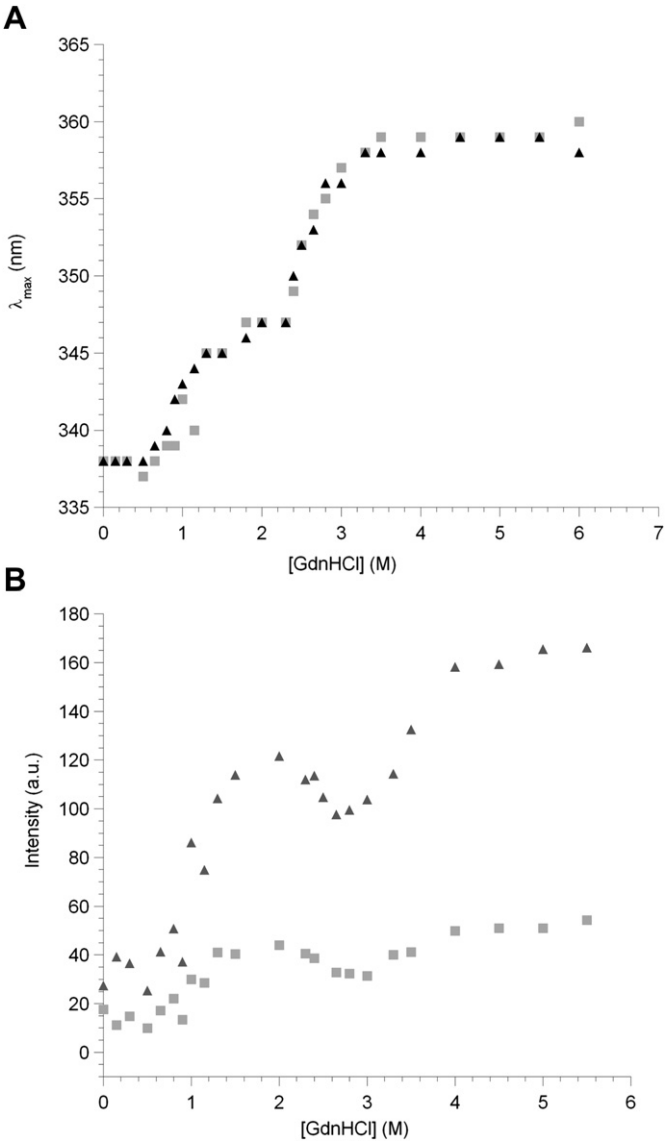

Fig. 8. Guanidine hydrochloride induced-denaturation curves of *Sm*SOD in 10 mM Tris HCl buffer, pH 7.8 at 25 °C. The red-shift of λ_{max} (panel A) and the fluorescence intensity at λ_{max} (panel B) were recorded upon excitation at λ_{exc} = 280 nm (triangle) and at λ_{exc} = 295 nm (square).

3.5. Structural comparison of the unfolding intermediates

In order to compare the structure of the GdnHCl-induced intermediate with that of the temperature-induced one, both fluorescence and CD spectra of *Sm*SOD in the presence of 2 M GdnHCl were superimposed to those of the native protein registered at 20 °C and 50–55 °C (data not shown). As we have already mentioned, the comparison between CD spectra suggests that both the thermal and GdnHCl-induced intermediates present an α-helical content comparable to that observed in the native protein. Fluorescence spectra of the two intermediates are both characterized by a red-shift of λ_{max} and by a net increase of the signal intensity after excitation at 280 nm, when compared to spectra of the native protein. The behaviour is slightly different upon excitation at 295 nm. On the basis of these data it can be speculated that the two intermediates could have a similar secondary structure, but a slightly different dimeric interface.

To further compare the structural features of the two intermediates we have also examined their ability to bind 1-Anilino-8-naphthalene sulfonate (ANS). Fluorescence spectra of ANS in the presence of the two intermediates are both characterized by a red-shift of λ_{max} and by a net decrease of the signal intensity when compared to spectra of the native protein (Fig. S9). This is a further indication of the overall structural similarity of the two intermediates. These results also suggest that the intermediates have a non-hydrophobic solvent exposed surface.

4. Conclusions

The results described in this work reveal that *Sm*SOD is a very stable protein and that both its temperature- and chemical-induced denaturation can be rationalized as a three-state transition, characterized by an intermediate dimeric species. The formation of the intermediate is a reversible process, whereas the second transition is an irreversible unfolding. Although the dimeric Fe- or Mn- SODs display a highly conserved overall structure, their denaturation pathway is not unique. In the case of a three-state mechanism, monomeric [37], dimeric [20,21] and even tetrameric or high molecular weight intermediates [38,39] have been observed. According to the thermal inactivation studies [22] and catalytic activity measurements presented in this paper, the dimeric intermediate, obtained during the temperature-induced *Sm*SOD denaturation, retains an almost unaltered catalytic activity. The identification of a functional intermediate in the unfolding pathway of Fe- or Mn- superoxide dismutases might suggest the existence, even under native conditions, of a second higher energy active conformation that presumably possesses only modest structural differences with respect to the more stable one. This unexpected flexibility observed for *Sm*SOD may uncover a more complex regulation mechanism of its enzymatic activity that could have more general implications.

Conflict of interest statement

None.

Acknowledgements

The authors thank Lelio Mazzarella for critical reading of the manuscript and Elisa Giugliano for her help in preliminary fluorescence measurements. CIMCF (Centro Interdipartimentale di Metodologie Chimico-Fisiche) is also acknowledged.

Appendix. Supplementary material

Supplementary data related to this article can be found online at doi:10.1016/j.biochi.2011.11.008.

References

[1] C.R. Matthews, Pathway of protein folding, Annu. Rev. Biochem. 62 (1993) 653–683.
[2] K.E. Neet, D.E. Timm, Conformational stability of dimeric proteins: quantitative studies by equilibrium denaturation, Protein Sci. 3 (1994) 2167–2174.
[3] J.A. Rumfeldt, C. Galvagnion, K.A. Vassall, E.M. Meiering, Conformational stability and folding mechanisms of dimeric proteins, Prog. Biophys. Mol. Biol. 98 (2008) 61–84.
[4] P.S. Kim, R.L. Baldwin, Specific intermediates in the folding reactions of small proteins and the mechanism of protein folding, Annu. Rev. Biochem. 51 (1982) 459–489.
[5] S.M. Doyle, E.H. Braswell, C.M. Teschke, SecA folds via a dimeric intermediate, Biochemistry 39 (2000) 11667–11676.
[6] K. Bose, A.C. Clark, Dimeric procaspase-3 unfolds via a four-state equilibrium process, Biochemistry 40 (2001) 14236–14242.
[7] M.E. Chanez-Cardenas, G. Perez-Hernandez, B.G. Sanchez-Rebollar, M. Costas, E. Vazquez-Contreras, Reversible equilibrium unfolding of triosephosphate isomerase from *Trypanosoma cruzi* in guanidinium hydrochloride involves stable dimeric and monomeric intermediates, Biochemistry 44 (2005) 10883–10892.
[8] S. Gildenhuys, L.A. Wallace, J.P. Burke, D. Balchin, Y. Sayed, H.W. Dirr, Class Pi glutathione transferase unfolds via a dimeric and not monomeric intermediate: functional implications for an unstable monomer, Biochemistry 49 (2010) 5074–5081.
[9] J.M. McCord, I. Fridovich, Superoxide dismutase. An enzymic function for erythrocuprein (hemocuprein), J. Biol. Chem. 244 (1969) 6049–6055.
[10] J.M. McCord, I. Fridovich, The utility of superoxide dismutase in studying free radical reactions. I. Radicals generated by the interaction of sulfite, dimethyl sulfoxide, and oxygen, J. Biol. Chem. 244 (1969) 6056–6063.
[11] V.C. Culotta, M. Yang, T.V. O'Halloran, Activation of superoxide dismutases: putting the metal to the pedal, Biochim. Biophys. Acta. 1763 (2006) 747–758.
[12] A.F. Miller, Superoxide dismutases: active sites that save, but a protein that kills, Curr. Opin. Chem. Biol. 8 (2004) 162–168.
[13] W.C. Stallings, K.A. Pattridge, R.K. Strong, M.L. Ludwig, Manganese and iron superoxide dismutases are structural homologs, J. Biol. Chem. 259 (1984) 10695–10699.
[14] J.A. Rumfeldt, P.B. Stathopulos, A. Chakrabarrty, J.R. Lepock, E.M. Meiering, Mechanism and thermodynamics of guanidinium chloride-induced denaturation of ALS-associated mutant Cu, Zn superoxide dismutases, J. Mol. Biol. 355 (2006) 106–123.
[15] G. Mei, N. Rosato, N. Silva Jr., R. Rusch, E. Gratton, I. Savini, A. Finazzi-Agro, Denaturation of human Cu/Zn superoxide dismutase by guanidine hydrochloride: a dynamic fluorescence study, Biochemistry 31 (1992) 7224–7230.
[16] M.E. Stroppolo, F. Malvezzi-Campeggi, G. Mei, N. Rosato, A. Desideri, Role of the tertiary and quaternary structures in the stability of dimeric copper, zinc superoxide dismutases, Arch. Biochem. Biophys. 377 (2000) 215–218.
[17] A.F. Miller, in: A. Messerschimdt, R. Huber, K. Wieghardt, T. Paulos (Eds.), Handbook of Metalloproteins, Wiley and Sons, Chicester, 2001.
[18] M.E. Stroupe, M. Di Donato, J.A. Tainer, in: A. Messerschimdt, R. Huber, K. Wieghardt, T. Paulos (Eds.), Handbook of Metalloproteins, Wiley and Sons, Chicester, 2001.
[19] S. Wang, W.F. Liu, Y.Z. He, A. Zhang, L. Huang, Z.Y. Dong, Y.B. Yan, Multistate folding of a hyperthermostable Fe-superoxide dismutase (TcSOD) in guanidinium hydrochloride: the importance of the quaternary structure, Biochim. Biophys. Acta 1784 (2008) 445–454.
[20] H.L. Pedersen, N.P. Willassen, I. Leiros, The first structure of a cold-adapted superoxide dismutase (SOD): biochemical and structural characterization of iron SOD from *Aliivibrio salmonicida*, Acta Crystallogr. Sect. F Struct. Biol. Cryst. Commun. 65 (2009) 84–92.
[21] A. Merlino, I. Russo Krauss, I. Castellano, E. De Vendittis, B. Rossi, M. Conte, A. Vergara, F. Sica, Structure and flexibility in cold-adapted iron superoxide dismutases: the case of the enzyme isolated from *Pseudoalteromonas haloplanktis*, J. Struct. Biol. 172 (2010) 343–352.
[22] A. De Vendittis, M. Amato, A. Mickniewicz, G. Parlato, A. De Angelis, I. Castellano, R. Rullo, F. Riccitiello, S. Rengo, M. Masullo, E. De Vendittis, Regulation of the properties of superoxide dismutase from the dental pathogenic microorganism *Streptococcus mutans* by iron- and manganese-bound co-factor, Mol. Biosyst. 6 (2010) 1973–1982.
[23] M.M. Bradford, A rapid and sensitive method for the quantitation of microgram quantities of protein utilizing the principle of protein-dye binding, Anal. Biochem. 72 (1976) 248–254.
[24] A. Dello Russo, R. Rullo, G. Nitti, M. Masullo, V. Bocchini, Iron superoxide dismutase from the archaeon *Sulfolobus solfataricus*: average hydrophobicity and amino acid weight are involved in the adaptation of proteins to extreme environments, Biochim. Biophys. Acta 1343 (1997) 23–30.
[25] L. Whitmore, B.A. Wallace, DICHROWEB, an online server for protein secondary structure analyses from circular dichroism spectroscopic data, Nucleic Acids Res. 32 (2004) W668–W673.
[26] P. Liu, H.E. Ewis, Y.J. Huang, C.D. Lu, P.C. Tai, I.T. Weber, Structure of *Bacillus subtilis* superoxide dismutase, Acta Crystallogr. Sect. F Struct. Biol. Cryst. Commun. 63 (2007) 1003–1007.
[27] T.A. Jones, J.Y. Zou, S.W. Cowan, M. Kjeldgaard, Improved methods for building protein models in electron density maps and the location of errors in these models, Acta Crystallogr. A 47 (Pt 2) (1991) 110–119.
[28] D. Van Der Spoel, E. Lindahl, B. Hess, G. Groenhof, A.E. Mark, H.J. Berendsen, GROMACS: fast, flexible, and free, J. Comput. Chem. 26 (2005) 1701–1718.
[29] A. Merlino, L. Esposito, L. Vitagliano, Polyglutamine repeats and beta-helix structure: molecular dynamics study, Proteins 63 (2006) 918–927.
[30] M. Porcelli, M.A. Moretti, L. Concilio, S. Forte, A. Merlino, G. Graziano, G. Cacciapuoti, S-adenosylhomocysteine hydrolase from the archaeon *Pyrococcus furiosus*: biochemical characterization and analysis of protein structure by comparative molecular modeling, Proteins 58 (2005) 815–825.
[31] E. Pizzo, A. Merlino, M. Turano, I. Russo Krauss, F. Coscia, A. Zanfardino, M. Varcamonti, A. Furia, C. Giancola, L. Mazzarella, F. Sica, G. D'Alessio, A new RNase sheds light on the RNase/angiogenin subfamily from zebrafish, Biochem. J. 433 (2011) 345–355.
[32] I. Castellano, A. Merlino, M. Rossi, F. La Cara, Biochemical and structural properties of gamma-glutamyl transpeptidase from *Geobacillus thermodenitrificans*: an enzyme specialized in hydrolase activity, Biochimie 92 (2010) 464–474.
[33] I. Castellano, A. Di Salle, A. Merlino, M. Rossi, F. La Cara, Gene cloning and protein expression of gamma-glutamyltranspeptidases from *Thermus thermophilus* and *Deinococcus radiodurans*: comparison of molecular and structural properties with mesophilic counterparts, Extremophiles 15 (2011) 259–270.
[34] M. Wiederstein, M.J. Sippl, ProSA-web: interactive web service for the recognition of errors in three-dimensional structures of proteins, Nucleic Acids Res. 35 (2007) W407–W410.
[35] E. Padros, A. Morros, J. Manosa, M. Dunach, The state of tyrosine and phenylalanine residues in proteins analyzed by fourth-derivative spectrophotometry. Histone H1 and ribonuclease A, Eur. J. Biochem. 127 (1982) 117–122.
[36] M. Dunach, M. Sabes, E. Padros, Fourth-derivative spectrophotometry analysis of tryptophan environment in proteins. Application to melittin, cytochrome *c* and bacteriorhodopsin, Eur. J. Biochem. 134 (1983) 123–128.
[37] S. Wang, Y. Yan, Z. Dong, Contributions of the C-terminal helix to the structural stability of a hyperthermophilic Fe-superoxide dismutase (TcSOD), Int. J. Mol. Sci. 10 (2009) 5498–5512.
[38] J.B. Cooper, S. Saward, P.T. Erskine, M.O. Badasso, S.P. Wood, Y. Zhang, D. Young, X-ray structure analysis of an engineered Fe-superoxide dismutase Gly-Ala mutant with significantly reduced stability to denaturant, FEBS Lett. 387 (1996) 105–108.
[39] H.C.K. Hsieh, C.C. Chiu, C. Yu, Equilibrium unfolding of a oligomeric protein involved the formation of multimeric intermediate state, Biochem. Biophys. Res. Commun. 326 (2005) 108–114.
[40] B. Liujiao, Z. Than, Y. Xiaoyani, L. Li, Z. Xiaohui, Unfolding of bovine heart cytochrome *c* induced by urea and guanidine hydrochloride, Chin. J. Chem. 29 (2011) 813–821.